UC Santa Cruz

UC Santa Cruz Electronic Theses and Dissertations

Title

The Role of Biofilm Matrix Protein VbpA in Vibrio cholerae Biofilm Formation

Permalink

https://escholarship.org/uc/item/2t19c3rg

Author

Oguchi, Rino

Publication Date

2021

Peer reviewed|Thesis/dissertation

eScholarship.org Powered by the California Digital Library
University of California

UNIVERSITY OF CALIFORNIA
SANTA CRUZ

THE ROLE OF BIOFILM MATRIX PROTEIN VbpA in *Vibrio cholerae* BIOFILM FORMATION

A thesis submitted in partial satisfaction
of the requirements for the degree of

MASTER OF SCIENCE

in

MICROBIOLOGY AND ENVIRONMENTAL TOXICOLOGY

by

Rino Oguchi

September 2021

The thesis of Rino Oguchi is approved:

_____
Professor Fitnat H. Yildiz, Ph.D., Chair

_____
Professor Victoria Auerbuch Stone, Ph.D.

_____
Professor Seth Rubin, Ph.D.

_____
Peter Biehl
Vice Provost and Dean of Graduate Studies

Copyright © by
Rino Oguchi
2021

Table of Contents

List of Figures iv

Abstract vi

Acknowledgements vii

Chapter 1: Introduction 1

Chapter 2: Characterizing the Role of Biofilm Matrix Protein VbpA in *Vibrio cholerae* Biofilm Formation 17

References 124

List of Figures

Figure 1.1. Select proteins identified in biofilm matrix proteomic analysis of *V. cholerae* 24
Figure 1.2. The impact of VbpA on colony and spot biofilm morphology phenotypes 28
Figure 1.3. Genomic context showing 500 bp around *vbpA* 31
Figure 1.4. Top 5 homologs of *vbpA* 34
Figure 1.5. Colony and spot biofilm morphology of strains lacking predicted TRAP-TAXI systems in *V. cholerae* 38-39
Figure 1.6. Spot biofilm morphologies of *vbpA* and *vbpI* complementation 42
Figure 2.1. Analysis of cellular localization of VbpA 45
Figure 2.2. Analysis of VbpA periplasmic localization using alkaline phosphatase fusion. 48
Figure 2.3. Presence of VbpA in both cell and biofilm matrix in *V. cholerae* 51
Figure 2.4. Switching signal peptides to control VbpA localization 54
Figure 2.5. Biofilm morphologies of *vbpA* strains with altered signal peptide 57
Figure 2.6. Exogenous addition of purified VbpA to spot biofilms of RΔ*vbpA* 60
Figure 2.7. VbpA visualization in the *V. cholerae* biofilm matrix using CLSM and fluorescently labeled antibody 63
Figure 3.1. CLSM analysis of rugose and RΔ*vbpA* colony biofilms 67
Figure 3.2. BiofilmQ analysis of biofilms of Rugose-Tn7::GFP and RΔ*vbpA*-Tn7::GFP 70
Figure 4.1. Abundance of matrix proteins RbmA, RbmC, and Bap1 in *V. cholerae* biofilms lacking VbpA 74
Figure 4.2. Abundance of Vibrio Polysaccharide in *V. cholerae* mutant and complemented strains of *vbpA* 77
Figure 4.3. RbmA, RbmC, and Bap1 visualization in the *V. cholerae* biofilm matrix using CLSM and fluorescently labeled antibodies 81-82
Figure 4.4. VPS visualization in the *V. cholerae* biofilm matrix using CLSM and fluorescently conjugated lectins 85
Figure 5.1. Volcano plot of Rugose vs. RΔ*vbpA* proteome analysis 89
Figure 5.2. Colony and spot biofilm morphology of single and double deletions of gene of interest from proteomic analysis 93-94
Table 6.1. Transposon screen for identification of genes phenocopying RΔ*vbpA* 98
Table 7.1. List of bacterial strains 107-108
Table 7.2. List of plasmids 109

Table 7.3. List of primers 110

The role of biofilm matrix protein VbpA in *Vibrio cholerae* biofilm formation

By

Rino Oguchi

ABSTRACT

Vibrio cholerae is a human pathogen that is responsible for the diarrheal disease cholera. *V. cholerae* is able to persist in the aquatic environment due to its ability to form biofilms as a means of protection from environmental assaults. Biofilms are a surface-associated growth form where aggregated cells are encased by an extracellular matrix made of exopolysaccharides (EPS), extracellular and surface-associated proteins, and extracellular DNA. Biofilm-associated proteins have diverse roles in biofilm formation and have been shown to be important for biofilm survival and growth. We identified the *V. cholerae* biofilm matrix proteome and identified a previously uncharacterized biofilm matrix protein which we termed VbpA (Vibrio biofilm protein A). We found that VbpA is present both in the periplasm and in the extracellular matrix; the lack of VbpA drastically alters *V. cholerae* biofilm architecture, signifying that VbpA plays an important role in biofilm assembly. Further characterization of VbpA revealed how it impacts known matrix proteins and biofilm architecture. We also compared the biofilm matrix and cellular proteome of the "rugose strain" and a *vbpA* mutant. This analysis showed that the lack of VbpA does not result in global changes to the proteome. A better understanding of the function of this protein can provide insight into possible targets for disrupting *V. cholerae* biofilms, preventing the survival and transmission of the pathogen.

Acknowledgements

I would like to first thank my advisor, Dr. Fitnat Yildiz for this opportunity to conduct research in her lab. Her great passion for discovery, creativity in experimental design, and caring for her students' success has made her a major role model as a great scientist. Her support throughout my time here has given me courage as I dove into new experiments and degree milestones. I am leaving this program with the confidence to call myself a scientist, and I am grateful for her mentorship for helping me get to where I am now.

I would like to thank my committee members, Dr. Fitnat Yildiz, Dr. Victoria Auerbuch Stone, and Dr. Seth Rubin, who gave me valuable insights and advice for my project. To the rest of the METX faculty, it was a privilege to learn and study under your guidance.

To the Yildiz Lab members, both past and present—I feel so lucky to have been in the same group as all of you. I was honestly intimidated when I first joined the lab because every person was, and is, extremely intelligent and a passionate scientist. However, I quickly learned that in this lab, there is a strong culture of helping each other out, sharing experiment tips and teaching each other new methods. I would like to especially thank Dr. Carmen Schwechheimer, Dr. Kyle Floyd, and William Garvey for conducting the proteomic study that identified VbpA in the *V. cholerae* matrix and allowing my project to be born. Thank you, Dr. Jin Hwan Park, Dr. Jennifer Teschler,

Dr. Anna Potapova, Dr. Fernando Pagliai, Lizett Gonzalez, Avatar Joshi, Giordan Kitts, Michael Trebino, Bao Nguyen, Megan Mouw, and Joe Kiblen.

To all of the friends I have met here in the METX Department, especially my cohort. Thank you for the laughs and the camaraderie; you helped me feel that I was not alone.

Thank you to my parents and my sister for your support. I am lucky that I was able to attend a school close to family, and I was able to visit home over the weekend whenever I needed some rest. Spending time with you always allowed me to start again refreshed, energized, and ready to tackle it all.

Finally, thank you to my partner Daniel for his never-ending support through the graduate school process. I could not have done it without you.

CHAPTER 1: Introduction

Rino Oguchi & Fitnat H. Yildiz

Biofilms

Many microbes exist in the natural environment as biofilms, which are surface-attached three-dimensional aggregates encased in an extracellular matrix (1–3). Biofilms can form on both biotic and abiotic surfaces (4). Biofilms are common in many types of microbes—from bacteria to fungi, algae, and archaea (1), but in this study we will be focusing on Gram negative bacterial biofilms. Biofilms benefit bacteria by protecting the population from environmental stresses such as nutrient limitation, bacteriophage attack, and protozoan predation (5). In addition to increased survival in the environment, bacterial biofilms are often resistant to antimicrobial agents and can withstand the host immune response, making them a difficult problem to tackle in medicine (6).

Biofilms have been implicated in the persistence of many chronic infections such as pneumonia in cystic fibrosis patients and the contamination of medical devices like catheters and artificial joint implantations (7). For example, many cystic fibrosis (CF) patients are chronically infected with *Pseudomonas aeruginosa,* which persists by forming biofilms (8). Specifically, *P. aeruginosa* biofilms on CF airways produce exopolysaccharides Psl and Pel (which will be discussed in detail in a later section), and Pel binds to host extracellular DNA, increasing tolerance to aminoglycoside antibiotics (9). Biofilms are also important to the transmission of cholera, caused by the Gram-negative bacterium *Vibrio cholerae*. Growth in the biofilm form contributes to *V. cholerae* survival in the aquatic environment, which allows it to then be ingested

in contaminated food and water sources (10). Growth in the biofilm form also contributes to *V. cholerae* infectivity, as biofilm growth causes an upregulation of virulence regulators like *toxT, toxR, toxS* and *tcpH* as well as the virulence factors regulated by these genes like the toxin-coregulated pilus (TCP) and cholera toxin (CTX), causing *V. cholerae* to become hyperinfectious (11). In order to fully understand the benefits that biofilms bring to bacteria, it is important to consider the roles of the different components that make up the biofilm matrix.

Composition of Biofilms

The composition of the extracellular matrix in biofilms varies widely between species, but they are generally composed of exopolysaccharides, secreted proteins, lipids, and nucleic acids (1). Mechanisms of biofilm matrix assembly, the spatial distribution of biofilm matrix components, and the impact of the resulting architectural parameters on biofilm fitness are not well understood.

Exopolysaccharides:

Of the biofilm components, exopolysaccharides generally make up a major portion of the matrix and provide the three-dimensional structure of biofilms (1, 12). For example, in-frame deletions of the gene operons that are critical for Vibrio polysaccharide polysaccharide (VPS) biosynthesis resulted in a marked decrease in biofilm formation, emphasizing the importance of the exopolysaccharide for biofilm architecture (13). Exopolysaccharides are generally large structures composed of

various sugar polymers but can vary greatly in their chemical properties (12). Some are neutral macromolecules or polycationic, but the majority are polyanionic due to the presence of uronic acids or ketal-linked pyruvate (14). Exopolysaccharides also have important interactions with other matrix components like lectins and proteins (14). For example, VPS from *V. cholerae* is thought to bind to RbmA, one of the main matrix proteins (15). Importantly, RbmA is cleaved by proteases. While whole RbmA associates with biofilm cells in a VPS-dependent manner, cleaved RbmA is no longer dependent on VPS for biofilm association (16).

Another example of an exopolysaccharide that interacts with matrix proteins is one of the exopolysaccharides of *P. aeruginosa* biofilms, Psl, which binds to the matrix proteins LecB and CdrA (17, 18). Interestingly, *P. aeruginosa* biofilms produce three co-occurring types of exopolysaccharides that play differential roles—alginate, Psl, and Pel (8). However, they are produced divergently depending on the environment. Alginate is often secreted in highly viscous mucoid isolates of *P. aeruginosa* while Psl and Pel are often produced by rugose, small colony variants (19). The compositions of these three exopolysaccharides are also diverse—alginate is a linear polymer of guluronic and mannuronic acid; Psl is composed of repeated pentamers of mannose, rhamnose, and glucose; and Pel is made of partially acetylated *N*-acetylgalactosamine (GalNAc) and *N*-acetylglucosamine (GlcNAc) (19, 20). In fact, these three exopolysaccharides have different charges at different physiological pH,

likely allowing *P. aeruginosa* increased flexibility to adapt to various stressors in the environment (20).

Many studies through the years have explored both the structural roles and interactions that exopolysaccharides have in biofilms. Cellulose is an essential exopolysaccharide component of many bacteria in the family *Proteobacteria* including *Salmonella* spp. and *Escherichia coli*, contributing to biofilm architecture, resistance to harsh chemicals, and hydrophobicity (21–23). Cellulose is a glucose polymer with β-1,4 glycosidic linkage and is secreted by a cellulose synthase complex made of two subunits, BcsA and BcsB (24). Cellulose is co-occurring with thin aggregative fimbriae in both *Salmonella* spp. and *E. coli* biofilms, and together these two components form a highly hydrophobic network within a rigid matrix (22). Interestingly, many cellulose producing bacteria have symbiotic or pathogenic relationships with plants, which also produce cellulose in their cell walls; however, there is also evidence that cellulose acts as an anti-virulence factor in enteropathogenic bacteria (23).

eDNA:

Extracellular nucleic acid polymers, or eDNA, have been identified to be fundamental to many biofilms, though the degree of their importance differs depending on the microbial species. In general, in biofilms eDNA often acts as the glue to stabilize biofilm structures (25). For example, in *P. aeruginosa* eDNA has been shown to be

essential to the biofilm structure, as the addition of the enzyme DNase I that cleaves DNA prevents biofilm assembly (26). In *P. aeruginosa,* the polysaccharide Pel is thought to bind to eDNA in the biofilm stalk region through ionic bonding (20). This binding of Pel and eDNA has clinical implications; Psl and Pel are produced in *P. aeruginosa* infections on CF lungs, and the aggregation of Pel to eDNA is one of the factors causing the inefficacy of aggressive antibiotic treatments in eradicating *P. aeruginosa* infections (9). This is because the binding of these two components promotes both tobramycin tolerance and protection from nucleases (9). In *V. cholerae* biofilms, it was confirmed through lectin chromatography, cross-linking studies, *in silico* analysis and isothermal titration calorimetry that eDNA also binds to the exopolysaccharide, VPS (27). Although the effect of this binding on biofilm structure has not been tested, it is likely that it helps to stabilize biofilm structure as it does in *P. aeruginosa.* In *V. cholerae* the level of eDNA in the biofilm is controlled by two extracellular nucleases, Dns and Xds, and the activity of these two nucleases is fundamental for the development of a normal three-dimensional structure of the biofilm as the lack of these nucleases causes an uncontrolled and unstructured biofilm mass, further corroborating the role of eDNA in biofilm stability (28). As eDNA can play such large roles, their abundance is carefully kept in check by nucleases, which respond to signals such as quorum sensing and chemicals like iron (29).

Matrix Proteins:

Matrix proteins are also important molecules in biofilms and are an active area of research. These proteins are secreted proteins that have roles in biofilm structure and stability and are important for adhesion between matrix components as well as to surfaces, leading to cell-cell or cell-biofilm surface attachment. Matrix proteins include proteins found inside the biofilm matrix as well as cell surface proteins like flagella and pili and proteins inside outer membrane vesicles (30, 31). The role of matrix proteins is diverse—they have roles in attachment, development of three-dimensional structures, stabilization through interactions with biofilm components and the dispersal of biofilms through enzymatic degradation of biofilm components (3).

There has been notable advancement in research conducted on matrix proteins of *P. aeruginosa, E. coli,* and *V. cholerae*. In *P. aeruginosa,* two secreted, soluble lectin proteins LecA and LecB interact with specific sugars in the biofilm matrix (18). More specifically, LecB binds to the exopolysaccharide Psl, and this interaction stabilizes the biofilm matrix; a mutant strain deficient in LecB had impaired cell aggregation and biofilm formation compared to the wildtype strain, supporting its importance in the biofilm formation process (18, 32). In addition to its structural role in the biofilm, LecB is also a virulence factor, inhibiting epithelial wound healing and helping disseminate bacteria along the cell-basement membrane interface (33). Another *P. aeruginosa* matrix protein CdrA also binds to the exopolysaccharide Psl and promotes Psl-dependent cell aggregation (17). However, CdrA promotes biofilm

aggregation across isolates that depend on different polysaccharides, showing that CdrA does not depend on the presence of Psl for its role in the biofilm (34). In addition to Psl, CdrA binds to another type of polysaccharide in the *P. aeruginosa* biofilm, Pel (34). CdrA exists as a full-length, cell-associated protein and as a processed, smaller form secreted to the extracellular matrix and proteolyzed by the periplasmic protease LapG (17, 35). Interestingly, CdrA can mediate bacterial aggregation and biofilm formation even in the absence of polysaccharides, though this CdrA-only biofilm matrix is more susceptible to proteolysis (36). In addition to these structural matrix proteins, the matrix protein ecotin, a serine protease inhibitor, has also been described (37). This protein inhibits neutrophil elastase, a bactericidal enzyme produced by the host immune system during infections. This protein protects biofilm cells from neutrophil elastase-mediated killing. Ecotin, along with LecB and CdrA, also binds to Psl (37).

In *E. coli,* the fiber-forming amyloid protein curli plays a structural role in the biofilm matrix (38). Curli extracellular fiber networks are well conserved between *E. coli* and *Salmonella* species and are important for providing essential structure, initial adhesion, and hindering predatory phage from the interior of the biofilm community (38). Curli subunits are secreted across the inner membrane through the Sec pathway and the curli fibers are produced by a dedicated type VIII secretion system (39). In *E. coli,* seven curli-specific genes (*csg*) make the structural and assembly components of the curli fibers (39). Amyloid filaments have a characteristic ‘cross-β spine’

architecture, where perpendicular-oriented β-strand units are repeated on the fiber axis (39).

In *V. cholerae,* three proteins RbmA, RbmC, and Bap1 are relatively well-studied and contribute to biofilm formation. RbmA is a critical protein in the *V. cholerae* biofilm matrix that enhances intercellular adhesion during biofilm assembly (40). In *V. cholerae,* biofilm matrix production can be observed by the corrugation of colonies on the solid-air interface; one example is the rugose variant of *V. cholerae* that harbors a single point mutation in the *vpvC* gene*,* showing increased corrugation as a result of increased matrix production (41). This allows for the clear observation of genes that have direct effects on the biofilm architecture. The deletion of *rbmA* from the rugose variant resulted in a smooth colony corrugation and a loss of cell clusters and associated RbmC and Bap1 envelopes, indicating that RbmA plays an important role in the biofilm structure (42, 43). Crucial from the beginning of biofilm formation, RbmA was noted to be the first known matrix protein to appear post surface attachment on the cell surface and then aid in mother-daughter cell aggregation (43). It is particularly important in biofilm assembly because in addition to mother-daughter cell aggregation, RbmA undergoes limited proteolysis to RbmA*, which recruits planktonic cells (16). The crystal structure of RbmA showed that it is made of tandem fibronectin type III (FnIII) folds (44). One of the FnIII domains binds to VPS directly (45). RbmA has a binary switch in its conformation and dimerization that alters biofilm architectural properties and the formation of higher order VPS-RbmA

structures (45). Bap1 and RbmC on the other hand both form envelopes around cell clusters, and Bap1 plays a role in biofilm adhesion to surfaces (43). These two proteins have some similarities such as their shared EF hand domains and sequence similarity, but a complementation study found that they can partially complement each other but are not functionally redundant (40). RbmC and Bap1 contain two and one β-prism domains, respectively (46). RbmCs' β-prism domains showed high affinity to complex *N*-glycans that are present on mammalian cell surfaces, showing RbmC's possible role in biofilm adhesion in the host environment (46). The β-prism domain in Bap1 separates the two domains in the crystal structure, made up of an eight-bladed β-propeller (47). Unlike RbmC, Bap1 does not bind to *N*-glycans and instead shows affinity for anionic or linear polysaccharides (47). Taken together, these different affinities may imply that RbmC and Bap1 both have adhesive roles in the biofilm, differing in the substrates that they adhere to.

The diversity of matrix proteins points to their importance in the biofilm, and a greater understanding of these proteins will allow us a better insight to the inner workings of the biofilm matrix.

Proteomic Studies

Proteomics, referring to the comparative identification of entire sets of proteins expressed by bacteria in certain conditions, has played a great role in gaining more understanding of the biofilm lifestyle (48). The major functions of proteins regulating

bacterial biofilms identified through proteomic studies so far are in the categories of proteins related to metabolism, motility, transport, and stress response (49). The technology of proteomic studies is still evolving as this approach is increasingly utilized for studying biofilm formation.

In *P. aeruginosa,* a study was carried out to identify the proteome associated with the *P. aeruginosa* PAO1 biofilm extracellular matrix, where cell, matrix, and OMV fractions were isolated and investigated using a combination of 1D-SDS-PAGE and an LTQ-ICR-FT Ultra mass spectrometer (50). The matrix proteome contains secreted protein (13.3%), cytoplasmic proteins (28.9%), cytoplasmic membrane proteins (2.2%), periplasmic proteins (11.1%), outer membrane proteins (35.6%) and proteins of unknown localization (8.9%) (50). CdrA was identified in the matrix, confirming the efficacy of this sample preparation (50). This study showed a surprisingly large portion of matrix proteins originate from OMVs. A more recent study also compared the total proteomes of 27 clinical isolates of *P. aeruginosa* grown under planktonic and biofilm conditions using protein digestion and qualitative liquid chromatography tandem mass spectrometry (LC-MS/MS) (51). This study found that there were distinct proteomic differences between the two growth forms, and that biofilm proteome profiles were much more divergent in the different clinical isolates compared to planktonic (51). Proteins involved in fatty acid phospholipid metabolism and adaptation to the environment were highly enriched in the biofilm form (51). There is also a study examining the proteome of whole cell *P. aeruginosa*

PAO1 grown in biofilm cultures (52). Whole cell lysates of planktonic and biofilm cultures collected at three different time points were digested and analyzed with LC-MS/MS. Through this study, it was found that *P. aeruginosa* biofilm proteomes change over time, with an increase in secreted factors and transcriptional regulators at 24 hours but a decrease by 48 hours (52). Fifty-eight proteins were identified exclusively in the biofilm, largely in the categories of putative enzymes, secreted factors, and transcriptional regulators (52). Several proteomic studies on *P. aeruginosa* have focused on quorum sensing. A proteomic analysis of extracellular proteins of *P. aeruginosa* PAO1 has been done to specifically observe proteins regulated by the Las and Rhl quorum sensing systems (53). This study used two-dimensional gel electrophoresis of wildtype and mutant strains deficient in *lasRI*, *rhlRI* and *vfr* genes. This study allowed for the characterization of previously unknown QS-regulated proteins in the *P. aeruginosa* biofilm matrix including an aminopeptidase and an endoproteinase (53). Recently, a study was conducted to identify proteins enriched in the biofilm matrix of *P. aeruginosa* by biotinylating the extracellular proteins of mature biofilms prior to biofilm disruption. This extracellular matrix proteome was compared to the total biofilm proteome, which included both intracellular and extracellular proteins (37). Proteins that were enriched in the matrix included proteins involved in protection of the biofilm matrix, oxidoreductase activity, redox processes, facilitating protein folding, and protease activity (37). A serine protease inhibitor ecotin was identified in this proteomic study and was studied further on its protection of the biofilm from neutrophil elastase (37).

In *V. cholerae*, a study by Absalon et al. (2011) identified the proteome associated with the biofilm matrix. In this study, biofilm-grown *V. cholerae* was disrupted by glass beads and the extracytoplasmic proteins were biotinylated, then pellicles disrupted by vortexing with and without beads or sonication (40). 74 predicted extracytoplasmic proteins were identified—10 of these were secreted, 17 were located in the outer membrane, 26 were located in the periplasm, and 18 could not have their location predicted with certainty. Secreted proteins identified included proteins forming bacterial appendages such as the mannose-sensitive hemagglutinin type IV pilus (MshA) as well as the flagellum (FlaA-FlaD), and the now well-studied matrix proteins RbmA and RbmC (40). Other proteins not previously associated with the biofilm matrix were identified including a hemolysin (HlyA), a chitinase, and a hemagglutinin protease (HAP) (40). Also of note, a proteome reference map for the *V. cholerae* El Tor strain has been established using 2-dimensional electrophoresis and peptide mass fingerprint (54).

Vibrio cholerae, **Causative Agent of Cholera**

V. cholerae, a pathogen with global health importance, is one of the main model organisms for studying biofilms. *V. cholerae* is a facultative human pathogen that is the causative agent of the disease cholera, an acute diarrheal disease (5). It is caused by the ingestion of contaminated food or water, and between 12 hours and 5 days after ingestion, can cause severe diarrhea that can kill within hours if left untreated

(55). There have been seven cholera pandemics throughout history, starting in Southeast Asia in the regions north of the Bay of Bengal, where the disease is endemic (56). Each year, an estimated 3 to 5 million cases occur, with 100,000 to 120,000 leading to death (57). Even in recent years, almost one billion people lack access to safe drinking water, putting them at risk of cholera (58). One of the main components leading to *V. cholerae* persistence is biofilms, which are important to both its survival in the aquatic environment and its pathogenesis in the human intestine (59). In fact, when in the biofilm state *V. cholerae* is hyperinfective, meaning the number of cells required to cause disease is decreased (60). Thus, understanding biofilms of *V. cholerae* is key to tackling this persistent global health issue.

Conclusion

Biofilms are three-dimensional aggregates of bacteria encased in a self-produced extracellular matrix. This mode of growth provides numerous advantages to microbes including environmental protection and survival in the harsh host environment. Biofilm-producing pathogens pose a serious threat to human health, as they contribute to chronic disease persistence, contamination of medical devices, tolerance of antibiotics, and the hyperinfectivity of certain biofilm-forming pathogens. It is essential to understand the composition of biofilms to tackle the issue of biofilm-forming pathogens. Exopolysaccharides are abundant in biofilms and often perform structural roles in biofilm architecture, commonly interacting with matrix proteins.

Extracellular DNA often acts as the glue to hold biofilms together and have been shown to bind to some specific exopolysaccharides. Matrix proteins are diverse and proteomic analysis has been an increasingly popular way to identify and quantify all proteins in the biofilm. Proteins identified in biofilm proteomes include well-studied matrix proteins like CdrA in *P. aeruginosa* and RbmA in *V. cholerae* as well as previously unstudied proteins like ecotin in *P. aeruginosa* and hemolysin (HlyA) in *V. cholerae* biofilm matrix. Biofilms are particularly important to the *V. cholerae* life cycle and infection, as biofilms contribute to its survival in the aquatic environment and in the host. In fact, growing as a biofilm makes *V. cholerae* hyperinfective.

Understanding the components and mechanisms of biofilms provides a platform for the development of anti-biofilm strategies. Anti-biofilm molecules that can interfere with one or more steps in the process of biofilm formation are a focus in the field of anti-biofilm drug development. For example, to prevent reversible biofilm attachment to medical devices, a number of methods have been identified to make these surfaces highly hydrophilic (61). To block irreversible adhesion, compounds blocking carbohydrate-binding adhesins are a promising strategy; an example is lectin-blocking glycodecoys from seed extracts (61). Compounds that specifically target pili and curli biogenesis are also interesting ways to prevent adhesion—for example, curlicides FN075 and BibC6 inhibit the assembly of type 1 pili, which are required for *E. coli* (UPEC) pathogenesis in urinary tract infection (61, 62). In order to disrupt mature biofilm structures, extracellular enzymes such as hydrolases that target

specific polysaccharides, nucleases that act on eDNA, and proteases acting on matrix proteins are promising anti-biofilm compounds (61). A study by Baker et al (2016) identified naturally derived glycoside hydrolases PelAh and PslGh which catalyze the disruption of Pel and Psl in *P. aeruginosa* biofilms, respectively (63). The more that can be understood about the different matrix components and their biogenesis, the more targets that can be developed to combat biofilm-forming pathogens.

CHAPTER 2: Characterizing the Role of Biofilm Matrix Protein VbpA in *Vibrio cholerae* Biofilm Formation

Rino Oguchi & Fitnat H. Yildiz

Introduction

Biofilms are surface-attached microbial communities encased in self-produced extracellular, three-dimensional matrices (1). Biofilms are ubiquitous in microbes including bacteria, fungi, and archaea and provide many benefits including protection from harsh environmental factors such as nutrient limitation, bacteriophage attack, and protozoan attack (5) as well as to host-associated factors like the immune clearance and antimicrobial agents (6). Because of these protective qualities, biofilms often play a role in transmission and infectivity of pathogenic microorganisms; hence, understanding the composition of the biofilm components and their role biofilm formation are important for developing anti-biofilm strategies to combat biofilm-forming pathogens.

The composition of the extracellular matrix in biofilms varies widely between species, but they are generally composed of exopolysaccharides, secreted proteins, lipids, and nucleic acids (1). These matrix components work to facilitate surface attachment, determine structural properties and stability of biofilms, and enhance population fitness (64). Exopolysaccharides are generally large structures composed of sugar polymers that contribute to the development of the three-dimensional architecture of biofilms (12). Many exopolysaccharides have important interactions—VPS in *V. cholerae* to matrix protein RbmA (16), Psl from *P. aeruginosa* to matrix proteins LecB and CdrA (17, 18), and Pel in *P. aeruginosa* to eDNA (20).

Extracellular nucleic acid polymers, or eDNA, often acts as the glue to stabilize biofilm structures (25). eDNA has been found to be fundamental for many biofilms' structures; adding nucleases that break down eDNA can cause restructuring and a loss of biofilm structure (28).

Some well-studied matrix proteins include RbmA, RbmC, and Bap1 in *V. cholerae* (42, 43, 65); CdrA, LecA, and LecB in *P. aeruginosa* (33, 36, 66); and amyloid protein curli in *E. coli* (39, 67). Matrix proteins play diverse roles in biofilms. These include retention of daughter cells to founder cells by RbmA, thereby mediating cell-cell interaction (42, 43, 45) and interaction with other matrix components such as exopolysaccharide in the case of RbmA and CdrA (16, 34). RbmA plays a fundamental architectural role in *V. cholerae* biofilms; biofilms formed by *rbmA* mutants are more fragile than those by wild type *V. cholerae* (42). CdrA in *P. aeruginosa* binds to the exopolysaccharide Psl and promotes biofilm aggregation (34). However, there are many more proteins in the biofilm matrix that have not been examined in detail.

Many studies have employed total or matrix-only proteomic analysis to identify and quantify all proteins in the biofilm matrix. These studies are shedding light on the diversity and function of the biofilm proteome. One method that is used to identify matrix proteomes is to separate the biofilm matrix from the cells and to conduct

proteomic analysis on the matrix. In *P. aeruginosa,* the matrix proteome was identified by suspending colony-grown biofilms and analyzing the filtered and precipitated supernatant (50). From this study, 45 proteins were identified that were found exclusively in the matrix. Of these, 35.6% were predicted to be localized to the outer membrane, 28.9% cytoplasmic, 13.3% extracellular secreted, 11.1% periplasmic, 2.2% inner membrane, and 8.9% of an unknown localization (50). Matrix proteins identified in proteomic studies include well-studied matrix proteins like CdrA in *P. aeruginosa* and previously unstudied proteins like a protease inhibitor ecotin which protects the biofilm matrix from neutrophil elastase and proteins involved in metabolism, motility, transport, and stress response (37, 49). In *V. cholerae,* the matrix proteome was identified by biotinylating the extracytoplasmic proteins and disrupting the pellicles mechanically (40). 74 proteins were identified in the matrix, and their predicted localizations were analyzed. 10 were predicted to be secreted, 17 in the outer membrane, 26 periplasmic, and 18 of an unknown localization (40). Secreted proteins identified in this study included bacterial cell-surface appendage proteins like the mannose-sensitive hemagglutinin type IV pilus (MshA) and the flagellum (FlaA-FlaD) and matrix proteins RbmA and RbmC (40). This study advanced the field of *V. cholerae* matrix proteomics by identifying proteins that had previously been unknown. While these studies in *V. cholerae* provided information on the general composition of biofilm proteome, it was qualitative, and it did not give information on biofilm sub-proteome i.e. matrix components present on outer membrane vesicles. To fill this knowledge gap, we

previously conducted a proteomic study of the isolated matrix and OMVs from biofilm-grown cells and quantified them with relative spectral counts. We identified a previously uncharacterized and highly abundant protein in the matrix proteome that we have termed VbpA (Vibrio biofilm protein A). This protein was also identified in the proteomic study by Absalon et al, (2011) but was not characterized. The objective of this study was to characterize VbpA and elucidate its role in *V. cholerae* biofilm formation.

The absence of VbpA had particularly drastic effects on the morphology of biofilms grown at the solid-air interface, suggesting that VbpA plays an important role in biofilm assembly. We determined VbpA's localization to be in the periplasmic and in the extracellular space, distributing around microcolonies in the biofilm matrix. To gain further insight into VbpA's function in biofilm matrix assembly, we analyzed both composition and spatial distribution of known biofilm components and found that VbpA does not affect the abundance but may be affecting the localization of structural biofilm components. Finally, a proteomic comparison between rugose and RΔ*vbpA* showed that the lack of VbpA does not alter biofilm or cellular proteome suggesting that VbpA's impact on biofilm formation is not mediated through signal transduction.

Results

Section 1. Identification and Bioinformatic analysis of *vbpA*

A matrix proteome analysis of a matrix overproducing rugose variant of *V. cholerae* biofilms was conducted. The biofilm matrix was isolated, and the samples were run on SDS-PAGE gels. Gels were stained with Coomassie, and bands were excised and sent for proteomic analysis using mass spectrometry. This proteomic analysis revealed that there are 339 proteins in the biofilm matrix. The known matrix proteins RbmA, RbmC, and Bap1 were identified and quantified in the matrix, showing the effectiveness of this study. One uncharacterized protein encoded by the VC0430 gene that we have termed VbpA (Vibrio biofilm protein A), was found in the matrix to be highly abundant: VbpA abundance was 400 spectral counts while RbmA was around 100 spectral counts (Fig 1.1).

Figure 1.1. Select proteins identified in biofilm matrix proteomic analysis of *V. cholera*. Spectral count of selected proteins from mass spectrometry analysis of *V. cholerae* A1552 rugose variant biofilm matrix (Yildiz Lab, Unpublished).

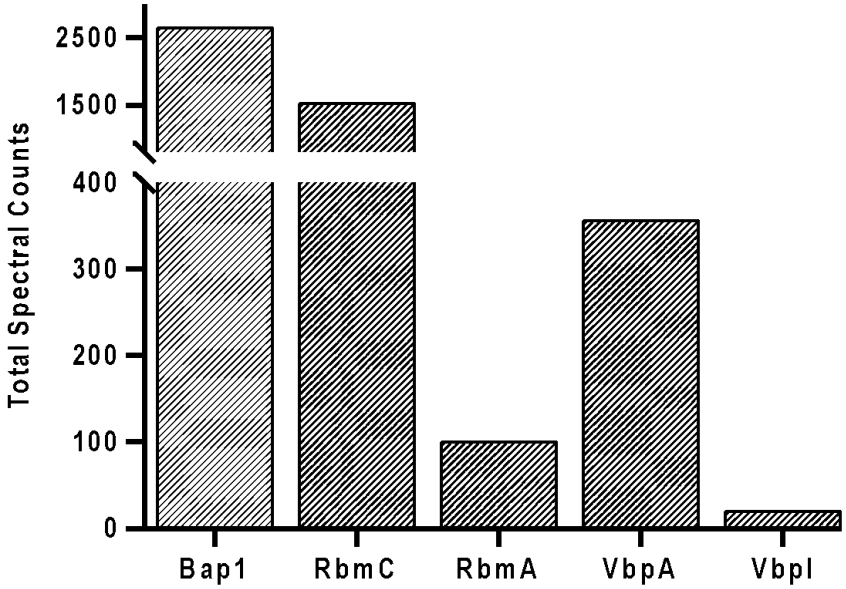
Total Spectral Counts
2500
1500
400
300
200
100
0
Bap1
RbmC
RbmA
VbpA
VbpI

Having seen that VbpA is an abundant *V. cholerae* matrix protein; we set out to determine whether VbpA plays a role in biofilm formation i.e., development of biofilm architecture and biofilm matrix assembly. We first analyzed the effect that *vbpA* has on the biofilm architecture. We generated a strain with an in-frame deletion of *vbpA* in the rugose parent strain and analyzed its biofilm properties. The rugose strain was used for the proteomic study. Due to increased production of biofilm matrix components and their interactions with each other, the rugose strain has characteristic colony biofilm architecture and any changes in corrugation patterns directly represents changes to the biofilm architecture (41). At least 2 biological replicates and 3 technical replicates were examined. RΔ*vbpA* forms significantly larger colonies—in colony dimensions, RΔ*vbpA* was an average of 8.84 mm in diameter compared to the rugose parent strain at 5.04 mm ($p<0.0001$) (Fig 1.2A) and in spot biofilm dimensions, RΔ*vbpA* was an average of 9.67 mm and the rugose strain was 7.13 mm (Fig 1.2B). Another noticeable change is that in RΔ*vbpA,* biofilm architecture, especially the outer ring of the colony biofilm, is markedly different from the parent strain. In the spot biofilm corrugation pattern, the rugose strain also has a tightly corrugated center and an outer ring that spreads out laterally. This outer ring takes up 2mm in the rugose strain (28.6% of the spot biofilm) while in RΔ*vbpA,* the outer ring takes up 4 mm (36.3% of the spot biofilm). When Δ*vbpA* mutation was complemented at a neutral Tn7 site by introducing the wild-type copy of the *vbpA* and its upstream regulatory regions, the biofilm size was restored to the rugose strain biofilm dimensions (average 5.01 mm in colony, 7.03 mm in spo3t morphology) as

well as the biofilm architecture. This confirms that the change in phenotype observed was due to the deletion of *vbpA*. Overexpression of *vbpA* by induction under an IPTG inducible promoter in the pMMB67EH plasmid also caused a change in biofilm architecture; in this case the biofilm corrugation appeared more compact relative to the rugose parent strain (Fig 1.2.C). These findings indicate that the presence and absence of VbpA impacts biofilm assembly.

Figure 1.2. The impact of VbpA on colony and spot biofilm morphology phenotypes. (A) Colony morphology of the following strains: Rugose, RΔ*vbpA,* RΔ*vbpA*-Tn7::*vbpA.* Overnight cultures grown at 30˚C shaking (200 rpm) were diluted up to 10^{-8} in LB medium and 100 µl was plated on LB agar plates and incubated at 30˚C for 120 hours. (B-C) Spot morphology of Rugose, RΔ*vbpA,* RΔ*vbpA*-Tn7::*vbpA* (B) and Rugose-pMMB and Rugose-pMMB/*vbpA* (C). Overnight cultures were diluted 1:200 and 3 µl spotted onto LB agar plates (B) or LB agar plates containing 100 µg/µl Ampicillin and 100 µM IPTG (C) and incubated at 30˚C for 72 hour.

.

A.

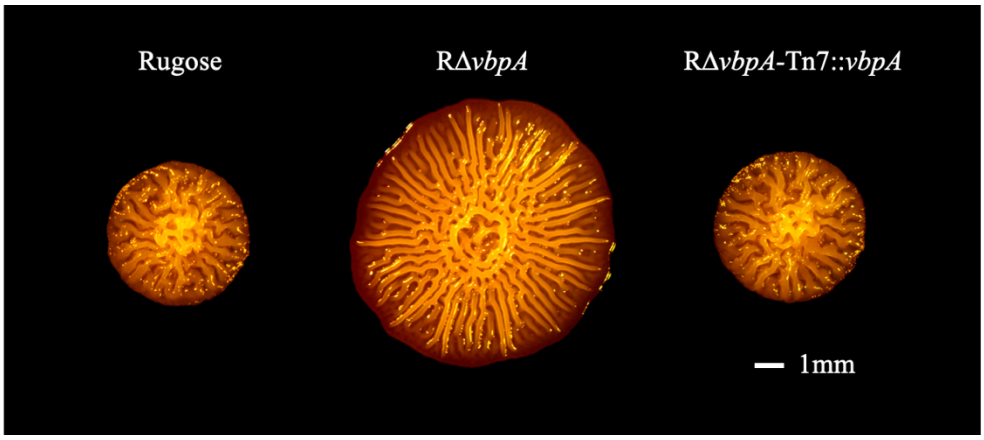
Rugose
RΔ*vbpA*
RΔ*vbpA*-Tn7::*vbpA*
1mm

B.

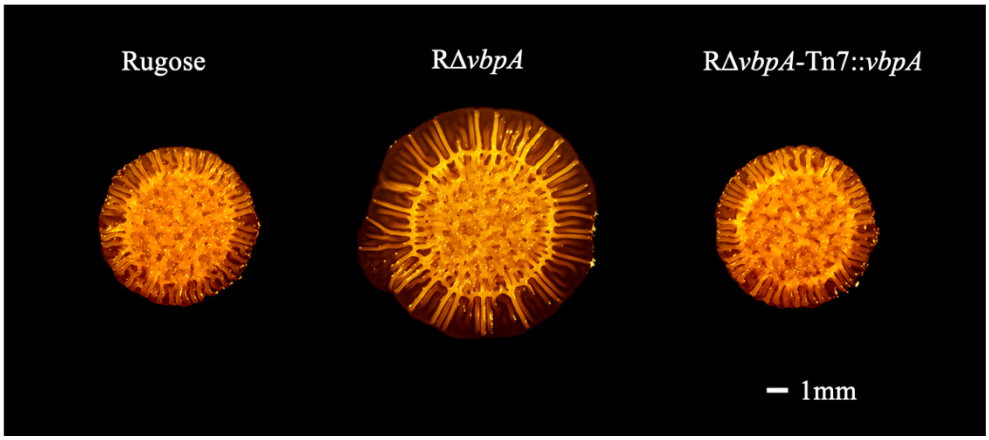
Rugose
RΔ*vbpA*
RΔ*vbpA*-Tn7::*vbpA*
1mm

C.

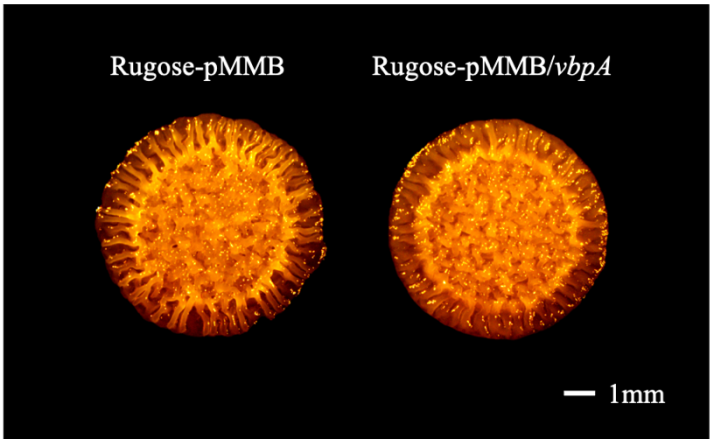
Rugose-pMMB
Rugose-pMMB/*vbpA*
1mm

To better understand how VbpA could impact biofilm architecture, we next used sequence homology analysis of *vbpA* to find similar proteins and generate hypotheses about its functions. *vbpA* is monocistronic and is located between VC0429, an unstudied protein, and VC0431, an arginine repressor protein ArgR (Fig 1.3).

Figure 1.3. Genomic context showing 500 bp around *vbpA*. Image showing genomic context of *vbpA* was obtained using Gene Graphics (68). *vbpA* (987 bp) is located between *vbpB* (2565 bp) and *argR* (471 bp).

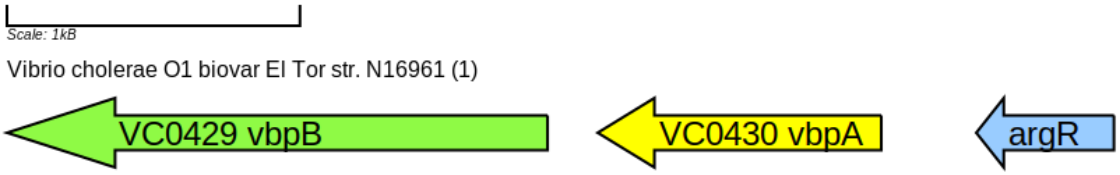
Scale: 1kB
Vibrio cholerae O1 biovar El Tor str. N16961 (1)
VC0429 vbpB
VC0430 vbpA
argR

The top five structural homologs of VbpA were identified by the Phyre2 web portal for protein modeling, prediction, and analysis (69). The highest homology was to an immunogenic protein from *Ehrlichia chaffeensis* (91% coverage, 100% confidence, 41% identity) (Fig 1.3). This protein is predicted to be the periplasmic component of a TRAP-type transport system. The second homologous protein is a periplasmic protein (90% coverage, 100% confidence, 38% identity) that is predicted to be a TRAP solute receptor, TAXI family in *Thermus thermophilus*. The other three structural homologs are predicted to be periplasmic transport proteins in *Bordetella pertussis* and *Polaromonas* sp. The homologs of VbpA determined by position-specific iterative BLAST (PSI-BLAST) showed VbpA exhibits high homology to various "TRAP transporter solute receptors, TAXI family" proteins in archaeal and several Gram-negative bacterial species (Fig 1.4).

Figure 1.4. Sequence alignment of homologs of *vbpA*. Alignments were determined by position-specific iterative BLAST using sequences detected by the Phyre2 web portal for protein modeling, prediction and analysis (69). VEx25_0128 is predicted TRAP transporter, solute receptor, TAXI family in *Vibrio antiquaries* (strain Ex25), 86.6% identity, E-value 2e-68. Arcpr_1316 is predicted TRAP transporter, solute receptor, TAXI family in *Archaeoglobus profundus* (strain DSM 5631 / JCM 9629 / NBRC 100127 / Av18), 32.4% identity, E-value 33e-62. HCH_04583 is predicted TRAP-type uncharacterized transport system, periplasmic component in *Hahella chejuensis* (strain KCTC 2396), 53.1% identity, E-value 63e-62. Tola_1378 is predicted TRAP transporter, TAXI family in *Tolumonas auensis (strain DSM 9187 / TA4),* 44.9% identity, E-value 5e-61. Sdel_0314 is predicted TRAP transporter solute receptor, TAXI family in *Sulfurospirillum deleyianum* (strain ATCC 51133 / DSM 6946 / 5175), 46.8% identity, E-value 8e-60. Alignment figure was constructed using Jalview. Highlighted residues show 100% identity matches. Identities were normalized by aligned length.

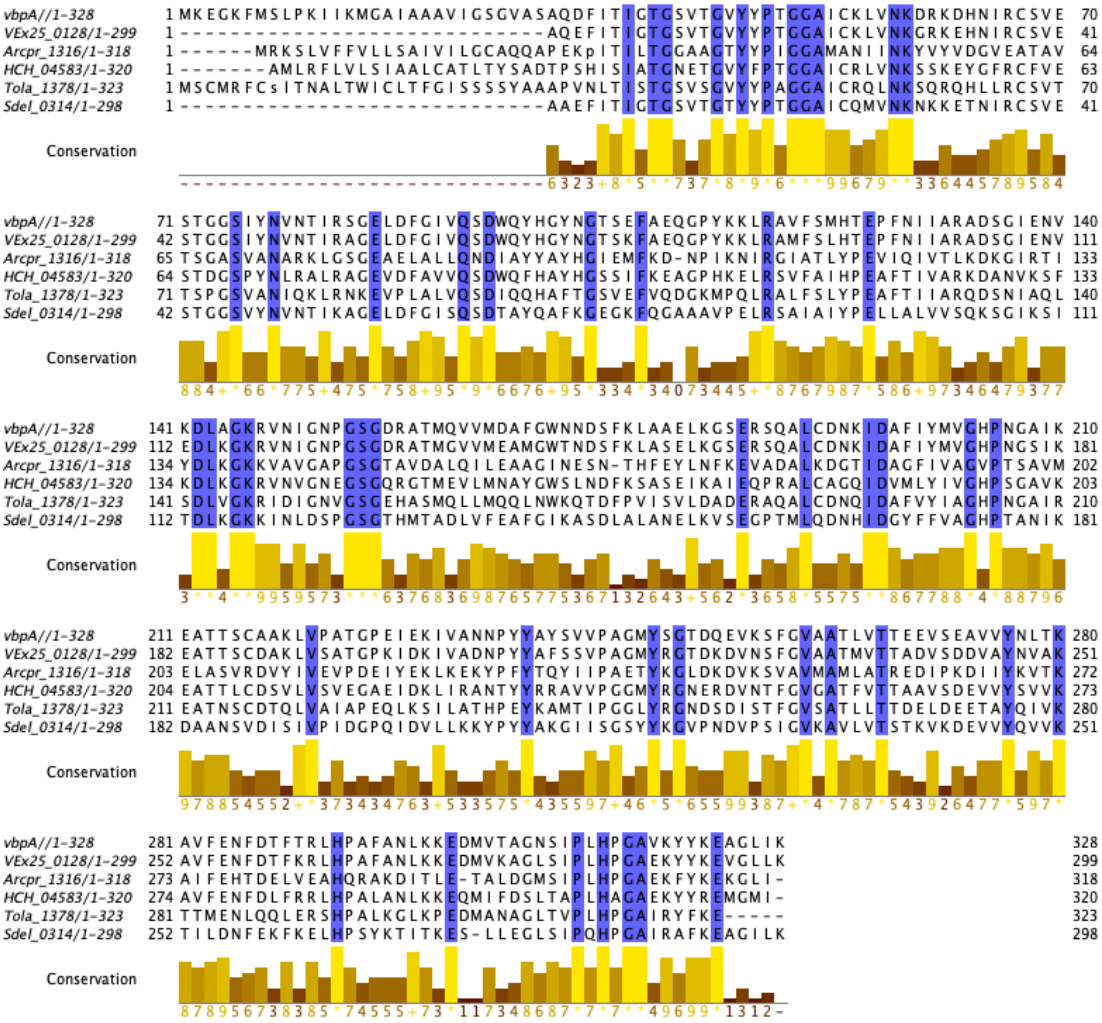
vbpA//1-328
VEx25_0128/1-299
Arcpr_1316/1-318
HCH_04583/1-320
Tola_1378/1-323
Sdel_0314/1-298
Conservation

Tripartite ATP-independent periplasmic (TRAP) transporters are a group of secondary transporters in bacteria that are composed of three protein components: a solute binding protein (SBP), also known as extracytoplasmic solute receptor (ESR) and two distinct integral membrane proteins, one large and one small (70). SBPs were historically thought to strictly be associated with the primary transporter group, ATP-binding cassette (ABC); TRAP transporters are more recently discovered and relatively unstudied (70, 71). TRAP transporters are common in bacteria and archaea that can be found in marine environments. TRAP associated SBPs that have very low K_d values for their ligands, making them suitable for environments with low concentrations of substrates (70, 71). The SBPs have also been shown to impose unidirectionality on transport, in comparison to most other secondary transporters, where the directionality of transport can reverse depending on the concentration of the substrate inside and outside of the cell (72). The substrates that TRAP transporters have been shown to bind to and transport are diverse and include sialic acid, C4-dicarboxylates, ectoine/hydroxyectoine, Gluconate/malonate and 2,3-diketo-L-gulonate (2,3-DKG), a-Keto acids/lactate, Taurine (2-aminoethanesulphonic acid), aromatic acids, and specific amino acids (73). Trap-associated extracytoplasmic immunogenic (TAXI) proteins, which VbpA is predicted to be, are a discrete family of SBPs that are usually components of TRAP transporters (70). The distinguishing features of TAXI proteins are that they are distinct in sequence from TRAP SBPs, and the TRAP transporters that function with a TAXI protein have a fusion of the two integral membrane protein subunits (70). The gene next to *vbpA,* VC0429 which we

have termed *vbpB,* is homologous to *dctQ* and *dctM* in *Rhodobacter capsulatum,* making up the small and large integral membrane proteins of ESR (70). This suggests that VbpA and VbpB form a TAXI-TRAP transporter group in *V. cholerae.* Interestingly, all archaeal TRAP transporters are in the TAXI family, suggesting that this may be a more ancient form of the TRAP transporter (70).

A review by Kelly and Thomas (2001) reported one other TAXI protein in *V. cholerae*: VCA0144, which we have termed VbpI (70). Interestingly, VbpI was also identified in the *V. cholerae* biofilm matrix proteome study, though at a much lower quantity compared to VbpA (Fig 1.1). VbpI is predicted to interact with the integral membrane protein VCA0146, which we have termed VbpJ. To better evaluate the role of these proteins in *V. cholerae* biofilm formation, we generated strains lacking *vbpA, vbpB, vbpI,* and *vbpJ* in the rugose genetic background. Analysis of colony and spot biofilm morphology showed that there is no significant change in biofilm morphology in Δ*vbpB* and Δ*vbpJ* (Fig 1.5)*,* and there is a drastic change in Δ*vbpA* and a slight change in Δ*vbpI*. We surmised that the two putative SBPs, VbpA and VbpI, and the two integral membrane proteins VbpB and VbpJ may have redundant functions or that they are produced under different environmental conditions. To begin to test this hypothesis, we made double deletion strains RΔ*vbpA*Δ*vbpI* and RΔ*vbpB*Δ*vbpJ* and examined the resulting colony and spot biofilm morphologies (Fig 1.5).

Figure 1.5. Colony and spot biofilm morphology of strains lacking predicted TRAP-TAXI systems in *V. cholerae*. Strains (Rugose, RΔ*vbpA,* RΔ*vbpI,* RΔ*vbpA*Δ*vbpI,* RΔ*vbpB,* RΔ*vbpJ,* RΔ*vbpB*Δ*vbpJ*) were grown overnight in 30˚C shaking overnight (200 rpm). Overnight cultures were diluted up to 10^{-8} and 100 µl spread onto LB agar plates and incubated at 30˚C for 120 hours (A), or overnight cultures were diluted 1:200 in LB medium and 3 µl spotted onto LB agar plates and incubated at 30˚C for 72 hours (B).

A.

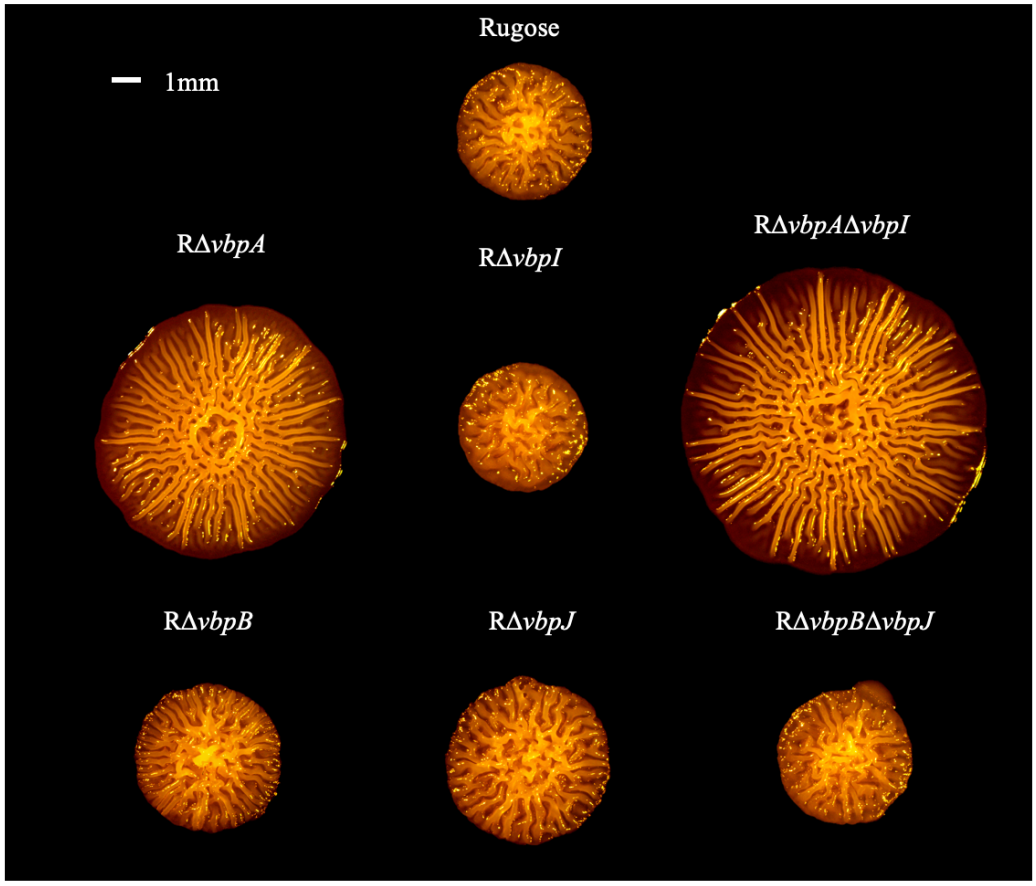
Rugose
1mm
RΔvbpA
RΔvbpI
RΔvbpAΔvbpI
RΔvbpB
RΔvbpJ
RΔvbpBΔvbpJ

B.

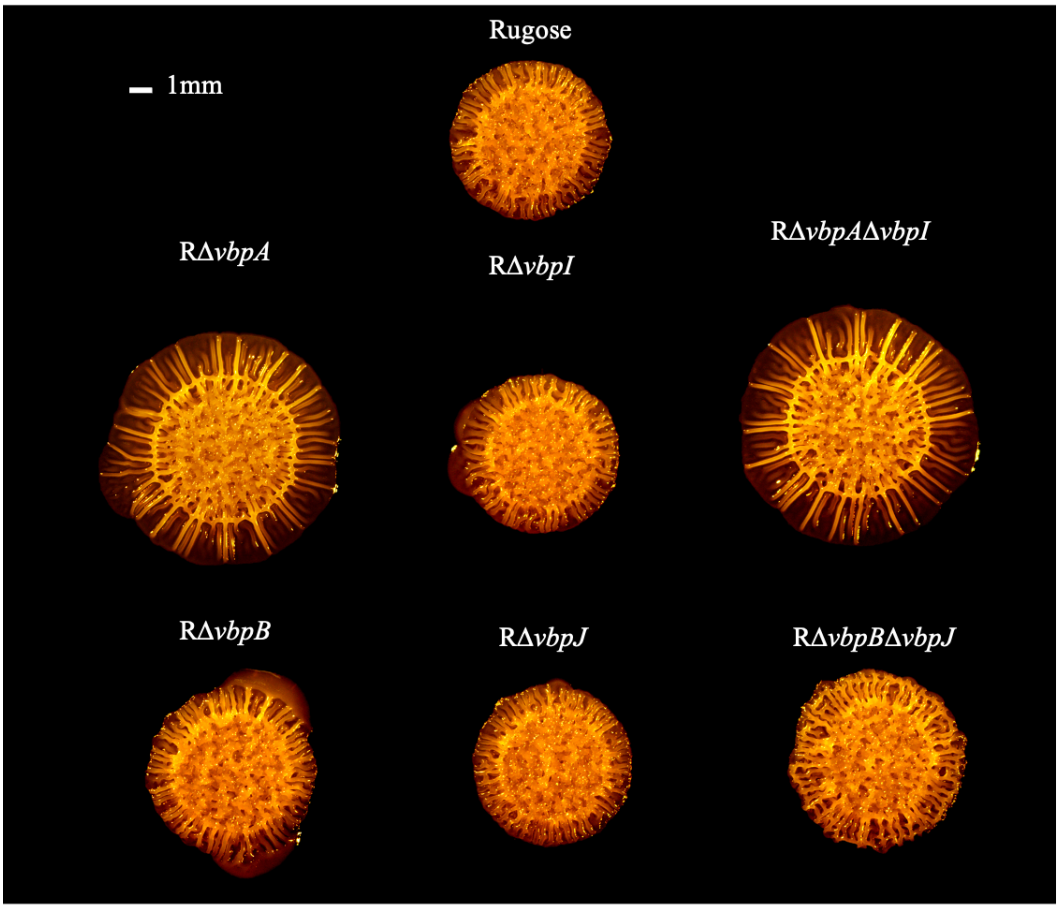
Rugose
1mm
RΔvbpA
RΔvbpI
RΔvbpAΔvbpI
RΔvbpB
RΔvbpJ
RΔvbpBΔvbpJ

To evaluate possible redundant functions in the two putative TAXI-TRAP transporter SBPs VbpA and VbpA, we also generated cross-complementation strains. In such strains, *vbpA* and *vbpI* expression was under an IPTG-inducible promoter in the pMMB plasmid (Fig 1.6). We noticed that introduction of the wild type copy of *vbpA* into the RΔ*vbpA* strain using a multi-copy plasmid from an inducible promoter (RΔ*vbpA*-pMMB/*vbpA*) partially complemented the defect in biofilm formation where the corrugation pattern became similar to the rugose strain. The colony biofilm size became an intermediate of Rugose-pMMB (vector only control) and RΔ*vbpA*-pMMB (vector only control): the spot biofilm diameters of the strains are Rugose-pMMB at roughly 6.5 mm, RΔ*vbpA*-pMMB at 9.5 mm, and RΔ*vbpA*-pMMB/*vbpA* at 8 mm. When *vbpI* was introduced to the *vbpA* mutant, the resulting phenotype was similar to *vbpA* complementation but had a different corrugation on the colony edges that is more circular compared to RΔ*vbpA*-pMMB/*vbpA*. This led us to hypothesize that VbpI and VbpA are functionally redundant. However, Δ*vbpA* causes a much more drastic change in biofilm corrugation patterns than Δ*vbpI* (Fig 1.5). Our observations thus far led us to predict that VbpA and VbpI play a role in the biofilm formation. VbpA and VbpI are predicted to be TAXI-TRAP transporter SBP; it is yet to be determined if VbpA and VbpI's role in biofilm formation is apart from their role as a TAXI-TRAP transporter SBP. Expression levels and conditions for VbpA and VbpI also remain to be determined.

Figure 1.6. Spot biofilm morphologies of *vbpA* and *vbpI* complementation. Overnight cultures for each strain were diluted 1:200 and 3 µl were spotted onto standard LB agar plates containing 0.1 mM IPTG + ampicillin 100 µg/µl. These were incubated at 30˚C for 72 hours before imaging. All images are at the same magnification. The experiment was repeated in two biological replicates with three technical replicates each. Images presented are representative of isolated trials.

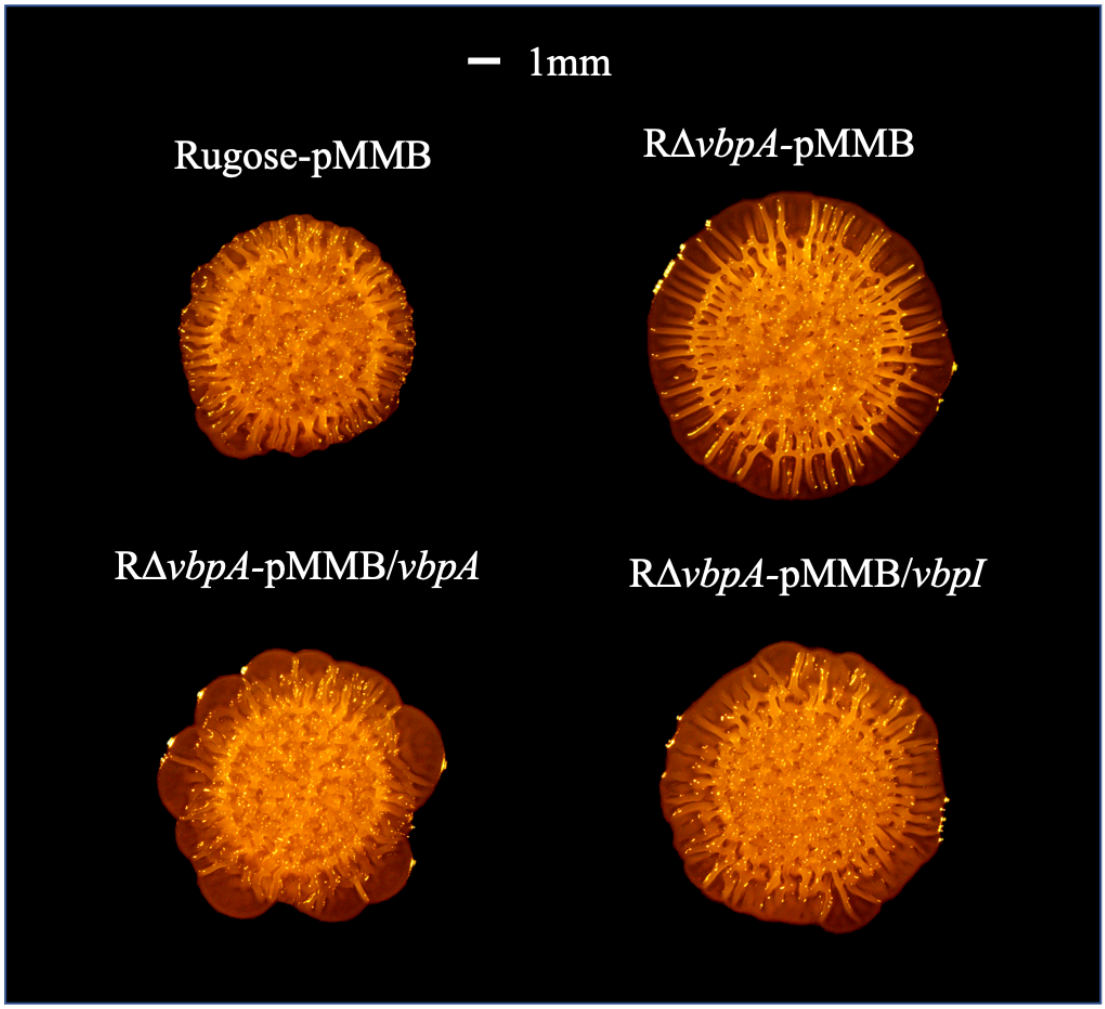
1mm
Rugose-pMMB
RΔ*vbpA*-pMMB
RΔ*vbpA*-pMMB/*vbpA*
RΔ*vbpA*-pMMB/*vbpI*

Section 2. Localization of VbpA

To understand the function of VbpA,we first determined its localization. VbpA was identified in the *V. cholerae* matrix proteome by Absalon et al (2011), but its localization could not be determined with certainty and was grouped in the "unknown" category (40). We looked to bioinformatics for clues to VbpA's localization. SignalP predicted the presence of a signal peptide with a probability of 1.0. Protter, a predictive protein visualization tool, also predicted that VbpA exists outside of the inner membrane, getting secreted out of the inner membrane through the Sec pathway (74). The top three structural homologs identified by Phyre2 analysis included two periplasmic binding proteins with 38% and 15% identities (Fig 1.3). Taken together, these data predict VbpA to be a periplasmic or secreted protein.

To uncover the localization of VbpA, we first performed subcellular fractionation of the rugose strain and determined VbpA localization using an antibody specific to VbpA. For these experiments, cell suspensions of rugose and negative control RΔ*vbpA* strains were separated into whole cell, spheroplast (containing cytoplasm and membranes), periplasm, and supernatant (secreted) fractions. These samples were analyzed using western blots and probed using an antibody specific to VbpA (Fig 2.1). We found that VbpA is present in the whole cell, periplasm, and supernatant fractions. This affirmed the predictions from bioinformatic analyses that VbpA was a periplasmic protein, and our proteomic result showed its presence in the matrix.

Figure 2.1. Analysis of cellular localization of VbpA. Rugose and RΔ*vbpA* cultures were grown overnight, shaking at 30˚C (200 rpm) and diluted 1:200 in 100 ml LB medium, then grown at 30˚C (200 rpm) until OD_{600} 1.1. Whole cell sample was collected. The rest of the culture was separated from the extracellular supernatant by centrifugation at 12,250xg for 15 mins at 4℃. The supernatant was precipitated using TCA and BSA was added for loading control. The pellet was separated to the periplasm and the spheroplast, which contains cytoplasmic and membrane fractions. The pellet was incubated in 20% sucrose in 20 mM Tris pH 8 (4 ml/g cells), 0.1 EDTA (0.2 ml/g cells) and 0.5 mM PMSF on ice for 1 hr. 0.5 MgCl2 (600 µl/g cells) was added, and then centrifuged at 9500 xg for 20 mins at 4℃. The supernatant contains the periplasmic fraction. The pellet, containing the spheroplast, was resuspended in 10 mM Tris pH 8. Samples were run on SDS-PAGE and VbpA analyzed via western analysis. Antibodies specific to RNA polymerase (RnaP) were used as a loading control for whole cell and spheroplast, BSA, which is spiked into the samples for protein precipitation control. RbmA was used as positive control for secreted protein fraction. This experiment was repeated in three biological replicates and one representative image is shown.

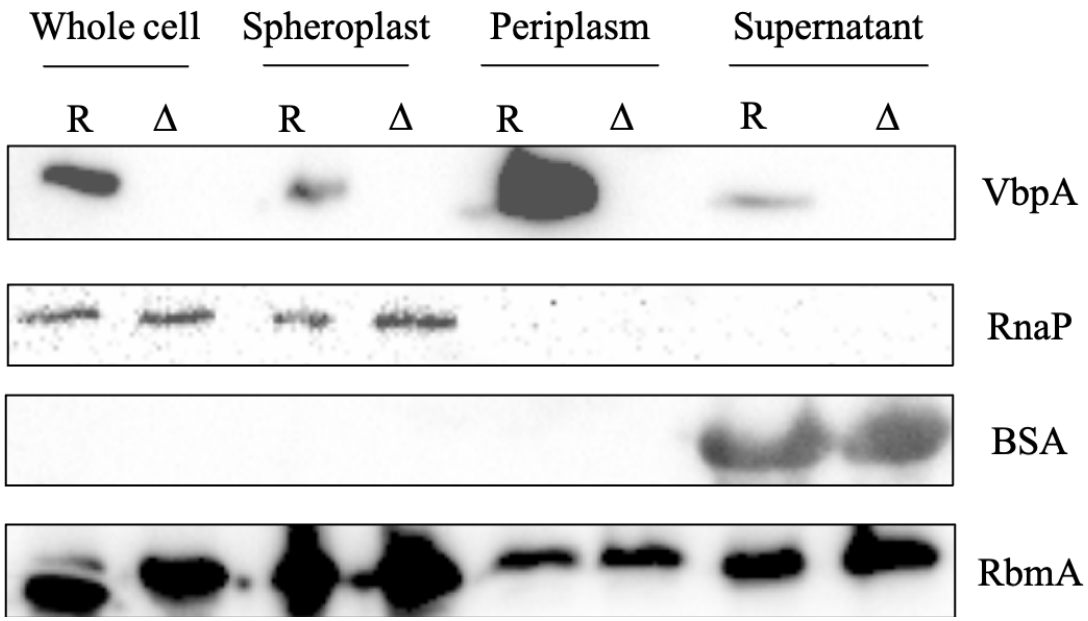
Whole cell
Spheroplast
Periplasm
Supernatant
R
Δ
R
Δ
R
Δ
R
Δ
VbpA
RnaP
BSA
RbmA

To further confirm periplasmic localization, we first constructed a strain where *vbpA* was fused to the *E. coli* alkaline phosphatase gene, *phoA,* where gene expression was controlled by an IPTG-inducible promoter. We next conducted an alkaline phosphatase enzymatic assay; this assay utilizes the property of PhoA in which it is only active when localized to the periplasm—thus by measuring PhoA activity, it is possible to see if the fused protein is localized to the periplasm (75). The negative control strains showed little to no enzymatic activity while the *vbpA-phoA* fusion strain showed a PhoA enzymatic activity (Fig 2.2) suggesting that VbpA is found in the periplasm.

Figure 2.2. Analysis of VbpA periplasmic localization using alkaline phosphatase fusion. Overnight cultures were diluted 1:200 and grown at 30˚C shaking (200 rpm) until OD 0.1 and induced with 100 µg IPTG and grown for 2 hours. Pellets were collected and lysed with a buffer containing Triton X-100. The lysate was collected and loaded to 96 well plates with para-Nitrophenylphosphate (*p*NPP), a chromogenic substrate when cleaved by alkaline phosphatase forms a product that absorbs light at 405 nm. Absorbance was read at 405 nm every 15 min for 1 hour. Above is absorbance normalized to protein concentration at 45 min. The experiment was repeated in 3 biological replicates and 3 technical replicates, this is an average of these replicates

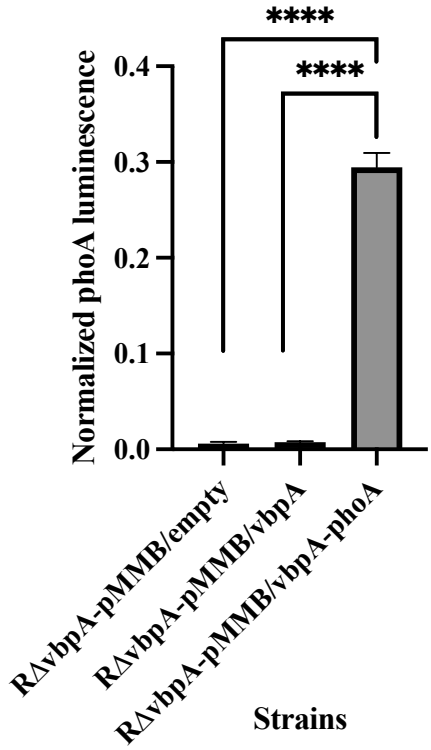
****
****
Normalized phoA luminescence
0.4
0.3
0.2
0.1
0.0
RΔvbpA-pMMB/empty
RΔvbpA-pMMB/vbpA
RΔvbpA-pMMB/vbpA-phoA
Strains

As a complementary study to confirm VbpA presence in the extracellular biofilm matrix, we also analyzed isolated matrix proteins from biofilm-grown cells. We collected plate-grown biofilms of rugose and RΔ*vbpA* strains and separated the biofilm matrix from the cells through centrifugation and concentrated using trichloroacetic acid (TCA) precipitation. Both biofilm proteome and whole-cell fractions from both strains were run on SDS-PAGE and the western blots were probed with the VbpA antibody and loading controls (Fig 2.3). This analysis showed VbpA is present in both the cell and matrix fractions, further confirming the presence of VbpA in the biofilm matrix.

Figure 2.3. Presence of VbpA in both cell and biofilm matrix in *V. cholerae*. The matrix was isolated and concentrated by TCA precipitation as described in the Materials and Methods section. VbpA and RbmA were analyzed via western analysis. RbmA was used as a positive control. The experiment was repeated in two biological replicates, one representative image is shown.

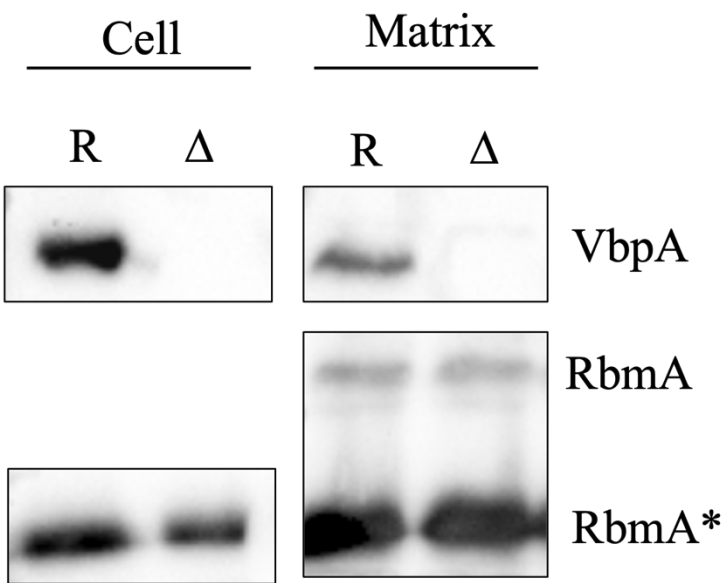
Cell
Matrix
R
Δ
R
Δ
VbpA
RbmA
RbmA*

The findings discussed above showed that VbpA exists in the cell in the periplasmic space as well as in the secreted space. We wanted to further understand how the localization of VbpA affects its protein function. In other words, we wanted to control where VbpA goes and see the effect of different locations on the biofilm phenotype. To do this, we generated strains where *vbpA* was expressed from a pTac IPTG-inducible promoter using a multi-copy plasmid on a Δ*vbpA* background and controlled its cellular localization by changing its signal peptide. In one strain, the signal peptide was deleted to localize VbpA to the cytoplasm, and the other strain the signal peptide of *vbpA* was switched to the signal peptide of *rbmA* as RbmA is a protein that is known to localize to the extracellular biofilm matrix. To experimentally test where VbpA would be localized in these strains, the strains were grown in LB medium supplemented with 100 µg IPTG. We then separated the cell from the supernatant by centrifugation and TCA precipitated the proteins in the supernatant. We ran these samples on SDS-PAGE and probed for VbpA using the VbpA antibody (Fig 2.4). We also ran samples of Δ*rbmA* with empty vector as well as complementation strain of *rbmA and* probed for RbmA presence using RbmA antibody. We found that when the signal peptide is deleted, VbpA is not produced, as we could not detect VbpA. This may suggest that secretion to the periplasm is critical for VbpA stability. In the strain with the *rbmA* signal peptide, VbpA was present both in the whole cell and in the secreted space, similar to what we observe in our RbmA positive control.

Figure 2.4. Switching signal peptides to control VbpA localization. Overnight cultures were diluted 1:200 in LB-Amp medium, induced with 100 μM IPTG at OD_{600} 0.1, and harvested two hours later. The cells were separated from supernatant through centrifugation. Cells were resuspended in PBS, boiled after addition of SDS to a final concentration of 2% SDS. Supernatant was precipitated with 12.5% TCA. VbpA and RbmA were analyzed via western analysis. BSA and RnaP are used as sample loading controls. WC refers to the whole cell, and SN refers to supernatant.

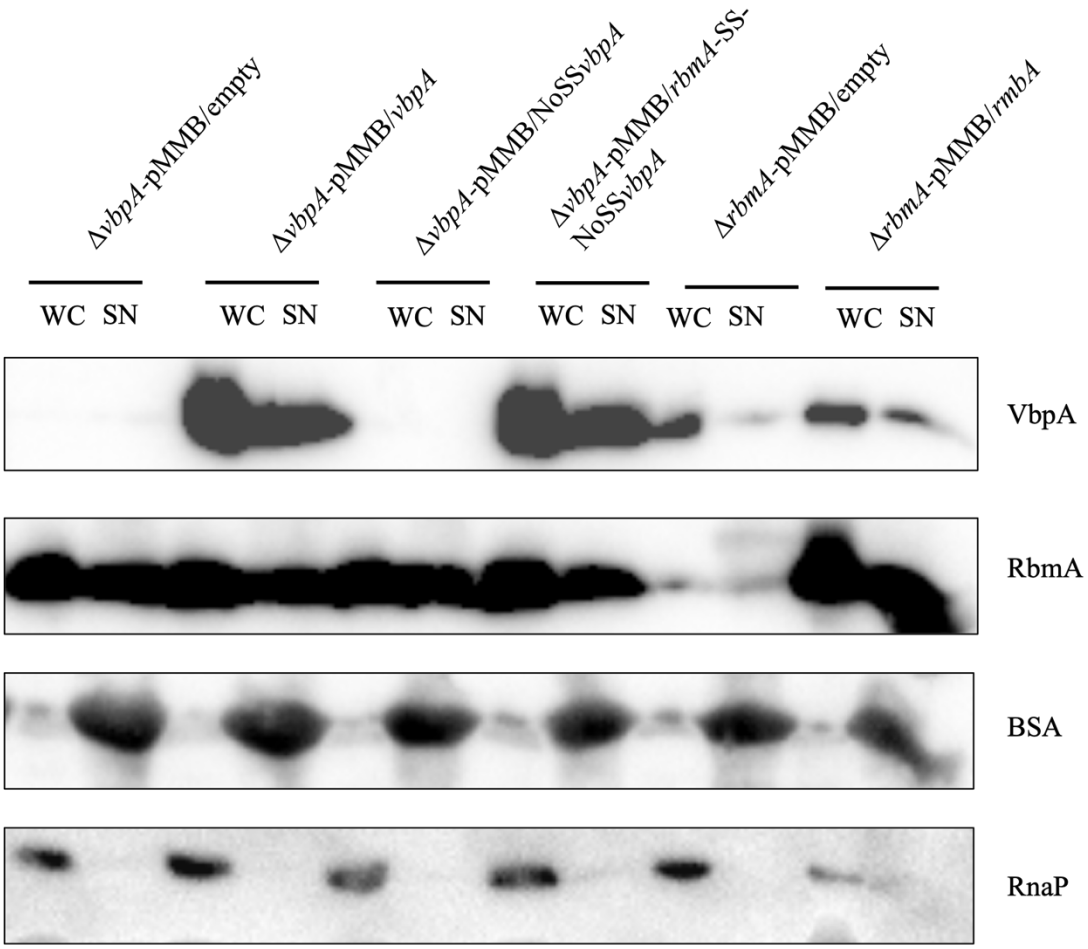
ΔvbpA-pMMB/empty
ΔvbpA-pMMB/vbpA
ΔvbpA-pMMB/NoSSvbpA
ΔvbpA-pMMB/rbmA-SS-NoSSvbpA
ΔrbmA-pMMB/empty
ΔrbmA-pMMB/rmbA
WC SN
WC SN
WC SN
WC SN
WC SN
WC SN
VbpA
RbmA
BSA
RnaP

We then analyzed spot and colony biofilm morphology of these strains on LB-Amp containing 100 μM IPTG (Fig 2.5). We observed that the deletion and switching of signal peptides in *vbpA* caused changes in morphologies in both colony and spot biofilms, but the changes were more evident on spot biofilms. The spot morphology of RΔ*vbpA*-pMMB is similar to RΔ*vbpA*-pMMB/noSS*vbpA*; this phenotype is expected as RΔ*vbpA*-pMMB/noSS*vbpA* does not produce VbpA (Fig 2.4). The spot biofilm morphology of RΔ*vbpA*-pMMB/*vbpA* mirrored that of RΔ*vbpA*-pMMB/*rbmA*-ss-noSS*vbpA* with the characteristic webbed, curved edges of the biofilm. This suggests that the strain with *rbmA* signal peptide functions similarly to when VbpA is in its native location, implying that VbpA functions in the secreted space to affect biofilm assembly.

Figure 2.5. Biofilm morphologies of *vbpA* strains with altered signal peptides. Overnight cultures of each strain were diluted 1:200 in LB-Amp medium and 3 µl spots plated onto 20 ml LB agar medium containing 100 µM IPTG and 100 µg/µl ampicillin. Spots were grown at 30˚C and imaged after 72 hours (A). 100 µl of serially diluted overnight cultures (final dilution of 10^{-8}) were plated on LB-Amp + 100 µM IPTG agar medium. Colonies were grown at 30˚C and imaged after 120 hours (B). The experiments were repeated in biological replicates; images presented are representative of isolated trials.

A.

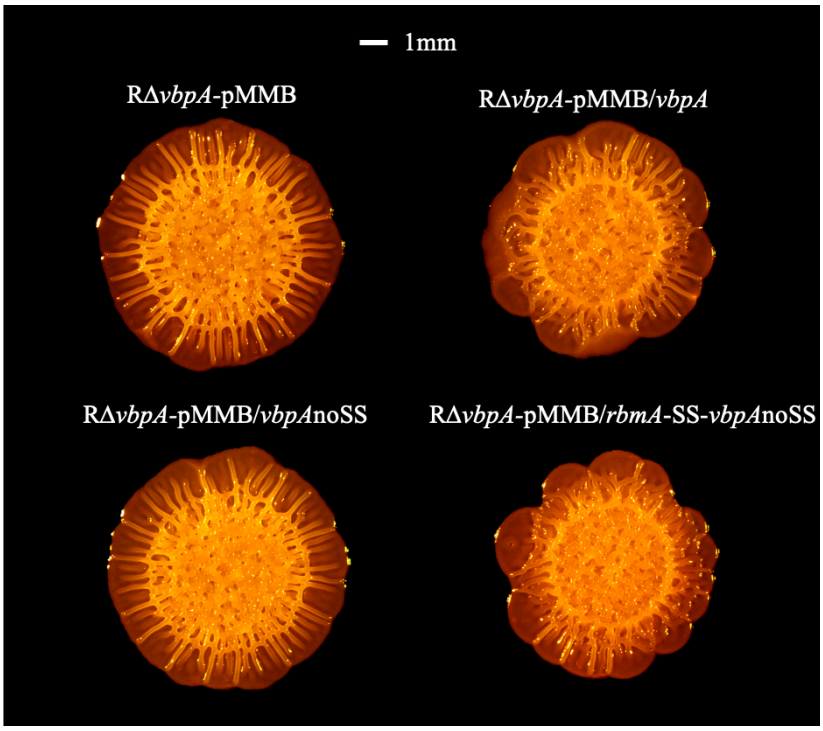
1mm
RΔvbpA-pMMB
RΔvbpA-pMMB/vbpA
RΔvbpA-pMMB/vbpAnoSS
RΔvbpA-pMMB/rbmA-SS-vbpAnoSS

B.

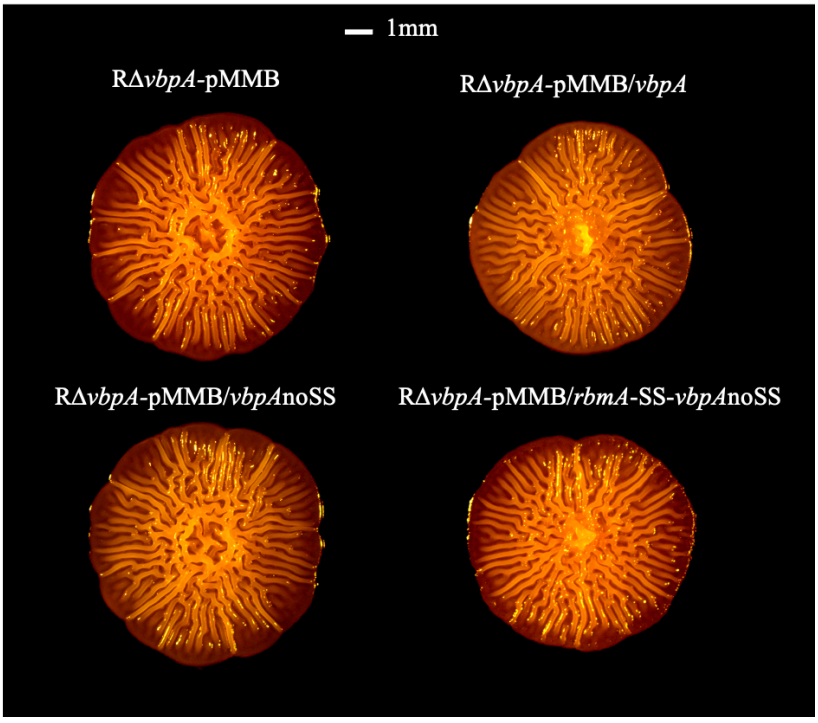
1mm
RΔvbpA-pMMB
RΔvbpA-pMMB/vbpA
RΔvbpA-pMMB/vbpAnoSS
RΔvbpA-pMMB/rbmA-SS-vbpAnoSS

To further confirm the action of VbpA in the extracellular space, we purified VbpA and added purified VbpA exogenously to spot biofilms of RΔ*vbpA* to observe changes in spot biofilm corrugation pattern (Fig 2.6). We hypothesized that the addition of VbpA exogenously in the extracellular space may restore the phenotype to the rugose parent strain. We tested the addition of purified VbpA with the GST tag and purified VbpA without the GST tag. As controls, we included BSA suspended in the buffer as well as the buffer alone. We supplemented 10 µl of RΔ*vbpA* cell suspensions, diluted 1:200 in LB medium from overnight grown cultures, with 1, 10, 50, and 100 µg of VbpA or BSA and spotted onto LB agar plates. The addition of the buffer alone and 1, 10, 50, and 100 µg of BSA did not affect the spot morphology. The addition of purified VbpA containing the GST tag altered the morphology drastically, causing the center of the spot biofilm to become markedly corrugated. The addition of VbpA without the GST tag also caused the center to become tightly corrugated, but to a lesser extent. Although the addition of purified VbpA did not cause the RΔ*vbpA* spot morphology to be restored to the rugose parent strain, this drastic change in morphology shows that extracellular presence of VbpA causes a change in *V. cholerae* biofilm architecture/assembly.

Figure 2.6. Exogenous addition of purified VbpA to spot biofilms of RΔ*vbpA*. Purified VbpA, with and without the GST tag were exchanged to a buffer containing 20 mM Tris (pH 8) and 300 mM NaCl. Protein content was quantified using BCA. 1, 10, 50, and 100 µg of protein was added to 10 µl of 1:200 diluted overnight cultures. 10 µl of the buffer alone and the buffer with 1, 10, 50, and 100 µg of BSA were added as control. Each of these were mixed and 3 µl spotted on 20 ml LB agar plates and incubated at 30˚C for 72 hours. The experiment was repeated in two biological replicates, images presented are representative of isolated trials.

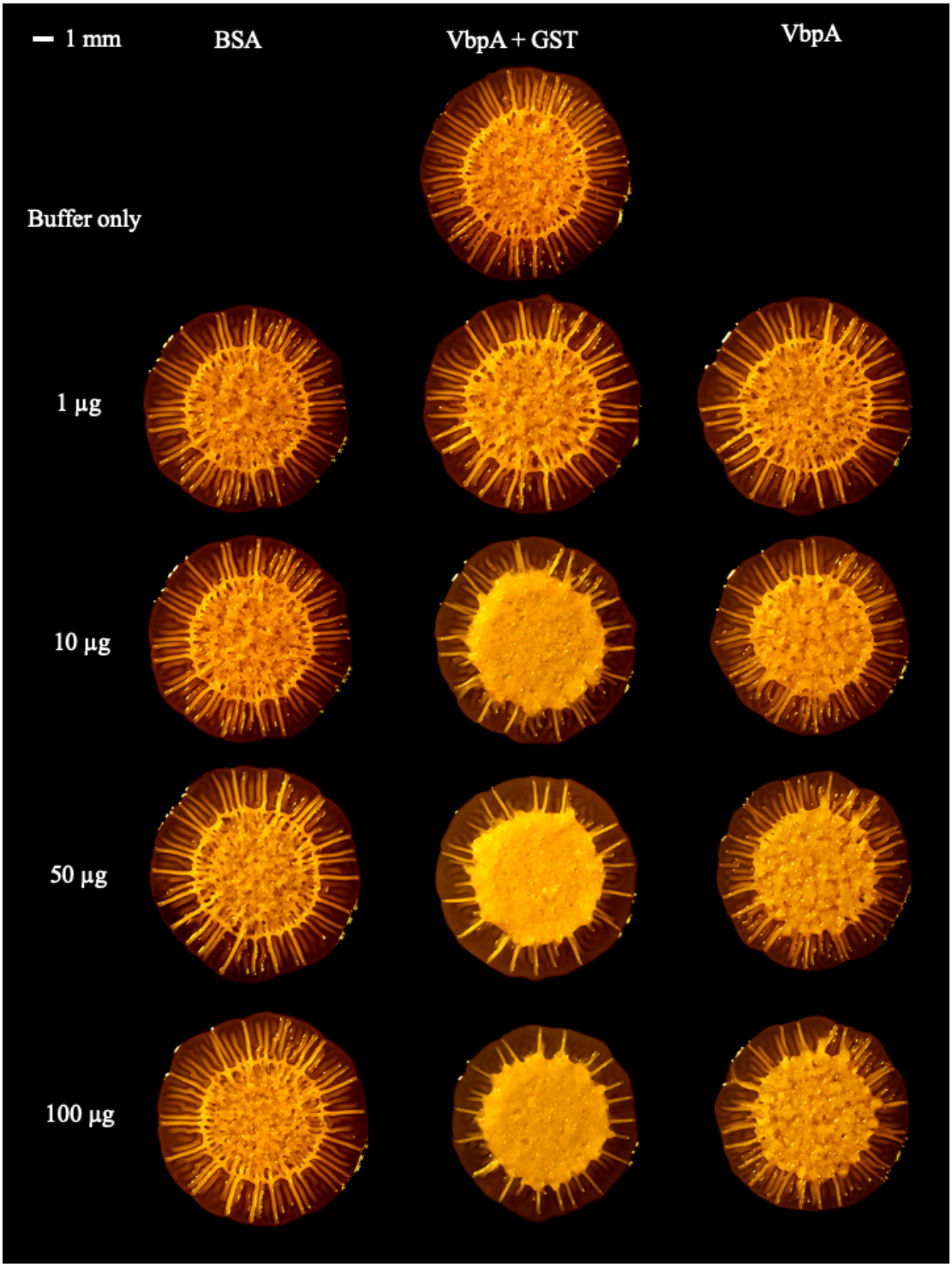
1 mm
BSA
VbpA + GST
VbpA
Buffer only
1 µg
10 µg
50 µg
100 µg

The exogenous addition of VbpA to spot biofilms of RΔ*vbpA* showed us that VbpA affects *V. cholerae* biofilms from the extracellular space (Fig 2.6). We also know from matrix isolation experiments that VbpA naturally localizes to the extracellular space as well as to within the cell (Fig 2.3). As the next step, we wanted to visualize VbpA within the biofilm matrix to visually confirm its extracellular location and to see its localization within the matrix. We constructed the strain R-*vbpA*-HA-Tn7::GFP where *vbpA* is chromosomally tagged at the N-terminus and the strain is also tagged with the GFP tag at the neutral Tn7 locus. We then grew biofilms of the strain under static conditions in LB medium and imaged the biofilm using confocal laser scanning microscopy (CLSM), visualizing VbpA using an HA antibody fluorescently conjugated to Alexa Fluor 647 (Fig 2.7). We were able to visualize VbpA in the biofilm matrix. This is the first demonstration of VbpA in the biofilm matrix. We found that VbpA was clustered around microcolonies and spread throughout within the biofilm matrix.

Figure 2.7. VbpA visualization in the *V. cholerae* biofilm matrix using CLSM and fluorescently labeled antibody. Rugose-HA-*vbpA*-Tn7::GFP was grown statically for 6 hours before washing with 1xPBS containing 1 mg/ml BSA. The biofilm was blocked in 1xPBS containing 5 mg/ml BSA for 5 min and then incubated in HA Tag Monoclonal Antibody, Alexa Fluor 647 (Thermo Fisher 26183-A647) at 1 µg/µl in 1xPBS containing 2 mg/ml BSA for 45 min. The biofilm was washed again in 1xPBS containing 1 mg/ml BSA and imaged using CLSM. Image was created using Imaris 9.7.2. Cells are shown in cyan, VbpA is shown in pink.

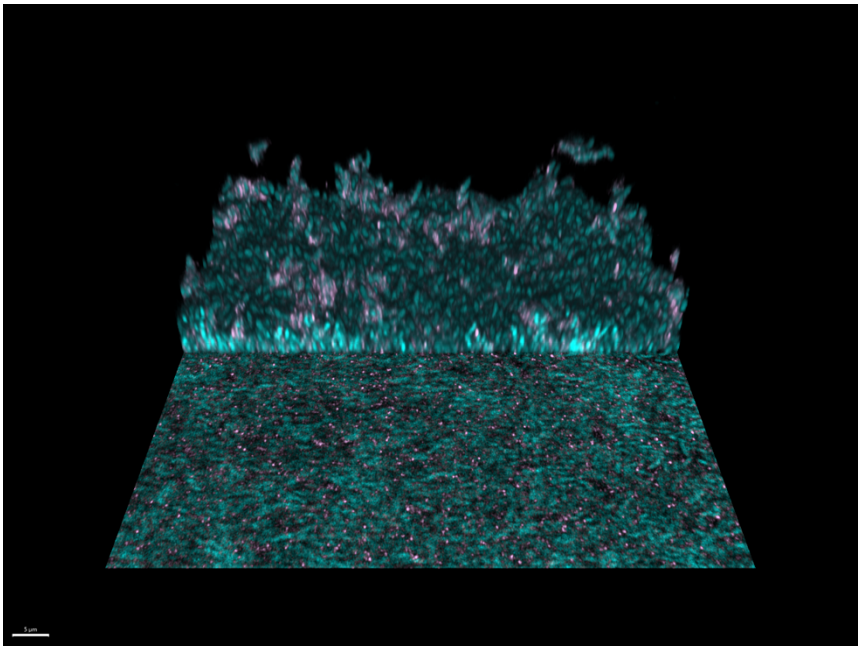

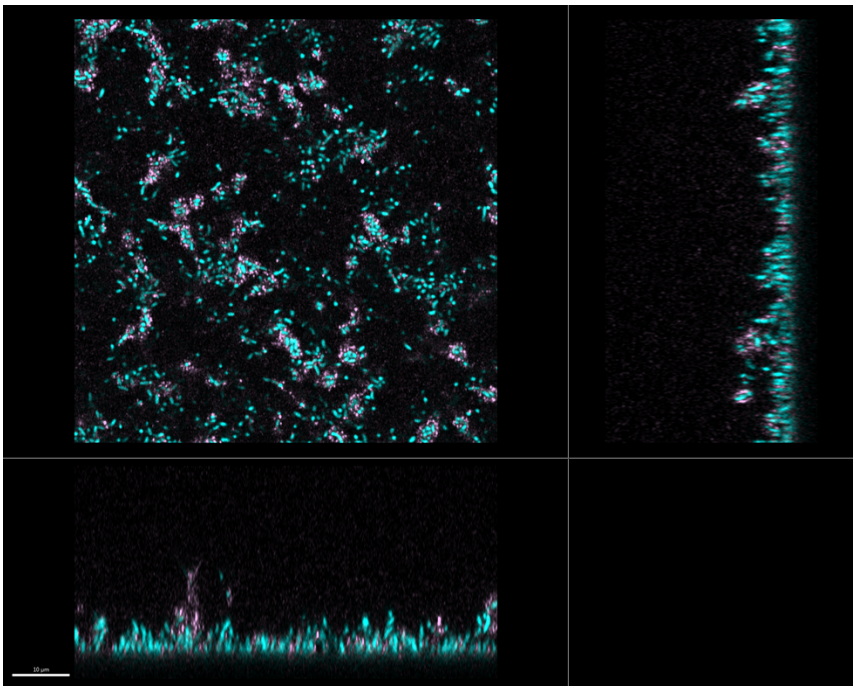

Section 3. Impact of VbpA on biofilm structure

Our studies described above showed that there are marked differences in biofilm forming abilities of the rugose strain and RΔ*vbpA* when biofilms were grown in an air-solid interface, i.e., colony and spot biofilms. In order to view potential changes at the single cell level, we grew colonies of Rugose-Tn7::GFP and RΔ*vbpA*-Tn7::GFP and visualized the edge and center of colony biofilms using CLSM (Fig 3.1). In general, both colonies showed the orderly, vertical packing of cells that was also observed in a similar study visualizing colonies of *V. parahaemolyticus* (75). The wrinkles in rugose colonies were apparent in the CLSM images (Fig 3.1A). Both the center of the colony and the edge had wrinkles, but there was a difference in the cell packing visible at the *xz* plane (Fig 3.1A-iii). The cells were more spaced out in the wrinkles at the edge of colonies compared to the center. The cells are also less ordered in their packing compared to the packed, orderly vertical alignments of the cells at the center, and this is also visible from the *xy* cross-section where more cells appear sideways than circular (Fig 3.1A-ii). In RΔ*vbpA* colonies, the edges appear as long, radially spreading prongs with thin biomass at the bottom. When imaged with CLSM, we saw that all of the cells at the edges are centered in these prongs and there are no cells in the thin biomass connecting these prongs. We do not know what is in this thin, connective biomass—it could be VPS or dead cells unable to be stained by GFP. This would be an intriguing area to pursue further. When we took an image at the *xy* plane in these prongs, we saw that there were chambers in which there were very few cells (Fig 3.1B-ii). This is a new finding that we had not been able to

observe previously with dissecting microscope images of colonies. In a portion of the edge prong that does not contain the empty chamber, the cell packing was tight and ordered (Fig 3.B-iii). In comparison, in the center of the RΔ*vbpA* colony, cells were not packed as tightly, and the cell orientation was more randomized (Fig 3.B-ii/iii). We are in the process of quantifying cell to cell spacing and cell orientation within biofilms. Even without quantification, though, through confocal imaging of colonies we were able to visualize differences at the cell level that had been previously undiscovered.

Figure 3.1. CLSM analysis of rugose and RΔ*vbpA* colony biofilms. Rugose-Tn7::GFP and RΔ*vbpA*-Tn7::GFP were grown overnight in 5 ml LB medium at 30˚C shaking (200 rpm), then serially diluted up to 10^{-8} and 100 µl spread onto 20 ml LB agar plates. Colonies were excised and placed on glass coverslips before examination with CLSM of Rugose-Tn7::GFP (A) and RΔ*vbpA*-Tn7::GFP (B). Imaris 9.7.2 was used to process images and visualize the three-dimensional rendering (i), *xy* plane cross section (ii), and *xz* plane cross section (iii) from both the edge and the center of colonies. 2 biological replicates and at least 2 technical replicate images were taken, shown are representative images.

A.

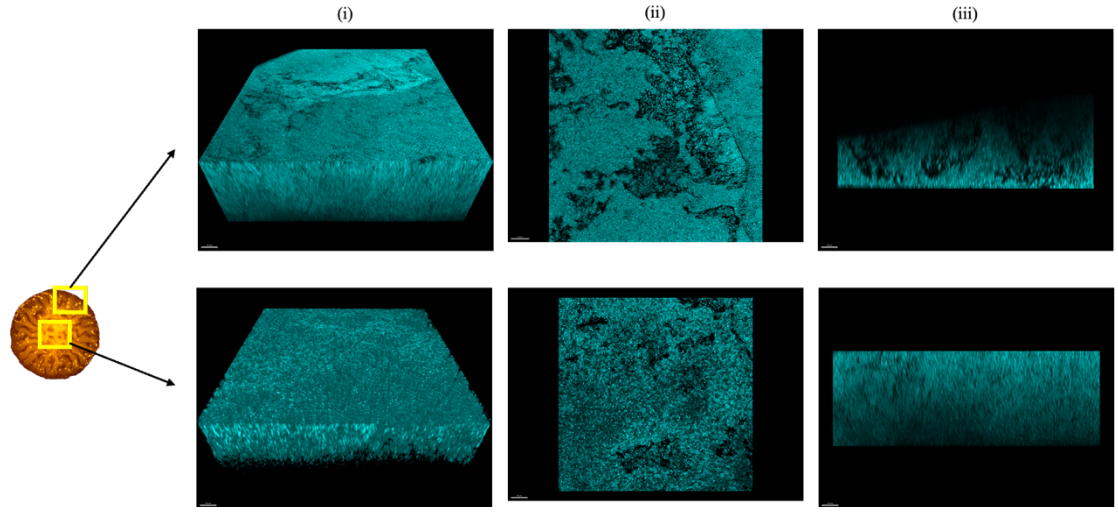

B.

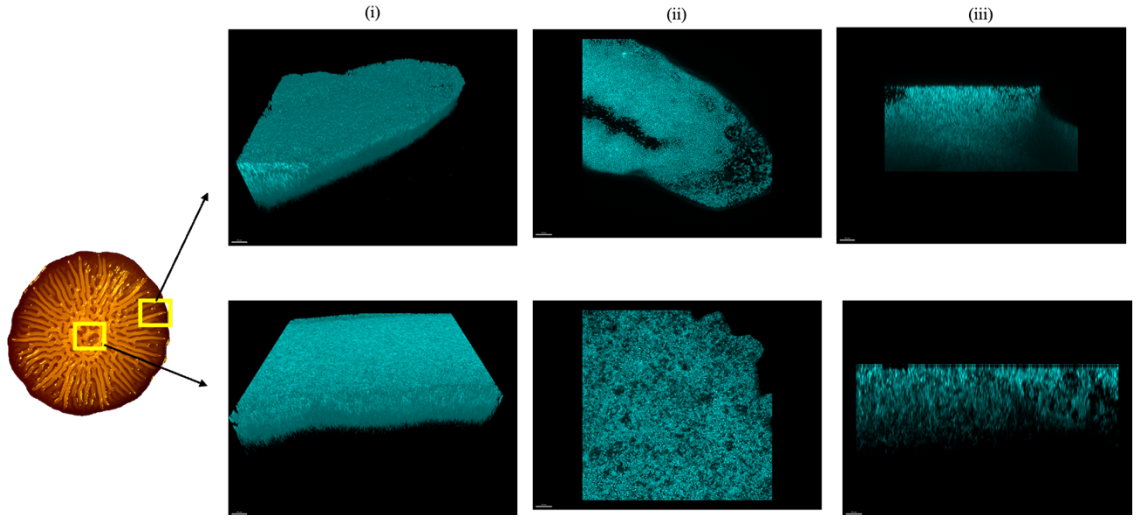

We wanted to visualize and quantify any changes that RΔ*vbpA* has on biofilms at a solid-liquid interface, which could be more indicative of biofilms grown in *V. cholerae*'s native habitats in aquatic environments and in the host. We grew Rugose-Tn7::GFP and RΔ*vbpA*-Tn7::GFP, which are tagged with GFP in a neutral Tn7 locus, statically for 6 hours and visualized the biofilms using CLSM. We used the quantitative analysis program BiofilmQ (76) to calculate biofilm volume, thickness, and roughness at 6 hours. We saw that there was no significant difference in biofilm parameters at the solid-liquid interface (Fig 3.2). This tells us that the phenotypic differences that RΔ*vbpA* causes is condition specific. For example, the phenotypic change may be specific to the solid-air interface, or specific to softer surfaces like those on agar plates. Understanding the conditions specific to VbpA's effect on biofilm structure can give us more insight into its functions.

Figure 3.2. BiofilmQ analysis of biofilms of Rugose-Tn7::GFP and RΔ*vbpA*-Tn7::GFP. 6 hours static biofilms were imaged using confocal microscopy and the biofilm volume (A), thickness (B), and roughness (C) calculated using BiofilmQ. The bar graphs show means from biofilm data from 2 biological replicates and 2 technical replicate z-series image stacks. Error bars show standard deviation. Significance was determined by unpaired t-test.

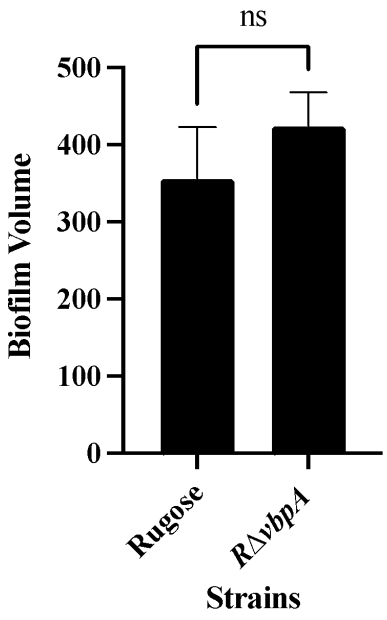
ns
500
400
300
200
100
0
Biofilm Volume
Rugose
RΔvbpA
Strains

A.

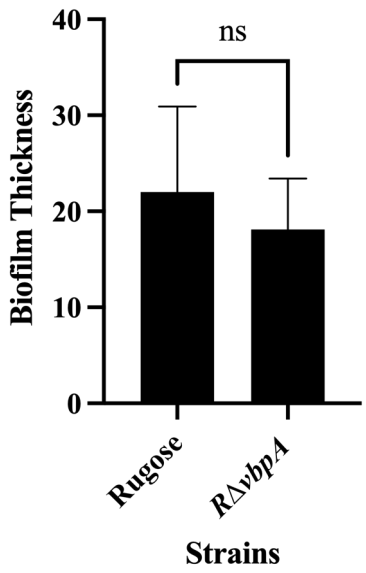
ns
40
30
20
10
0
Biofilm Thickness
Rugose
RΔvbpA
Strains

B.

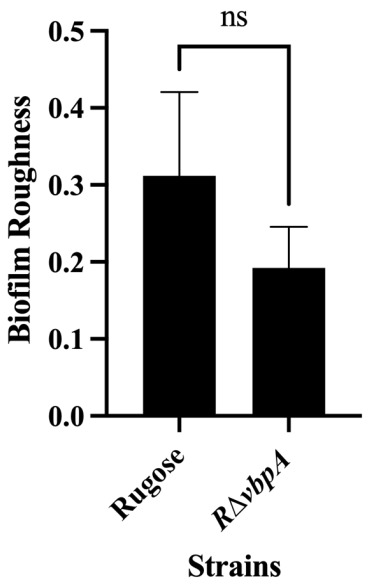
ns
0.5
0.4
0.3
0.2
0.1
0.0
Biofilm Roughness
Rugose
RΔvbpA
Strains

C.

Section 4. Impact of VbpA on known biofilm structural components

Our studies showed that the presence and absence of VbpA in the extracellular space had an effect on biofilm assembly and architecture. However, the specific role of VbpA in the biofilm and how it was causing these changes was unknown. One hypothesis that we decided to investigate was whether VbpA impacts the abundance or localization of the known matrix components that affect *V. cholerae* biofilm structure. The three canonical matrix proteins RbmA, RbmC, and Bap1 and the exopolysaccharide VPS are well documented to affect biofilm structure. We investigated the effect the presence and absence of VbpA had on these biofilm components.

We first investigated whether the absence of VbpA from the rugose parent strain affects the production of the three matrix proteins. We analyzed production of known matrix components in rugose and RΔ*vbpA* as well as strains harboring single deletions of the matrix proteins (RΔ*rbmA,* RΔ*rbmC,* RΔ*bap1*) which were used as negative control. The biofilm spots were resuspended and lysed, and total proteins were analyzed on SDS-PAGE and imaged using western blots. We used antibodies specific to RbmA, RbmC, and Bap1 and RnaP was used for sample loading control. There was no observed variation in RbmA, RbmC, and Bap1 in RΔ*vbpA*, suggesting that the biofilm phenotype of RΔ*vbpA* is not the result of altered abundance of the canonical matrix proteins (Fig 3.1). We also wondered if the presence or absence of

the canonical matrix proteins RbmA, RbmC, and Bap1 would affect the abundance of VbpA. We tested this in a similar way, by analyzing for the abundance of VbpA in strains lacking the matrix proteins singly, doubly, and triply (Fig 4.1). We found that there was no detectable difference in the abundance of VbpA in these strains, showing us that VbpA production is not controlled by the presence of the three canonical matrix proteins of *V. cholerae.*

Figure 4.1. Abundance of matrix proteins RbmA, RbmC, and Bap1 in *V. cholerae* biofilms lacking VbpA. 3 µl of diluted overnight culture (1:200) was plated in triplicate on agar plates. Biofilms were grown at 30˚C, harvested after 24 hours, and resuspended in sterile H_2O containing protease inhibitors. Samples were boiled after the addition of 10% SDS to a final concentration of 2% SDS. VbpA, RbmA, RbmC, and Bap1 were analyzed by western analysis. RnaP is used as a sample loading control. This experiment was repeated in three biological replicates.

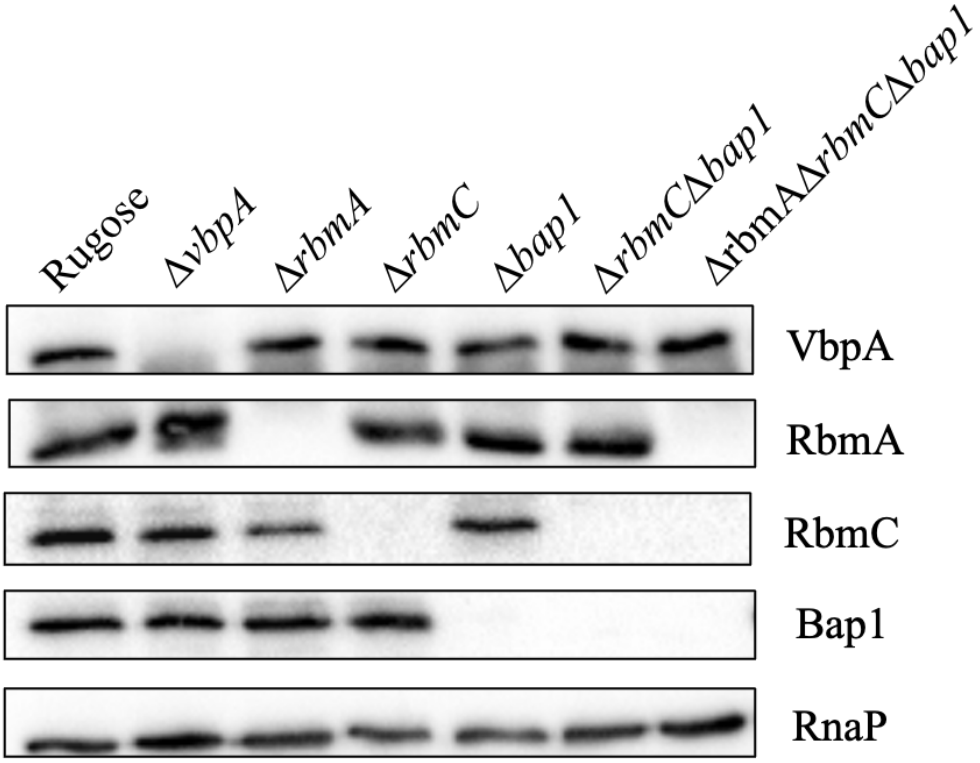
Rugose
ΔvbpA
ΔrbmA
ΔrbmC
Δbap1
ΔrbmCΔbap1
ΔrbmAΔrbmCΔbap1
VbpA
RbmA
RbmC
Bap1
RnaP

We also investigated whether the presence or absence of VbpA affects the production of VPS. Matrix-associated VPS was quantified by immunoblotting for VPS from rugose, RΔ*vbpA,* RΔ*vbpA*-Tn7::*vbpA* complement strain, and Δ*vps*-I Δ*vps*-II as a negative control (Fig 4.2). We isolated VPS by ethanol precipitation and quantified it using immunoblots. We did not see a significant change in abundance of VPS between the parent strain and the mutant strain. This finding showed that VPS abundance is not responsible for the observed phenotypic change in the RΔ*vbpA* strain. We observed an increase in VPS abundance in RΔ*vbpA*-Tn7::*vbpA* compared to the parent and mutant strains; it is unclear if this is biologically significant or an artifact. VPS is a very sticky substance; VPS quantification can be challenging and VPS levels need to be analyzed using complementary approaches.

Figure 4.2. Abundance of Vibrio Polysaccharide in *V. cholerae* mutant and complemented strains of *vbpA*. 200 µl of overnight cultures were plated on 20 ml LB agar plates and incubated overnight at 30˚C. Half plates were harvested and suspended in 5 ml 10 mM Tris (pH 8) with glass beads and vortexed. Cells were removed via centrifugation. Crude VPS was prepared by ethanol precipitation. Abundance of VPS in samples was determined by immunostaining and quantified using ImageJ software. The data was analyzed and graphed using GraphPad. Unpaired t-tests were calculated to find P values. The experiment was repeated in two biological replicates and two technical replicates, shown as the average of these replicates.

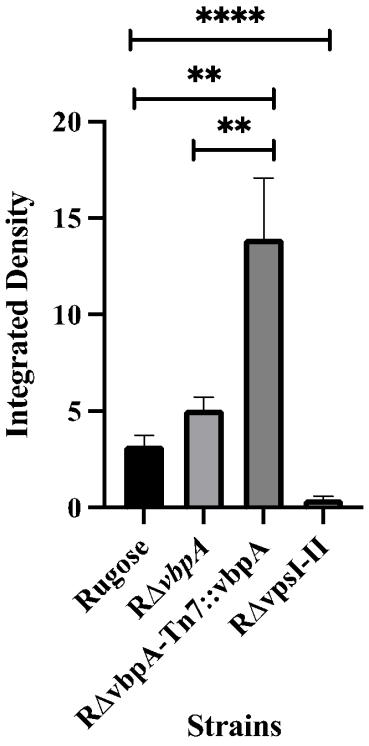
****
**
**
20
15
10
5
0
Integrated Density
Rugose
RΔvbpA
RΔvbpA-Tn7::vbpA
RΔvpsI-II
Strains

We saw that the absence of VbpA did not cause a change in abundance of the known structural components of the *V. cholerae* biofilm: the matrix proteins RbmA, RbmC, and Bap1 and the exopolysaccharide VPS. We next investigated whether VbpA could be causing a change in localization of these important biofilm matrix components. We previously developed a method to visualize biofilm matrix components using epitope tagged matrix proteins paired with corresponding fluorescent antibodies and fluorescently labeled lectins to visualize VPS. Our earlier work showed that the matrix proteins and VPS have specific localizations in the rugose strain biofilm—RbmA was detected throughout the biofilm, RbmC and Bap1 found around cell clusters, Bap1 was additionally concentrated at the biofilm-surface interface, and VPS was present around cell clusters and in the interstitial space between clusters (43). The localizations of these components are important for their functions; for example, the localization of Bap1 at the biofilm-surface interface directly ties to its role in biofilm surface adhesion (40, 43).

To investigate if VbpA may be affecting the localizations of canonical biofilm matrix components, we compared protein localization in biofilms of the rugose parent strain and Δ*vbpA,* both harboring Myc, FLAG, and human influenza hemagglutinin (HA) epitopes at 3' ends of *rbmA, rbmC,* and *bap1* genes, respectively and GFP inserted at the Tn7 locus. We formed biofilms at air-liquid interface under static conditions and labeled these matrix proteins by incubating the biofilms in corresponding fluorescently labeled primary antibodies (Fig 4.3). In the rugose strain we saw similar

localizations of matrix proteins as was seen in Berk et al, 2012, where RbmA was found throughout the biofilm as well as the biofilm-substrate interface, RbmC and Bap1 formed envelopes around cell clusters, and Bap1 concentrated at the biofilm-substrate interface. In Δ*vbpA,* the localizations of these proteins looked similar. For better evaluation, we are in the process of quantifying both abundance and localization patterns of matrix proteins in the Δ*vbpA* strain.

Figure 4.3. RbmA, RbmC, and Bap1 visualization in the *V. cholerae* biofilm matrix using CLSM and fluorescently labeled antibodies. RΔ*ctxAB* RbmA-Myc RbmC-3xFLAG Bap1-3xHA Tn7::GFP and RΔ*vbpA* RbmA-Myc, Bap1-HA, RbmC-FLAG Tn7::GFP were grown statically for 6 hours before washing with 1xPBS containing 1 mg/ml BSA. The biofilm was blocked in 1xPBS containing 5 mg/ml BSA for 5 min and then incubated in one of: c-Myc Monoclonal Antibody, Alexa Fluor 555 (Thermo Fisher MA1-980-A555) at 2 µg/µl for RbmA (A); DYKDDDDK Tag (FLAG) Monoclonal Antibody, Alexa Fluor 647 (Thermo Fisher MA1-142-A647) at 2 µg/µl for RbmC (B), or HA Tag Monoclonal Antibody, Alexa Fluor 647 (Thermo Fisher 26183-A647) at 1 µg/µl for Bap1 (C) in 1xPBS containing 2 mg/ml BSA for 45 min. The biofilm was washed again in 1xPBS containing 1 mg/ml BSA and imaged using CLSM. Visualization image was created using Imaris 9.7.2. Cells are cyan, RbmA is red, RbmC is yellow, and Bap1 is magenta.

A.

Rugose

RΔ*vbpA*

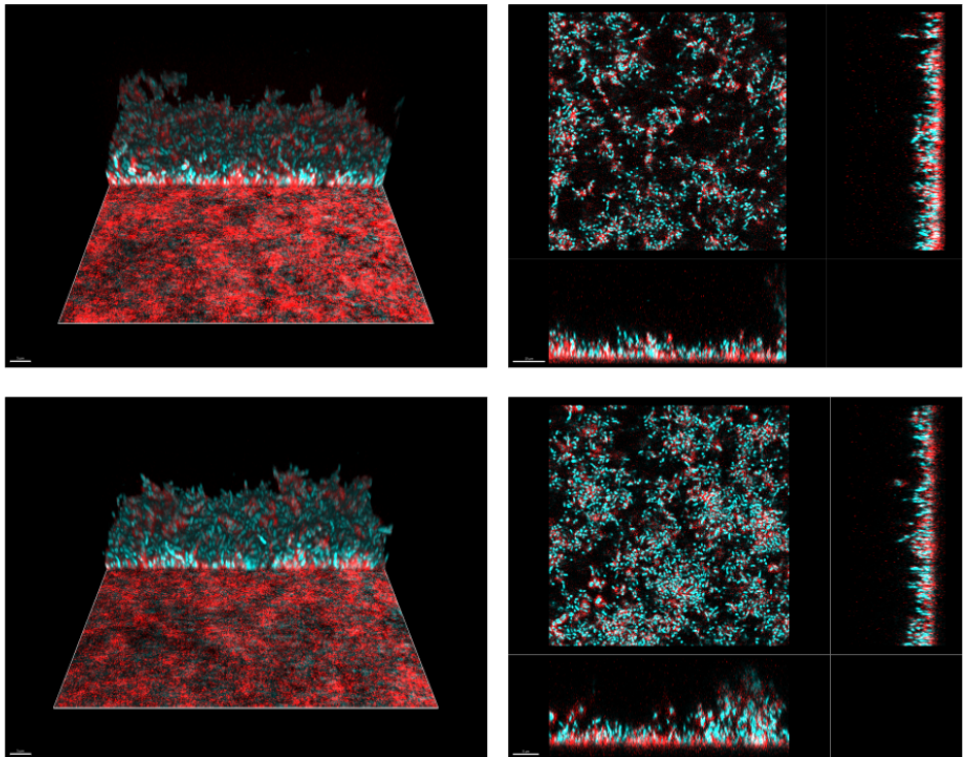

B.

Rugose

RΔ*vbpA*

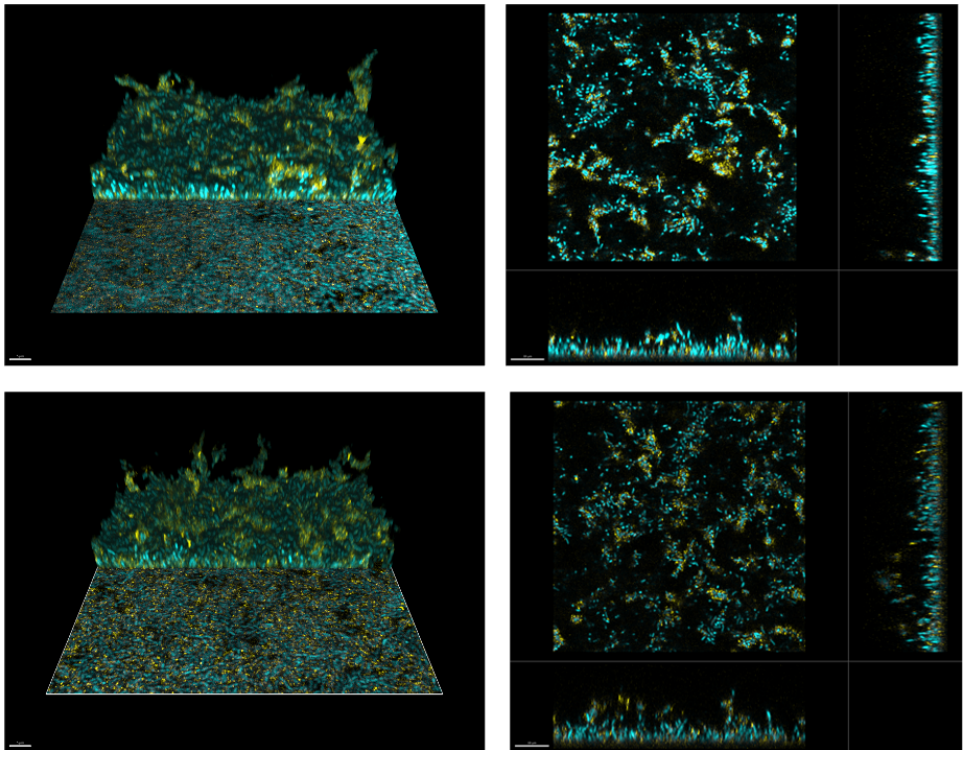

C.

Rugose

RΔ*vbpA*

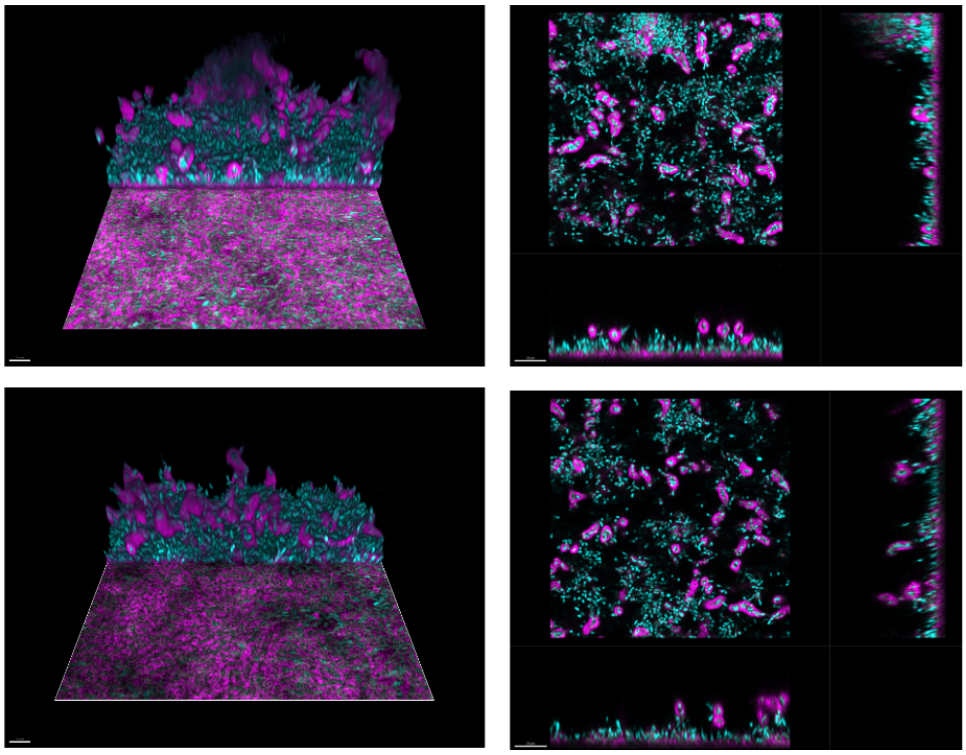

To visualize VPS, we used two types of lectins: Wheat Germ Agglutinin (WGA), a plant lectin which binds to the sugars NeuNAc and GlcNAc found in the minor variant of VPS (77) and concanavalin-A, a plant lectin that binds to Con A selectively binds to a-mannopyranosyl and a-glucopyranosyl residues, allowing binding to both the major structure and the minor variant of VPS (78, 79). The minor variant is present in ~20% of VPS and using both lectin types allowed us to differentiate the two forms of VPS (77). We visualized the fluorescent confocal images and observed the localizations of the major and minor variants of VPS in rugose and RΔ*vbpA* biofilms (Fig 4.4). Both minor and major forms of VPS clustered around microcolonies, and the major form concentrated at the biofilm-substrate interface. This pattern of VPS localization was the same in rugose and RΔ*vbpA.* For better evaluation, we are in the process of quantifying both abundance and localization patterns of VPS forms in the Δ*vbpA* strain.

Figure 4.4. VPS visualization in the *V. cholerae* biofilm matrix using CLSM and fluorescently conjugated lectins. Rugose-Tn7::GFP and RΔ*vbpA*-Tn7::GFP were grown statically for 6 hours before washing with 1xPBS containing 1 mg/ml BSA. The biofilm was blocked in 1xPBS containing 5 mg/ml BSA for 5 min and then incubated in one of: Wheat Germ Agglutinin, Alexa Fluor 555 Conjugate (Thermo Fisher W32464) 5 µg/ml (A); or Concanavalin A, Alexa Fluor 647 Conjugate (Thermo Fisher C21421) at 50 µg/ml (B) in 1xPBS containing 2 mg/ml BSA for 45 min. The biofilm was washed again in 1xPBS containing 1 mg/ml BSA and imaged using CLSM. Visualization image was created using Imaris 9.7.2. Cells are cyan, WGA is orange, and Concanavalin A is green.

A.

Rugose

RΔ*vbpA*

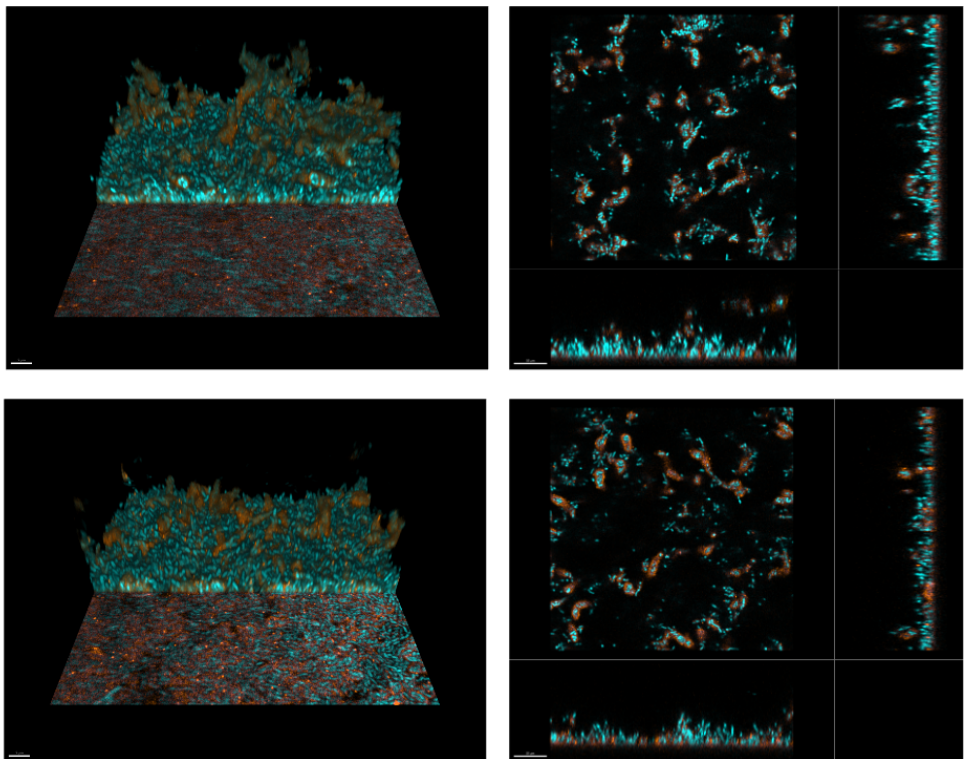

B.

Rugose

RΔ*vbpA*

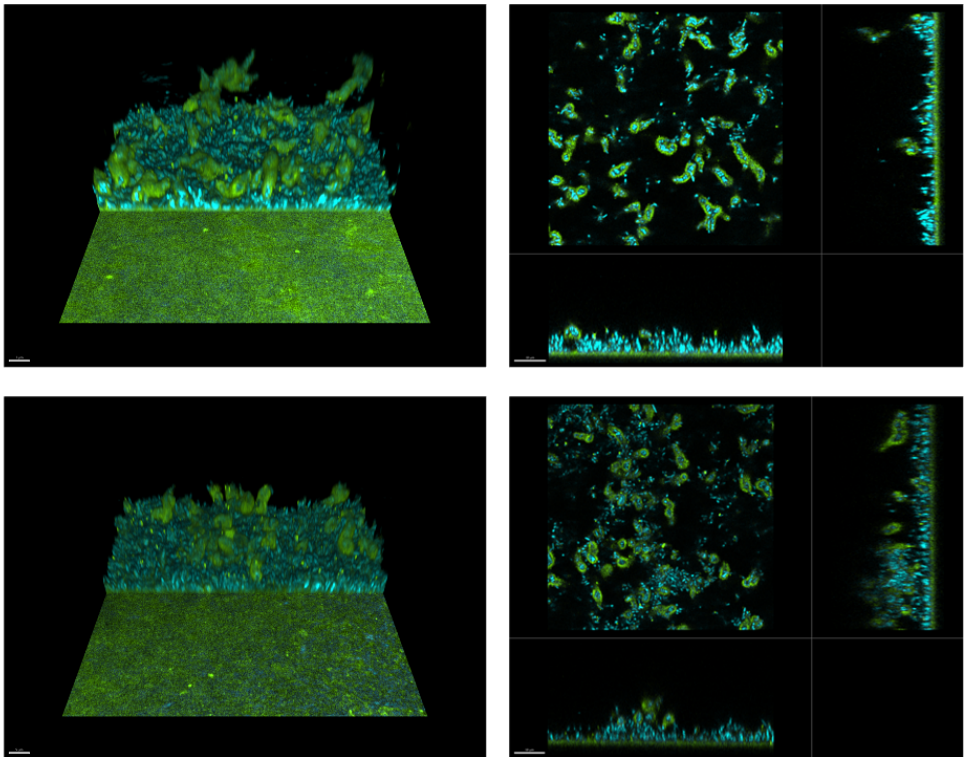

Section 5. Impact of VbpA on biofilm proteome and architecture

In previous sections, we analyzed the effect that VbpA has on known components that are known to have large roles in forming the *V. cholerae* biofilm architecture. In this investigation, we were exploring the hypothesis that VbpA plays a structural role in the biofilm matrix, causing architectural change through acting on the major structural components. On the other hand, we wanted to explore the possibility that VbpA plays a regulatory role to affect the biofilm matrix, with a possible involvement in signal transduction pathways. Although we examined the effect of VbpA on the major known players that affect biofilm architecture, there are many components that we are not aware of that could be playing large roles. We hypothesized that VbpA is a regulatory protein that affects the biofilm matrix proteome composition. To test this hypothesis, we compared the total proteomes of the rugose parent strain and RΔ*vbpA.* We decided to investigate the total proteome from spot biofilms rather than examining the matrix proteome exclusively because VbpA is a periplasmic and extracellular protein and may have important regulatory interactions both intra- and extracellularly. For proteome analysis, we used tandem mass tag (TMT) labeling which allows robust quantification.

We examined proteins that had over 1 log2 fold change between rugose and RΔ*vbpA* (Fig 5.1). Interestingly, the only protein that was downregulated in RΔ*vbpA* over 1 log2 fold change was VbpA, with log2 fold change of -4.13 and t-test p-value of

2.51e-5. There were 5 proteins that were upregulated in RΔ*vbpA* with over 1 log2 fold change. These proteins are: VC2696 (log2 fold change 2.62, p-value 9.67E-9), VCA0645 (log2 fold change 1.49, p-value 1.07E-7), VC1202 (log2 fold change 1.229, p-value 2.58E-7), VC2651 (log2 fold change 1.14, 9.68E-4), and VC0414 (log2 fold change 1.05, p-value 3.23E-5).

Figure 5.1. Volcano plot of Rugose vs. RΔ*vbpA* proteome analysis. Whole proteomes were comparatively analyzed using TMT-labeled peptides. 24 hour plate-grown biofilms were harvested, digested, TMT-labeled, and cleaned in preparation for LC-MS/MS analysis as described in Materials and Methods section. Volcano plot was prepared using SimpliFi. Vertical black lines show the log2 fold>1 cutoff. Y-axis shows $\log_{10}$ p-value. Proteins > -1 log2 fold change and <1 log2 fold change are labeled. 2 biological samples were analyzed, shown is the mean of those replicates.

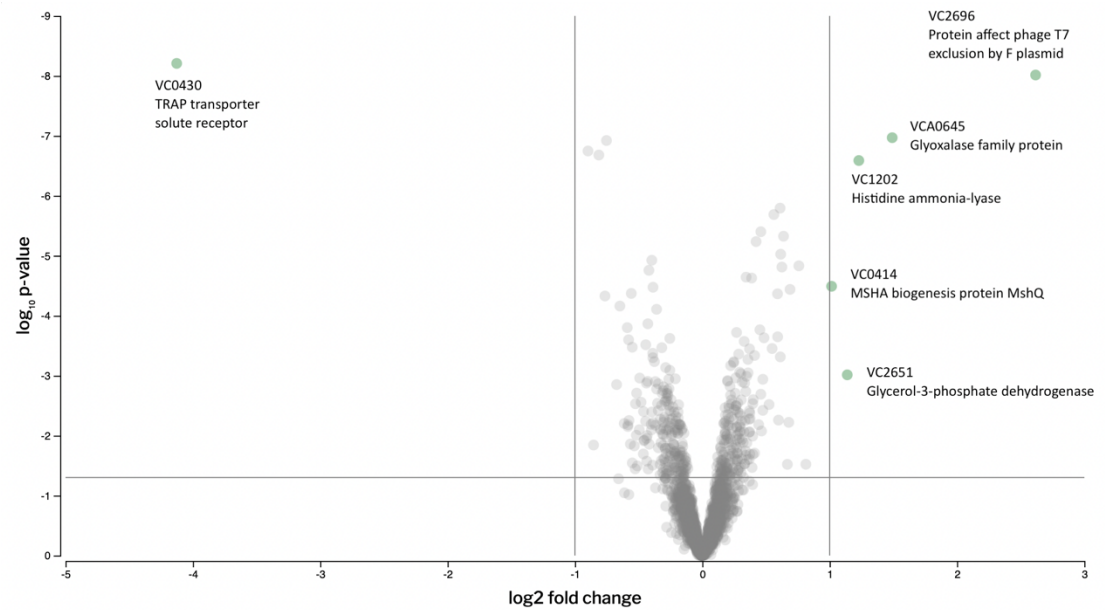
VC2696
Protein affect phage T7
exclusion by F plasmid
VC0430
TRAP transporter
solute receptor
VCA0645
Glyoxalase family protein
VC1202
Histidine ammonia-lyase
VC0414
MSHA biogenesis protein MshQ
VC2651
Glycerol-3-phosphate dehydrogenase
log10 p-value
log2 fold change

We conducted bioinformatic analysis of these proteins to understand more of its functions and investigate any potential involvement with VbpA. VC2696 is annotated as FxsA, which has not been studied in *V. cholerae* but has been identified in *E. coli* as a key player of F exclusion of bacteriophage T7 (80). VCA0645 is a putative glyoxalase that has been identified in other *V. cholerae* proteome and transcriptome assays such as the comparative proteome analysis of wildtype and Δ*nqr* strains (81), the comparative transcriptome analysis of wildtype and an Δ*oscR* mutant (82), and the comparative transcriptome analysis of RΔ*cdgA*Δ*vpsR* versus RΔ*cdgA*Δ*vpsT* mutants (83). VC1202 is annotated as a histidine ammonia-lyase HutH, that was also identified in the comparative proteome analysis of wild-type and Δ*nqr* strains as a protein that decreased in abundance in the mutant (81). VC2651 is annotated as a glycerol-3-phosphate dehydrogenase that is homologous to other similar proteins in Gram-negative bacteria such as GpsA in *Yersinia pestis* (84). VC0414 is known to be part of the mannose-sensitive hemagglutinin (MSHA) pilus operon in *V. cholerae*, and the MSHA pilus has been shown to be important for surface attachment in biofilm assembly (30, 85). VC0414 is known as MshQ. The genes required for the biogenesis of MshA pilus are clustered in two operons in a 16.7 kb region, and *mshQ* is in the second operon harboring 7 genes from *mshB-Q* (85). The pilus is composed of repeats of the major pilin, MshA. MshA pili, along with the single polar flagellum, are critical for initial attachment, biofilm formation, and motility (30, 85). Although the function of MshQ has not been well studied, we speculate that it is involved in surface sensing (Yildiz Lab, unpublished).

To evaluate the effect that these proteins may have on biofilm formation, we decided to construct in-frame deletions of VC2696, VCA0645, and VC1202, and VC0414, *mshQ.* We were particularly interested in MshQ because we have studied the important role that the MSHA pilus has on biofilm assembly. We predicted that VbpA may be involved in surface sensing, and this caused MshQ to increase in abundance in RΔ*vbpA*. To investigate this further, we also generated a double mutant of *vbpA* and *mshQ* as well as deletions of genes encoding the major pilin and flagellar subunits-*mshA* and *flaA.* We observed colony and spot biofilm morphology of these strains (Fig 5.2). We observed that biofilms formed by the deletion of *mshQ,* both in the rugose background and in the RΔ*vbpa* background, formed larger biofilms. This pattern was also seen in the deletion of *mshA.* This suggests to us that the MSHA pilus system is playing a role in biofilm architecture, though the mechanism of this has yet to be determined. Our hypothesis was that the phenotype that we see from RΔ*vbpA* on agar plates may be in part coming from the increased production of the proteins that were identified in the proteomic analysis. Of the other proteins identified by the proteomic analysis, only RΔVCA0645 changed biofilm architecture, the biofilm becoming smaller and less corrugated. Further investigation of this protein's role in biofilms is required.

Figure 5.2. Colony and spot biofilm morphology of single and double deletions of genes of interest from proteomic analysis. Strains (Rugose, RΔ*vbpA,* RΔVC2696, RΔVCA0645, RΔVC1202, RΔ*mshQ,* RΔ*vbpA*Δ*mshQ,* RΔ*mshA,* RΔ*vbpA*Δ*mshA,* RΔ*flaA*) were grown overnight in 30˚C shaking overnight (200 rpm). Overnight cultures were diluted up to 10^{-8} and 100 µl spread onto 20 ml LB agar plates and incubated at 30˚C for 120 hours (A), or overnight cultures were diluted 1:200 in LB medium and 3 µl spotted onto 20 ml LB agar plates and incubated at 30˚C for 72 hours (B).

A.

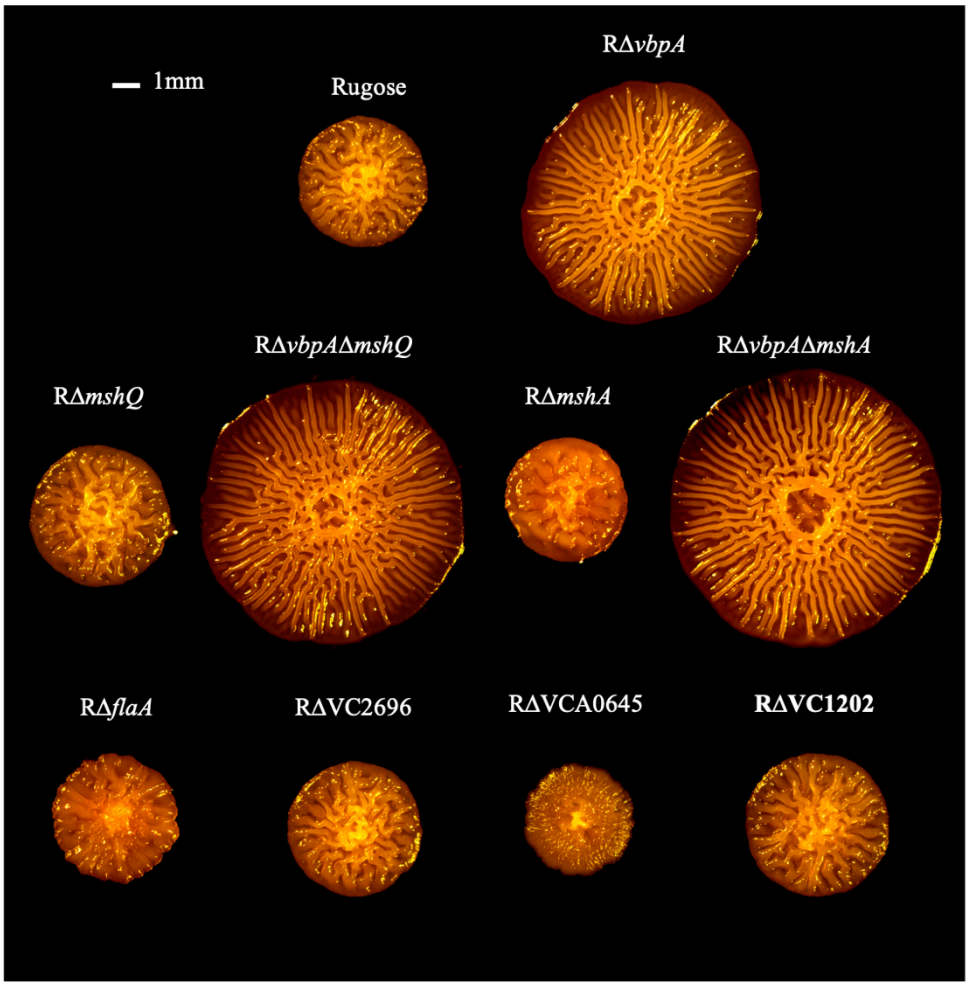
1mm
Rugose
RΔ*vbpA*
RΔ*mshQ*
RΔ*vbpA*Δ*mshQ*
RΔ*mshA*
RΔ*vbpA*Δ*mshA*
RΔ*flaA*
RΔVC2696
RΔVCA0645
RΔVC1202

B.

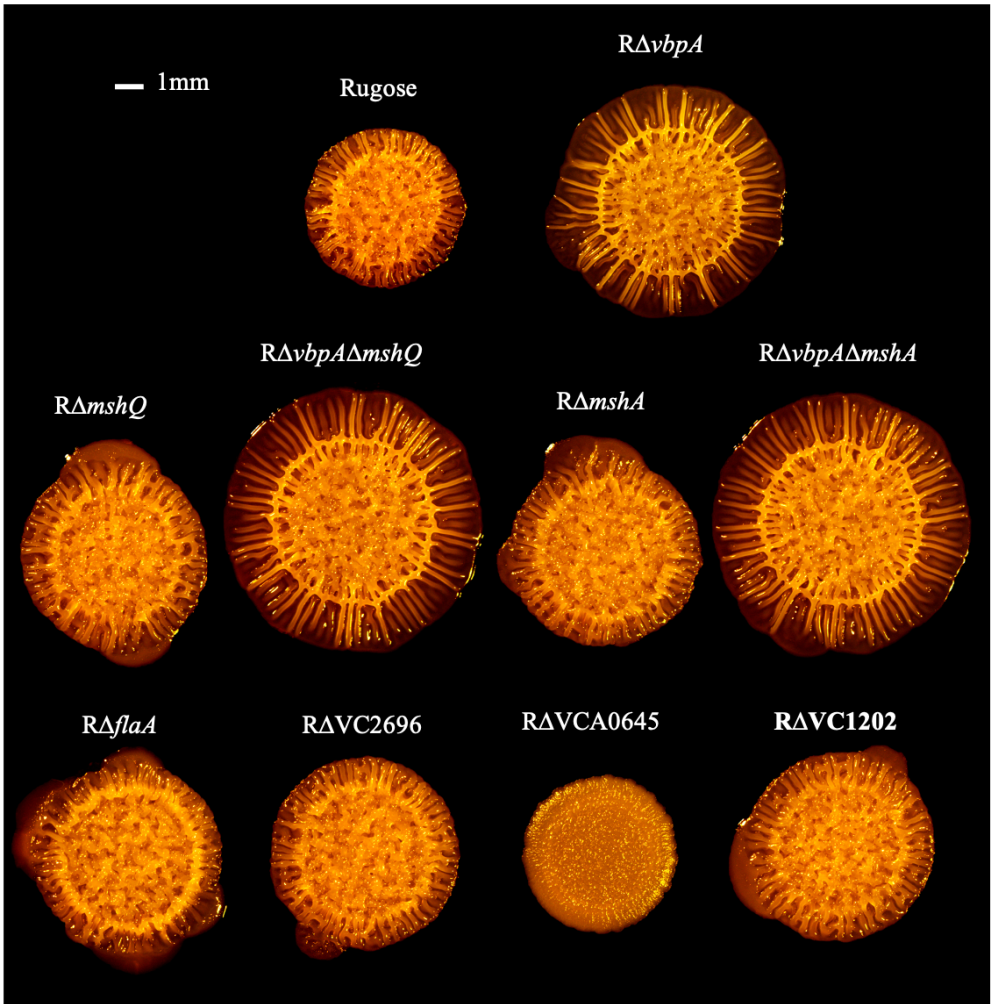
1mm
Rugose
RΔ*vbpA*
RΔ*vbpA*Δ*mshQ*
RΔ*vbpA*Δ*mshA*
RΔ*mshQ*
RΔ*mshA*
RΔ*flaA*
RΔVC2696
RΔVCA0645
RΔVC1202

Section 6. Genetic analysis to identify players that phenocopy RΔ*vbpA* biofilm architecture

The phenotype that RΔ*vbpA* has on the air-solid interface is one that we had not seen before, where the biofilm spreads out larger and the ring on the outside of the biofilm gets spread out and more defined. Because this phenotype is so unique and clearly distinguishable, we thought we could identify additional genes and proteins that may be participating in similar aspects of biofilm assembly. We decided to take an unbiased approach by carrying out transposon mutagenesis to identify other genes that, when mutagenized, cause a similar biofilm phenotype to RΔ*vbpA.* We generated a transposon mutant library on the rugose parent strain using the mTn10 transposon. Using this library, we screened colonies that have a similar colony biofilm phenotype as RΔ*vbpA* on LB agar plates—in particular, RΔ*vbpA* colonies grow larger than the typical at roughly 7 mm compared to the typical rugose phenotype colony, which is at around 5 mm. The corrugation pattern also becomes more spread out compared to the tight corrugation of rugose colonies. Colonies with a similar phenotype on plates were saved and their spot biofilm morphology examined through a dissecting microscope. In the spot morphology phenotype, we were also looking for larger spot biofilms at roughly 11 mm at 72 hours compared to the rugose colonies at 9 mm. From this secondary screen, we identified strains with a spot biofilm phenotype that was similar to RΔ*vbpA*. We then determined their transposon insertion site by arbitrary PCR.

21 genes were identified in the transposon mutagenesis from screening 12,000 mutants (Table 6.1). Interestingly, the top three genes with the highest number of hits were *vxrA, cdgH,* and *cdgM,* which are either known or predicted to be involved in cyclic di-GMP regulation (86, 87). We were expecting a transposon insertion in *vbpA* to be identified. However, we screened over 12,000 colonies but did not identify a transposon insertion in *vbpA.* It is possible that a transposon insertion does not lead to the same phenotype as an in-frame deletion of a gene and that we need to increase the number of mutants screened to identify a transposon insertion into *vbpA*. This study allowed us to identify the types of genes whose mutation results in biofilm phenotype similar to that of *vbpA*. In general, we identified genes related to cyclic di-GMP regulation, sensor histidine kinases, virulence, transport, as well as unstudied hypothetical genes.

Table 6.1. Transposon screen for identification of genes phenocopying RΔ*vbpA*. A transposon library of the rugose strain was constructed as described in detail in Materials and Methods section. A 1 ml aliquot of the library was thawed and grown in 5 ml LB medium overnight at 30˚C shaking and serially diluted to 10^{-7} and 100 µl spread onto LB agar plates. These plates were incubated for 72 hours at 30˚C and each colony screened under a dissecting microscope for the first screening. Those that had colonies that looked similar to RΔ*vbpA* underwent a second screening where spot biofilms were examined, and we conducted arbitrary PCR to amplify the transposition sites and sequenced them. Sequences were analyzed against the *V. cholerae* O1 biovar El Tor strain N16961 and *V. cholerae* O1 biovar El Tor strain A1552 genomes using Artemis, and sequences identified using MicrobesOnline (88).

Gene	Gene number	Number of insertions	Predicted function
vxrA	VCA0565	10	Sensor histidine kinase
cdgH	VC2285	8	GGDEF family protein
cdgM	VC1376	5	Diguanylate cyclase, periplasmic ligand-binding sensor domain
	VC1329	4	Opacity related protein
	VC2286	4	Conserved hypothetical protein
toxR	VC0984	3	Cholera toxin transcriptional activator
hlyA	VCA0219	2	Hemolysin
gsk-1	VC1129	2	Inosine-guanosine kinase
varK	VC0238	2	Transferase, hexapeptide repeat family
	VC2072	1	Peptidase insulinase family protein
	VC1067	1	Hypothetical protein
	VCA0691	1	Acetyl-CoA reductase
treB	VC0910	1	PTS system, trehalose-specific IIBC component
fexB	VC2369	1	Sensor histidine kinase
aldA-2	VC1819	1	Aldehyde dehydrogenase
	VCA0982	1	Transcriptional regulator, LysR family
vctP	VCA0227	1	Iron(III) ABC transporter substrate-binding protein
	VCA0802	1	Conserved hypothetical protein
toxS	VC0983	1	Transmembrane regulatory protein
	VC1066	1	Hypothetical protein
cpdB	VC2562	1	2`,3`-cyclic-nucleotide 2`-phosphodiesterase

Discussion

Matrix proteins have important roles in biofilm assembly. This study serves to illuminate the role of one unstudied matrix in the *V. cholerae* matrix proteome. We systematically characterized VbpA, starting with its effect on biofilm architecture and examining its cellular localization. We observed a drastic change in biofilm architecture on colony and spot biofilms at the solid-air interface in RΔ*vbpA* compared to the rugose parent strain. We also examined biofilm changes in single and double deletions of predicted homologous genes in *V. cholerae* that are also predicted to be in the TAXI-TRAP transport system. The single deletion of RΔ*vbpA* had the most drastic change compared to the other single deletions. However, there were noticeable differences, such as RΔ*vbpJ* forming larger colony/spot biofilms than the rugose strain. These observations suggest that the TAXI-TRAP system has a role in V. cholerae biofilm formation. A study of a TRAP-type solute binding protein DctB in *Bacilllus subtilis* found that in addition to acting as a solute binding protein, it forms a tripartite sensor unit with sensor kinase DctS and transporter DctA, acting as a cosensor along with DctS (89). Similarly to this example, the TAXI-TRAP system in *V. cholerae* may be playing an unknown role, affecting other aspects of bacterial function besides transportation. We found that *vbpA* mutation can be partially complemented with *vbpI,* a predicted homolog. VbpI may also be important for biofilm assembly; though we did not see a major difference in biofilm phenotype in RΔ*vbpI,* VbpA and VbpI may be functionally redundant and expressed under

different conditions or they have specific roles in biofilm matrix assembly. VbpI's lower abundance in the matrix under the conditions that we tested may be contributing to the lack of phenotypic difference seen in RΔ*vbpI.* A further characterization of the roles of the predicted *V. cholerae* TAXI-TRAP system would further our understanding of how this transport system can be affecting biofilm assembly.

In this study we were able to determine VbpA's localization through a series of complementary approaches. Cell fractionation as well as the alkaline phosphatase showed VbpA's periplasmic localization. The matrix isolation and the visualization of VbpA in the biofilm using fluorescently tagged antibodies confirmed VbpA's presence in the biofilm matrix. In addition to confirming its presence, through the confocal microscopy we were able to see that within the matrix, VbpA exists at the middle layer in the biofilm, localizing around microcolonies in a similar way to Bap1, RbmC, and VPS. Understanding VbpA's localization patterns helps us to understand how VbpA could contribute to biofilm matrix assembly. VbpA is a periplasmic protein but can also be found in the extracellular space; it is yet to be determined how it is getting secreted. It is possible that secretion is through presence inside outer membrane vesicles. In addition, matrix proteins RbmA, RbmC, and Bap1 as well as virulence factors like the cholera toxin are secreted to the extracellular space through the Type II Secretion (T2S) System (90). It is possible that VbpA is secreted through

the T2S system as well; this would be an area of further study that could identify further importance of T2S system in *V. cholerae* biofilm formation.

We examined the effect that VbpA's presence and absence has on biofilm architecture in detail. Because we saw that the mutant RΔ*vbpA* causes a drastic change in biofilm phenotype on agar plates at the solid-air interface, we observed this at the single cell level using CLSM. At this magnification, we saw that cell orientation was altered between the rugose strain and RΔ*vbpA.* Of note was the presence of empty chambers within the prongs at the edges or RΔ*vbpA* colonies that contained little to no cells. The exact cause of this has yet to be determined, but this points to a disruption in cell organization within the biofilm. This may also have implications in the role of cell death in biofilm corrugation. A study conducted in *B. subtilis* found that cell death is an important factor leading to the formation of wrinkle formation (92). VbpA's role in spatial patterning of cell death is an area we would like to investigate further. There was no significant change in biofilm volume, thickness, or roughness at statically grown biofilms at the solid-liquid interface between the rugose and RΔ*vbpA* strains. These results show that VbpA's effect on biofilm architecture is condition-specific, though it is unknown if it is specific to the solid-air interface or a softer surface like agar plates. A study by Yan et al (2019) found that mechanical instability of a non-growing substrate contributes to biofilm morphogenesis, meaning that different levels of the substrate softness causes different levels of stress on the biofilm growth, possibly causing different phenotypes (93).

Further investigation of RΔ*vbpA* biofilms on different substrates may elucidate VbpA's roles in surface adhesion.

In order to understand the mechanism by which VbpA is affecting biofilm architecture, we examined the effect VbpA has on known biofilm components—matrix proteins RbmA, RbmC, and Bap1 and the exopolysaccharide VPS. VbpA does not affect the abundance of the three canonical matrix proteins. We could not conclusively say whether VbpA affects VPS abundance through the VPS isolation experiment. One way to quantify VPS more accurately is flow-assisted cell sorting with lectins, as was done in a study analyzing Psl in *P. aeruginosa* (91). We also examined VbpA's effect on the localizations of these matrix components. The patterns seen in the images signify that VbpA does not cause major changes to matrix component localization, though the changes have yet to be quantified.

A proteomic comparison between the rugose strain and RΔ*vbpA* from plate-grown spot biofilms found 5 proteins that were more abundant in RΔ*vbpA* by over a log2 fold of 1. As RΔ*vbpA*'s whole proteome only differs in the abundances of 5 proteins, the architecture change in this mutant does not seem to be achieved through global changes in proteome composition. However, some of these proteins may be playing a large role in interaction with VbpA or separately acting on the biofilm. We are particularly interested in one of the proteins identified in the comparative proteomic analysis, MshQ because it is part of the MSHA pilus that we know is involved in

initial attachment to form biofilms. MSHA pilus assembly is promoted by c-di-GMP, which is an important small molecule that signals the switch from motile planktonic growth form to biofilm growth (85, 86). MshQ in particular is predicted to have roles in surface sensing (Yildiz Lab, unpublished). The fact that a surface-sensing protein is upregulated when VbpA is deleted could mean that VbpA is also playing a factor in surface sensing or surface adhesion. In addition, the genes that had the most transposon insertions that caused RΔ*vbpA*-like phenotype on agar plates were involved in c-di-GMP regulation or sensor histidine kinases. This leads to speculation that VbpA may be involved in c-di-GMP regulation pathways or signaling pathways affecting biofilm formation. One study that could further identify the types of proteins that VbpA is interacting with is a pull-down, and this is something we would like to pursue in future studies.

In conclusion, VbpA is a periplasmic and extracellular protein that plays an important role in biofilm formation. It is abundant in the matrix, and its secretion pathway needs to be investigated. The method to which VbpA is affecting biofilm architecture is unknown—it does not change the abundance or localization of known structural matrix proteins or VPS, and its effect on biofilm architecture is condition-specific. This characterization of VbpA is the first example of a TAXI protein that affects biofilm assembly. Further characterization may reveal if TAXI proteins like VbpA inherently affect biofilm architecture, or proteins like VbpA have functions outside of its role as a SBP that affects biofilm architecture. Examining protein interaction

partners of VbpA and VbpI through protein pull-down can reveal whether these TAXI SBP's interact with other TAXI system proteins or with other systems. We may also conduct a glycan array to investigate the substrate that VbpA transports, and study this substrate's effect on biofilm assembly.

More generally, this study elucidates one of many matrix proteins that have yet to be studied and adds a deeper understanding of the vast diversity of biofilm matrix proteins and their important roles in biofilms. Biofilms are implicated in chronic infections like cystic fibrosis and the contamination of medical devices, causing a great threat to human health. Understanding the components and mechanisms of biofilm formation provides a platform for the development of anti-biofilm strategies, and this deeper understanding of the role of biofilms allows for more potential specific protein targets.

Ending Notes

This project aimed to characterize an unknown protein, VbpA, that was discovered in a previous proteomic analysis of the *V. cholerae* biofilm matrix. The deletion strain of *vbpA* caused such a drastic change on plate-grown colony and spot biofilms that we knew it must be playing a role in *V. cholerae* biofilm formation. Of all of the project options I had in this laboratory for my Master's thesis project, I was drawn to this one because of the discovery aspect. This protein was a completely novel protein that had not been studied, and any finding we make would be novel information about this protein. My goal in entering this Master's program was to learn and soak in as much experience, skills, and knowledge as possible, and through this project I have been able to do exactly that. From the basic molecular skills like molecular cloning to complex techniques like confocal laser scanning microscopy and proteomic sample preparation, these were all skills that I learned and conducted for this study.

Two large accomplishments come to mind when thinking back on this thesis project. One is the proteomic comparison between rugose and RΔ*vbpA*. This was an informative study that allowed us to identify and quantify global proteomic changes in RΔ*vbpA* using TMT labeling. Although there were only five proteins with significant change in abundance, this is new information that VbpA's effect is likely not through global proteomic changes. Another large accomplishment is the use of fluorescently labeled antibodies and lectins to visualize matrix proteins and VPS in

the biofilm matrix. We had not conducted these staining experiments at our facilities before and we planned carefully to conduct these experiments, finding information and recommendations from published literature and communicating with microscopy personnel to make these experiments work specifically with the equipment that we have. Using this, we were able to visualize VbpA in the biofilm matrix. Comparing the localization patterns of VbpA with that of other proteins and other matrix components can lead us to make more hypotheses about VbpA's interaction partners. As a future direction, it would be informative to conduct a fluorescent microscopy experiment with two or more proteins together to understand colocalization patterns. In addition, we would like to examine matrix protein localization in colony and spot biofilms using fluorescent antibodies.

Through conducting these studies, I have learned about the process of conducting scientific experiments, from conducting a literature search to understand the established knowledge to experimental design, experiment conduction, optimization, result analysis, understanding the implications of results, and leading to more hypotheses and more experiments. Throughout all of this was communication with my faculty advisor who helped to guide me in the process, and other lab members who shared their knowledge with me. I am happy to take the valuable experience I have had in conducting this study among amazing people and apply it to my future career as a scientist.

Table 7.1 Bacterial Strains

***E. coli* strains**	**Relevant Genotype**	**Source**
S17λpir	TprSmrrecAthipror-Km-KRP4 : : 2- Tc : :MuKm Tn7 λpir	(95)
DH5α	F'endA1 hsdR17 supE44 thi-1 recA1 gyrA96relA1Δ(argF-lacZY A)U169(φ80dlacΔM15)	Promega
pGT2		
***V. cholerae* strains**		
FY_Vc_2	*V. cholerae* O1 El Tor A1552, rugose wild-type variant, Rif^r (Rugose)	(15)
FY_Vc_105	RΔ*rbmA*, Rif^r	(42)
FY_Vc_222	Rugose-Tn7::GFP , Rif^r, Gm^r	(42)
FY_Vc_339	RΔ*flaA*, Rif^r	(59)
FY_Vc_686	RΔ*rbmC*, Rif^r	(65)
FY_Vc_1376	RΔ*bap1*, Rif^r	(65)
FY_Vc_1400	RΔ*rbmC*Δ*bap1*, Rif^r	(65)
FY_Vc_4327	RΔ*vps*-I Δ*vps*-II, Rif^r	(13)
FY_Vc_4329	RΔ*rbmA*Δ*rbmC*Δ*bap1*, Rif^r	(43)
FY_Vc_10515	RΔ*rbmA*-pMMB/*rbmA*, Rif^r, Ap^r	Yildiz Lab Collection
FY_Vc_13393	RΔVC0430 (*vbpA*) , Rif^r	Yildiz Lab Collection
FY_Vc_13640	RΔ*ctxAB* RbmA-Myc RbmC-3xFLAG Bap1-3xHA Tn7::GFP, Rif^r, Gm^r	Yildiz Lab Collection
FY_Vc_13727	RΔ*vbpA*-Tn7::*vbpA*, Rif^r, Gm^r	Yildiz Lab Collection
FY_Vc_15245	RΔVCA0144 (*vbpI*)	Yildiz Lab Collection
FY_Vc_15249	RΔ*vbpA* RbmA-Myc, Bap1-HA, RbmC-FLAG Tn7::GFP, Rif^r, Gm^r	This study
FY_Vc_15251	RΔ*vbpA*-Tn7::GFP, Rif^r, Gm^r	Yildiz Lab Collection
FY_Vc_15254	RΔ*vbpA*Δ*vbpI*, Rif^r	Yildiz Lab Collection
FY_Vc_15255	RΔVC0429 (*vbpB*) , Rif^r	Yildiz Lab Collection
FY_Vc_15256	RΔVCA0146 (*vbpJ*) , Rif^r	Yildiz Lab Collection
FY_Vc_15790	RΔ*vbpB*Δ*vbpJ*, Rif^r	This study
FY_Vc_16380	Rugose-pMMB/*vbpA*, Rif^r, Ap^r	This study
FY_Vc_16382	RΔ*vbpA*/ pMMB-*vbpA*, Rif^r, Ap^r	This study
FY_Vc_16406	RΔ*vbpA*/ pMMB67EH empty, Rif^r, Ap^r	This study
FY_Vc_16428	RΔ*vbpA*-pMMB/*vbpI*, Rif^r, Ap^r	This study

FY_Vc_16652	RΔ*vbpA*-pMMB/NoSS*vbpA*, Rif^r, Ap^r	This study
FY_Vc_16653	RΔ*vbpA*-pMMB/*rbmA*-SSonly-NoSS*vbpA*, Rif^r, Ap^r	This study
FY_Vc_16820	RΔ*vbpA*-pMMB/*vbpA*-phoA, Rif^r, Ap^r	This study
FY_Vc_16893	RΔ*vbpA*Δ*mshQ*, Rif^r	This study
FY_Vc_16899	RΔ*mshQ*, Rif^r	Yildiz Lab Collection
FY_Vc_16963	RΔVC1202, Rif^r	This study
FY_Vc_16983	RΔVC2696, Rif^r	This study
FY_Vc_16984	RΔVCA0645, Rif^r	This study
FY_Vc_16985	RΔ*mshA*, Rif^r	Yildiz Lab Collection
FY_Vc_16986	RΔ*vbpA*Δ*mshA*, Rif^r	This study
FY_Vc_17038	Rugose-HA-*vbpA*-Tn7::GFP, Rif^r, Gm^r	This study
FY_Vc_17039	RΔ*rbmA*-pMMB67EH empty, Rif^r, Ap^r	Yildiz Lab Collection

Table 7.2. Plasmids

Plasmid vector	Relevant genotype	Source
pGP704sacB28	pGP704 derivative	Gary Schoolnik
pGP704S::Tn7-GFP	Mini-Tn*7* vector harboring a constitutively expressed *gfp* cassette	Gary Schoolnik
pUX-BF13	Helper plasmid containing transposase gene for mini-Tn*7*	Gary Schoolnik
pMMB67EH	Low copy number IPTG inducible vector	(95)
pGP704sacB28	pGP704SacB-ΔVC0430	In strain collection
pGP704sacB28	pGP704SacB-ΔVCA0144	In strain collection
pGP704sacB28	pGP704SacB-ΔmshQ	In strain collection
pGP704sacB28	pGP704SacB-ΔmshA	In strain collection
pGP704sacB28	pGP704SacB-HA-vbpA	This study
pGP704sacB28	pGP704SacB-ΔVC2696	This study
pGP704sacB28	pGP704SacB-ΔVCA0645	This study
pGP704sacB28	pGP704SacB-ΔVC1202	This study
pMMB67EH	pMMB67EH-VC0430	This study
pMMB67EH	pMMB67EH-VCA0144	This study
pMMB67EH	pMMB67EH-rbmA	This study
pMMB67EH	pMMB67EH-vbpA-phoA	This study
pMMB67EH	pMMB67EH-NoSSvbpA	This study
pMMB67EH	pMMB67EH-rbmA-ss-NoSSvbpA	This study

Table 7.3. Primers

pGT2_VC0430_F	acctgtacttccaatccaatCAGGATTTCATTACTATCGG
pGT2_VC0430_R	atccgttatccacttccaatTTACTTAATCAAACCCGC
pMMB_VC0430_F	attcgagctcggtacccgggATGAAGGAAGGGAAATTC
pMMB_VC0430_R	cctgcaggtcgactctagagTTACTTAATCAAACCCGC
pMMB_VCA0144_F	attcgagctcggtacccgggTTGGAAACGGTACAGCATC
pMMB_VCA0144_R	cctgcaggtcgactctagagTTACTGTGGCATCAAGTG
pMMB_VC0430_PhoA_F	caggaaacagaattcgagctATGAAGGAAGGGAAATTC
pMMB_VC0430_PhoA_R	gtgtccgggcCTTAATCAAACCCGCTTC
pMMB_PhoA_F	tttgattaagGCCCGGACACCAGAAATG
pMMB_PhoA_R	tgcatgcctgcaggtcgactTTATTTCAGCCCCAGAGC
pMMB_NoSSVbpA_F	caggaaacagaattcgagctCAGGATTTCATTACTATCGG
pMMB_NoSSVbpA_R	tgcatgcctgcaggtcgactTTACTTAATCAAACCCGC
pMMB_rbmA_SS_F	caggaaacagaattcgagctTTGTCTAACTTTAAAGGATCTATCATG
pMMB_rbmA_SS_R	tgaaatcctgCGCATAAGAAGCCGTTGAAAATAAC
rbmA_SS_VbpA_F	ttcttatgcgCAGGATTTCATTACTATCGG
rbmA_SS_VbpA_R	tgcatgcctgcaggtcgactTTACTTAATCAAACCCGC
VC2696_A	ccatggtgacgtcaccggttACCTGAGACGCTACTGGG
VC2696_B	taaggtattaCACAATGCCTCCTTGGTTTTG
VC2696_C	aggcattgtgTAATACCTTAGGTCAGTCGGTTAC
VC2696_D	gactagagggtaccagagctTCGCTCTCTACGAACCCG
VCA0645_A	ccatggtgacgtcaccggttTTACAGCCCAGCAGCTCG
VCA0645_B	gctgcatttaCATGATGTCACCTTTATTTTGATTGTCC
VCA0645_C	tgacatcatgTAAATGCAGCCAACGGCATAG
VCA0645_D	gactagagggtaccagagctGGTATGACGGTTGAGCAG
VC1202_A	ccatggtgacgtcaccggttCACTTCCAAGGTTTACCTG
VC1202_B	cagtcacttaCATGGTTTCTTTCCTCAC
VC1202_C	agaaaccatgTAAGTGACTGACAAATCAAC
VC1202_D	gactagagggtaccagagctCCACATGCTCAATAAAAGC

Materials and Methods

Bacterial strains, plasmids, and culture conditions

Bacterial strains and plasmids used in this study are listed in Table 7.1 and 7.2. *Escherichia coli* DH5αλpir was used for plasmid construction and *E. coli* S17 λpir was used for conjugation with *V. cholerae. E. coli* and *V. cholerae* were grown at 37˚C and 30˚C respectively, and both were grown aerobically. Cultures were grown in Luria-Bertani (LB) broth (1% Tryptone, 0.5% Yeast Extract, 1% NaCl), pH 7.5. Strain colonies were grown on LB agar medium containing 1.5% (wt/vol) granulated agar. Antibiotics were used at the following concentrations: ampicillin 100 µg/ml; rifampicin 100µg/ml; gentamycin 50µg/ml. For induction, IPTG was added at a concentration of 0.1 mM.

Recombinant DNA Technique and Genetic Manipulation

DNA manipulations were carried out according to manufacturer's instructions and standard molecular procedures. Restriction enzymes were purchased from New England BioLabs. PCRs were carried out using primers purchased from Integrated DNA Technologies and DNA polymerases purchased from New England BioLabs. In-frame gene deletion strains were constructed through homologous recombination, exchanging the native open reading frame to the truncated open reading frame not containing the gene of interest. For each deletion gene, 5' (500 bp) and 3' (500 bp) regions including start and stop codons were amplified by PCR with primers A, B, C,

and D. These primers are listed in Table 7.3. The AB primers amplified the upstream region of the gene, and the CD primers amplified the downstream region of the gene. The amplified 503 bp fragments were cloned into pGP704SacB via Gibson Assembly (NEB). The recombinant plasmids containing the upstream and downstream regions were transformed into *E. coli* DH5αλpir. Deletion constructs were purified and sequenced (Genewiz). Successful constructs were transformed to *E. coli* S17 λpir and were used for conjugation with *V. cholerae*. Trans-conjugants were selected on LB agar medium containing ampicillin (100 µg/ml) and rifampicin (100 µg/ml). Sucrose-based selection was used to select *V. cholerae* deletion clones that had undergone homologous recombination between the wild-type copy of the gene and rejected the plasmid. Ampicillin and rifampicin-resistant colonies were randomly selected and streaked on LB agar medium containing ampicillin and rifampicin with the same concentrations as above, and incubated at 37˚C. Single colonies were then inoculated into liquid LB and incubated overnight at 37˚C shaking (200 rpm). From liquid culture, 10 µl was streaked on LB agar plates containing 6% (wt/vol) sucrose without NaCl. Sucrose plates were incubated at room temperature for 48 hours. Single colonies were selected at random from sucrose plates and patched onto two LB agar plates—one containing ampicillin (100 µg/ml) and one without ampicillin. After incubation overnight at 37˚C, presence of the deletion was verified by PCR. Deletion mutants were stored at -80˚C in 10% (vol/vol) glycerol. Overexpression was made by cloning the gene of interest into the plasmid backbone of pMMB67EH, which

contains the IPTG inducible pTAC promoter. This construct was then conjugated with *V. cholerae*.

Colony Biofilm Morphology Analysis

For analysis of corrugated colony morphology development, cultures grown overnight at 30˚C shaking (200 rpm) were diluted to 10^{-8} with LB medium and 100 µl of the 10^{-7} and 10^{-8} dilutions were plated onto 20 ml LB agar medium. Samples were incubated at 30˚C for 120 hours before imaging.

Spot Biofilm Morphology Analysis

Cultures were grown overnight at 30˚C shaking (200 rpm), then diluted 1:200 in LB medium and 3 µl spots were plated onto LB agar medium (20 ml). Samples were incubated at 30˚C for 72 hours before imaging. For overexpression strains, LB agar medium supplemented with ampicillin (100 µg/µL) and 100 µM IPTG were used.

Western Blot Analysis

Biofilms were grown for 24 hours at 30˚C as described above (Spot Biofilm Morphology Analysis), then harvested and resuspended in 400µl protease inhibitor (Sigma S8830) water. Once samples were sufficiently resuspended, 100µl of 10% SDS was added, and samples were heated at 95˚C for 15 mins. Protein concentrations were determined using bicinchoninic acid assay (BCA) (Pierce). 30µg of protein was calculated, and β-mercaptoethanol was added to a final concentration of 5% (vol/vol).

Samples were run on 12% SDS-PAGE gels and transferred to nitrocellulose membranes with a Mini Trans-Blot Cell (Bio-Rad) in transfer buffer containing 25 mM Tris (pH 8.3), 192 mM glycine, 20% (vol/vol) methanol, and 0.1% (wt/vol) SDS. The blot was blocked in 5% (wt/vol) milk in a PBS buffer containing 250 mM NaCl and 0.1% (vol/vol) Tween 20 in a wash buffer containing a PBS buffer with 250 mM NaCl and 0.1% (vol/vol) Tween 20. Rabbit polyclonal antibody for VbpA was used to detect VbpA at a concentration of 1µg/µl. Horseradish peroxidase conjugate Anti-Rabbit IgG (H+L) (Promega) was used at a dilution of 1:2500. Immunoblots were developed with a SuperSignal West Pico chemiluminescent kit (Pierce).

Subcellular Fractionation

Cultures grown overnight shaking at 30˚C (200 rpm) were diluted 1:200 in 100 ml LB medium, then grown at 30˚C (200 rpm) until OD_{600} 1.1. 1 ml of culture was collected, and the cells separated by centrifugation at 12,250xg for 15 mins at 4˚C for the whole cell fraction. In the remainder of the culture, cells were separated from extracellular supernatant by centrifugation at 12,250xg for 15 mins at 4℃. The pellet was collected for further fractionation. 30 ml of supernatant was collected for trichloroacetic acid precipitation of extracellular proteins. 1 ml of 1mg/ml bovine serum albumin was added for loading control, and trichloroacetic acid was added to each sample to a final concentration of 12.5%. Samples were incubated overnight, shaking, at 4℃. Samples were centrifuged at 30,250xg for 1 hr at 4˚C. Supernatant was discarded and the resulting pellet was dried on ice in the fume hood for 20 minutes. The pellet was

suspended in 7 ml ice cold acetone and centrifuged at 30,250xg for 1 hr at 4℃. Supernatant was discarded, and the resulting pellet was allowed to dry on ice in the fume hood for 20 minutes. Samples were suspended in 400 µl PBS. The resuspended pellet was allowed to hydrate overnight at 4˚C shaking and was analyzed the next day as the supernatant fraction.

The pellet was separated to the periplasm and the spheroplast, which contains the cytoplasmic and membrane fractions. The pellet was homogenized and incubated in 20% sucrose in 20 mM Tris pH 8 (4 ml/g cells), 0.1 EDTA (0.2 ml/g cells) and 0.5 mM PMSF on ice for 1 hr. 0.5 $MgCl_2$ (600 µl/g cells) was added, and then centrifuged at 9500 xg for 20 mins at 4˚C. The supernatant is the periplasmic fraction. The pellet, containing the spheroplast, was resuspended in 10 mM Tris pH 8.

Isolation of Extracellular Matrix

Cultures grown overnight shaking at 30˚C (200 rpm) were diluted to OD_{600} 0.1 and 200 µl were spread on 20 ml LB agar medium plates using sterile glass beads. Samples were grown at 30˚C overnight; 2 plates of biofilms per strain were harvested and resuspended in 1 ml of PBS containing an EDTA-free protease inhibitor. The OD_{600} of the strain's sample was adjusted to within one OD_{600} unit. 900 µl of each sample was transferred to new tubes and constantly rotated at 4˚C overnight. Cells were separated from the crude matrix with centrifugation twice at 10,000 xg for 10 min at 4˚C. The pellet from the first centrifugation was kept as the cell component. The supernatant was filtered through 0.45 µm membranes, centrifuged at 10,000 xg

for 5 min at 4˚C. The supernatant was transferred to organic acid-safe, polypropylene Eppendorf Safe-Lock Natural tubes. BSA and sodium deoxycholate were added to final concentrations of 35 µg/ml and 0.02%, respectively. Tubes were vortexed and incubated on ice for 1 hr. Trichloroacetic acid was added to each sample to a final concentration of 12.5% and vortexed and continuously rotated overnight at 4˚C. The sample was centrifuged at 21,130 xg for 1 hr at 4˚C and the supernatant was discarded, and the pellet dried on ice for 20 min. The pellet was resuspended in 1.5 ml ice cold acetone, then centrifuged again at 21,130 xg for 1 hr at 4˚C. The supernatant was discarded, and the pellet was dried on ice for 20 min. The sample was resuspended in 400 µl PBS containing EDTA-free protease inhibitor and boiled in a 95˚C heat block for 30-45 min to resuspend completely.

Alkaline Phosphatase Assay

SensoLyte pNPP Alkaline Phosphatase Assay Kit, Colorimetric (AnaSpec AS-72146) was used for this enzymatic assay. RΔ*vbpA*-pMMB/*vbpA-phoA,* a strain where *vbpA* is fused to *phoA,* the alkaline phosphatase gene from *E. coli* MG1655, was used for this assay. RΔ*vbpA*-pMMB and RΔ*vbpA*-pMMB/*vbpA* were used as negative controls. 5 colonies of these strains were inoculated and grown overnight at 30˚C (200rpm) in LB media containing ampicillin (100 µg/ml). This culture was diluted 1:200 and grown at 30˚C (200 rpm) until OD_{600} 0.1 and induced with 100 µg IPTG and grown for an additional 2 hours. 18 ml of cultures were moved to 50 ml conical tubes and centrifuged at 4000 rpm for 10 min at 4˚C. The pellets were then analyzed

according to the manufacturer's instructions. Briefly, the cells were washed with an assay buffer and lysed with Triton X-100. Then cell suspension was incubated for 10 min at 4˚C under agitation and centrifuged at 2500 xg for 10 min at 4˚C. The supernatant was collected for the alkaline phosphatase assay. 50 µl of biological samples were added to 96 well plates. 50 µl of *p*NPP substrate solution was added to each well and absorbance was read at 405 nm every 15 min for 1 hour. This experiment was repeated in 3 biological replicates and three technical replicates.

Protein Purification

Recombinant *E. coli* BL21 (DE3) cells carrying expression plasmid pGT2-*vbpA* was grown at 37˚C shaking (200 rpm) in LB medium containing ampicillin overnight, then diluted 1:200 in LB-Amp and grown at 37˚C shaking (2004pm) until OD_{600} reached 0.5. Induction was carried out by adding IPTG to a final concentration of 0.1 mM and the cultures were grown for 24 hours at 18℃. Cells were harvested by centrifugation at 6000 rpm for 15 min and frozen at -80˚C overnight. Cells were then resuspended and lysed in buffer containing 50 mM Tris (pH 8.0), 200 mM NaCl, 2 mM beta-mercaptoethanol, and Pierce™ Protease Inhibitor Tablets, EDTA-free (A32965) using sonication at a 10 sec on, 20 sec off cycle 10 times, for 3 cycles. Lysate was centrifuged at 20,000 rpm for 15 min at 4˚C and the supernatant was moved to fresh tubes. Lysate was filtered with a 0.45 µm filter. Protein was purified with the GST affinity column. The column was first washed with 20% ethanol and filtered water, and incubated with the lysate for 5 min. The column was then washed

with buffer containing 50 mM Tris (pH 8.0), 200 mM NaCl, and 2 mM beta-mercaptoethanol, followed by elution with 50 mM Tris (pH 8.0), 200 mM NaCl, 2 mM beta-mercaptoethanol, and 20 mM glutathione. The protein was further purified using a Ni-NTA column. The eluent from the GST column was mixed 1:1 with a buffer containing 20 mM sodium phosphate, 30 mM NaCl, and 10 mM imidazole and loaded to the Ni-NTA column. This was allowed to flow through, and the column was washed with a buffer containing 20 mM sodium phosphate, 30 mM NaCl, and 25 mM imidazole, and then followed by elution with 20 mM sodium phosphate, 30 mM NaCl, and 250 mM imidazole. Buffer exchange was carried out with the eluted protein using Amicon Ultra-15 centrifugal filter units to a storage buffer containing 20 mM Tris (pH 8), 300 mM NaCl, 0.1 mM EDTA, 0.1 mM DTT, and 40% glycerol. Proteolysis of the GST tag was carried out overnight at 4˚C with the tobacco etch virus (TEV) protease (Sigma Aldrich T4455-10KU). For the spot morphology experiments, both uncleaved and cleaved purified proteins were exchanged to a buffer containing 20 mM Tris (pH 8) and 300 mM NaCl. Proteins were quantified using BCA and 1, 10, 50, and 100 µg of cleaved and uncleaved proteins were added to 10 µl of 1:200 diluted overnight culture in LB medium. BSA suspended in the same buffer was added at the same amounts for control.

Isolation of Vibrio Polysaccharide

5 single colonies were inoculated to 5 ml LB medium and grown shaking overnight at 30˚C (200 rpm). 200 µl of the overnight culture was spread onto a 20 ml LB agar

plate and incubated overnight at 30˚C. Half of the plate was harvested and resuspended in 5 ml 10 mM Tris (pH 8) and vortexed with glass beads. OD_{600} of each sample was adjusted so they were within 1 unit of each other. 500 µl of OD_{600} adjusted cultures were transferred to tubes and mixed overnight on rotation. The cultures were centrifuged at 15,000 xg for 30 min at 4˚C and the supernatant was transferred to a new tube to be centrifuged at the same cycle. The resulting supernatant was transferred to new tubes and ice-cold ethanol was added at 3x the volume of the supernatant. The mixture was vortexed and incubated overnight at -20˚C. The mixture was centrifuged at 21,000 xg for 30 min at 4˚C and the supernatant discarded. The pellet was resuspended and washed with ice-cold 70% ethanol. This was centrifuged at 21,000 xg for 30 min at 4˚C and the supernatant discarded. The samples were left to dry on ice for 30 min. The pellet was resuspended in 200 µl sterile Millipore water and stored at 4˚C for short-term usage or at -20˚C for long-term storage.

Transposon Mutagenesis

The transposition plasmid *E. coli* SM10 λ-pir pDL1093 was introduced to the rugose strain. The pDL1093 was grown in LB medium containing antibiotics kanamycin (50µg/ml) and chloramphenicol (20µg/ml). To construct a transposition library, the 0.5 ml of the overnight culture of rugose strain containing pDL1093 grown at 30˚C was transferred to 100 ml of prewarmed 40˚C LB medium containing kanamycin (50 µg/ml) and shaken overnight at 40˚C (200 rpm). 100 µl of this overnight grown

culture was passed through another overnight growth in 100 µl of prewarmed 40˚C LB medium containing kanamycin (50 µg/ml) and shaken overnight at 40˚C (200 rpm). After each passage, samples were collected and grown on three different agar media—LB agar medium at 30˚C, LB agar medium containing kanamycin (50 µg/ml) at 40˚C and LB agar medium containing kanamycin (50 µg/ml) and chloramphenicol (25 µg/ml) at 30˚C to check for transposition efficiency. The contents of the second transposition passage were aliquoted and frozen at -80˚C. These library aliquots were screened for strains with a morphology similar to RΔ*vbpA*. A 1ml aliquot was thawed and grown in 5ml of LB medium overnight at 30˚C shaking (200 rpm). A 10^{-7} dilution of this overnight culture was made with LB medium and 100 µl spread onto 20 ml LB agar medium using sterile glass beads. These plates were incubated for 72 hours at 30˚C and each colony screened under a dissecting microscope. Those that looked similar to Δ*vbpA* were saved and underwent a second screening where spot biofilm morphology was examined as described in the Spot Biofilm Morphology section. Strains that also had spot biofilms similar to RΔ*vbpA* underwent Arbitrary PCR to sequence the location of the transposon.

Static biofilms and confocal scanning laser microscopy (CLSM) for biofilm parameters

Static biofilms were imaged using strains tagged with GFP. Cultures grown overnight in LB medium at 30˚C shaking (200 rpm) were diluted to OD_{600} 0.02 using LB medium, and 3 ml aliquots were inoculated in 2-well chambers (Ibidi 80287). The

biofilms were grown at 30˚C in static conditions for 6 hours. A sterile loop was used to remove pellicles at the liquid-air interface. The LB was removed from chambers and the biofilms were washed three times with LB medium. Confocal images were captured with Zeiss LSM880. The biofilm properties were quantified using BiofilmQ.

Protein and exopolysaccharide localization using CLSM and fluorescently labeled antibodies/lectins

Cultures were grown overnight at 30˚C as described above (Static biofilms and confocal laser scanning microscopy (CLSM) for biofilm parameters). 500 µl of cultures diluted to OD_{600} 0.02 were inoculated in 8-well chambers (Ibidi 80826). The biofilms were grown at 30˚C in static conditions for 6 hours. A sterile loop was used to remove pellicles at the liquid-air interface. The LB was removed from chambers and the biofilms were washed twice with PBS containing 1 mg/ml BSA. The biofilm was then blocked in PBS containing 5 mg/ml BSA for 5 min at room temperature, then the biofilm was incubated for 45 min at room temperature in PBS with 2 mg/ml BSA containing one of these fluorescently labeled antibodies or lectins: HA Tag Monoclonal Antibody, Alexa Fluor 647 (Thermo Fisher 26183-A647) at 1µg/µl; c-Myc Monoclonal Antibody, Alexa Fluor 555 (Thermo Fisher MA1-980-A555) at 2 µg/µl; DYKDDDDK Tag (FLAG) Monoclonal Antibody, Alexa Fluor 647 (Thermo Fisher MA1-142-A647) at 2 µg/µl; Concanavalin A, Alexa Fluor 647 Conjugate (Thermo Fisher C21421) at 50 µg/ml; and Wheat Germ Agglutinin, Alexa Fluor 555 Conjugate (Thermo Fisher W32464) at 5 µg/ml. The antibody or lectin solutions were

removed and the biofilm was washed three times in PBS containing 1 mg/ml BSA. Confocal images were captured with Zeiss 880 confocal microscope using the Airyscan Fast program and the images were quantified using BiofilmQ and visualized using Imaris.

Proteomic Analysis

Samples of the rugose strain and RΔ*vbpA* were TMT labeled for multiplexed quantification by liquid chromatography/tandem mass spectrometry (LC-MS/MS). 5 plate-grown colonies of rugose and RΔ*vbpA* were inoculated to 5 ml LB medium and grown overnight at 30˚C shaking (200 rpm). The overnight culture was diluted 1:200 in LB medium and 3 µl spotted onto 20 ml LB agar plates in triplicate and incubated for 24 hours at 30˚C. Spots were harvested and homogenized in 1X PBS and washed three times. The samples were then prepared for TMT labeling using the Easypep™ Mini MS Sample Prep Kit (Thermo Fisher A40006) following the manufacturer's instructions. Briefly, the sample pellet was resuspended in the provided lysis buffer and the universal nuclease, and mixed. The mixture was lysed via sonication and the lysate was centrifuged at 16,000 xg for 10 min. The protein concentration of the supernatant was determined using the Pierce™ BCA Protein Assay Kit (Thermo Fisher 23227). Protein sample was transferred to new microcentrifuge tubes and reduced and alkylated. The protein was then digested with the addition of the Enzyme Reconstitution Solution and the Trypsin/Lys-C Protease Mix and shaken at 37˚C for 1-3 hours. The digested proteins were labeled with TMT reagents using the

TMTpro™ 16plex Label Reagent Kit (Thermo Fisher A44521) following the manufacturer's instructions. Briefly, the protein digest was prepared in 100 mM TEAB pH 8.5. Anhydrous acetonitrile was added to the vials containing TMTpro Label Reagent, and the protein digest and the label reagent were incubated together for 1 hour at room temperature. 5% hydroxylamine was added to quench the reaction and incubated for 15 min. The labeled peptide samples were cleaned using the Easypep™ Mini MS Sample Prep Kit and vacuum dried. The labeled peptide samples were sent to UC Davis Proteomics Core Facility for quantitative proteomic analysis.

References

1. Flemming H-C, Wingender J. 2010. The biofilm matrix. 9. Nat Rev Microbiol 8:623–633.

2. Dragoš A, Kovács ÁT. 2017. The Peculiar Functions of the Bacterial Extracellular Matrix. Trends Microbiol 25:257–266.

3. Fong JNC, Yildiz FH. 2015. Biofilm Matrix Proteins. Microbiol Spectr 3.

4. Karatan E, Watnick P. 2009. Signals, Regulatory Networks, and Materials That Build and Break Bacterial Biofilms. Microbiol Mol Biol Rev 73:310–347.

5. Teschler JK, Zamorano-Sánchez D, Utada AS, Warner CJA, Wong GCL, Linington RG, Yildiz FH. 2015. Living in the matrix: assembly and control of Vibrio cholerae biofilms. 5. Nat Rev Microbiol 13:255–268.

6. Costerton JW, Stewart PS, Greenberg EP. 1999. Bacterial Biofilms: A Common Cause of Persistent Infections. Science 284:1318–1322.

7. Hobley L, Harkins C, MacPhee CE, Stanley-Wall NR. 2015. Giving structure to the biofilm matrix: an overview of individual strategies and emerging common themes. FEMS Microbiol Rev 39:649–669.

8. Ma L, Conover M, Lu H, Parsek MR, Bayles K, Wozniak DJ. 2009. Assembly and Development of the Pseudomonas aeruginosa Biofilm Matrix. PLoS Pathog 5.

9. Jennings LK, Dreifus JE, Reichhardt C, Storek KM, Secor PR, Wozniak DJ, Hisert KB, Parsek MR. 2021. Pseudomonas aeruginosa aggregates in cystic fibrosis sputum produce exopolysaccharides that likely impede current therapies. Cell Rep 34:108782.

10. Conner JG, Teschler JK, Jones CJ, Yildiz FH. 2016. Staying alive: Vibrio cholerae's cycle of environmental survival, transmission, and dissemination. Microbiol Spectr 4.

11. Gallego-Hernandez AL, DePas WH, Park JH, Teschler JK, Hartmann R, Jeckel H, Drescher K, Beyhan S, Newman DK, Yildiz FH. 2020. Upregulation of virulence genes promotes Vibrio cholerae biofilm hyperinfectivity. Proc Natl Acad Sci 117:11010–11017.

12. Watnick P, Kolter R. 2000. Biofilm, City of Microbes. J Bacteriol 182:2675–2679.

13. Fong JCN, Syed KA, Klose KE, Yildiz FH. 2010. Role of Vibrio polysaccharide (vps) genes in VPS production, biofilm formation and Vibrio cholerae pathogenesis. Microbiol Read Engl 156:2757–2769.

14. Sutherland IW. 2001. Biofilm exopolysaccharides: a strong and sticky framework. Microbiology 147:3–9.

15. Yildiz FH, Schoolnik GK. 1999. Vibrio cholerae O1 El Tor: Identification of a gene cluster required for the rugose colony type, exopolysaccharide production, chlorine resistance, and biofilm formation. Proc Natl Acad Sci 96:4028–4033.

16. Smith DR, Maestre-Reyna M, Lee G, Gerard H, Wang AH-J, Watnick PI. 2015. In situ proteolysis of the Vibrio cholerae matrix protein RbmA promotes biofilm recruitment. Proc Natl Acad Sci 112:10491–10496.

17. Borlee BR, Goldman AD, Murakami K, Samudrala R, Wozniak DJ, Parsek MR. 2010. Pseudomonas aeruginosa uses a cyclic-di-GMP-regulated adhesin to reinforce the biofilm extracellular matrix. Mol Microbiol 75:827–842.

18. Passos da Silva D, Matwichuk ML, Townsend DO, Reichhardt C, Lamba D, Wozniak DJ, Parsek MR. 2019. The Pseudomonas aeruginosa lectin LecB binds to the exopolysaccharide Psl and stabilizes the biofilm matrix. Nat Commun 10.

19. Franklin MJ, Nivens DE, Weadge JT, Howell PL. 2011. Biosynthesis of the Pseudomonas aeruginosa Extracellular Polysaccharides, Alginate, Pel, and Psl. Front Microbiol 2.

20. Jennings LK, Storek KM, Ledvina HE, Coulon C, Marmont LS, Sadovskaya I, Secor PR, Tseng BS, Scian M, Filloux A, Wozniak DJ, Howell PL, Parsek MR. 2015. Pel is a cationic exopolysaccharide that cross-links extracellular DNA in

the Pseudomonas aeruginosa biofilm matrix. Proc Natl Acad Sci U S A 112:11353–11358.

21. Solano C, García B, Valle J, Berasain C, Ghigo J-M, Gamazo C, Lasa I. 2002. Genetic analysis of Salmonella enteritidis biofilm formation: critical role of cellulose. Mol Microbiol 43:793–808.

22. Zogaj X, Nimtz M, Rohde M, Bokranz W, Römling U. 2001. The multicellular morphotypes of Salmonella typhimurium and Escherichia coli produce cellulose as the second component of the extracellular matrix. Mol Microbiol 39:1452–1463.

23. Serra DO, Hengge R. 2019. Cellulose in Bacterial Biofilms, p. 355–392. *In* Cohen, E, Merzendorfer, H (eds.), Extracellular Sugar-Based Biopolymers Matrices. Springer International Publishing, Cham.

24. Serra DO, Richter AM, Hengge R. 2013. Cellulose as an Architectural Element in Spatially Structured Escherichia coli Biofilms. J Bacteriol 195:5540–5554.

25. Sarkar S. 2020. Release mechanisms and molecular interactions of Pseudomonas aeruginosa extracellular DNA. Appl Microbiol Biotechnol 104:6549–6564.

26. Whitchurch CB, Tolker-Nielsen T, Ragas PC, Mattick JS. 2002. Extracellular DNA required for bacterial biofilm formation. Science 295:1487.

27. Kanampalliwar A, Singh DV. 2020. Extracellular DNA builds and interacts with vibrio polysaccharide in the biofilm matrix formed by Vibrio cholerae. Environ Microbiol Rep 12:594–606.

28. Seper A, Fengler VHI, Roier S, Wolinski H, Kohlwein SD, Bishop AL, Camilli A, Reidl J, Schild S. 2011. Extracellular nucleases and extracellular DNA play important roles in Vibrio cholerae biofilm formation. Mol Microbiol 82:1015–1037.

29. Yang L, Barken KB, Skindersoe ME, Christensen AB, Givskov M, Tolker-Nielsen T. 2007. Effects of iron on DNA release and biofilm development by Pseudomonas aeruginosa. Microbiol Read Engl 153:1318–1328.

30. Floyd KA, Lee CK, Xian W, Nametalla M, Valentine A, Crair B, Zhu S, Hughes HQ, Chlebek JL, Wu DC, Hwan Park J, Farhat AM, Lomba CJ, Ellison CK, Brun YV, Campos-Gomez J, Dalia AB, Liu J, Biais N, Wong GCL, Yildiz FH. 2020. c-di-GMP modulates type IV MSHA pilus retraction and surface attachment in Vibrio cholerae. 1. Nat Commun 11:1–16.

31. Schwechheimer C, Kuehn MJ. 2015. Outer-membrane vesicles from Gram-negative bacteria: biogenesis and functions. Nat Rev Microbiol 13:605–619.

32. Tielker D, Hacker S, Loris R, Strathmann M, Wingender J, Wilhelm S, Rosenau F, Jaeger K-E. 2005. Pseudomonas aeruginosa lectin LecB is located in the outer membrane and is involved in biofilm formation. Microbiology, 151:1313–1323.

33. Thuenauer R, Landi A, Trefzer A, Altmann S, Wehrum S, Eierhoff T, Diedrich B, Dengjel J, Nystrom A, Imberty A, Romer W. 2020. The Pseudomonas aeruginosa Lectin LecB Causes Integrin Internalization and Inhibits Epithelial Wound Healing. mBio 11.

34. Reichhardt C, Jacobs HM, Matwichuk M, Wong C, Wozniak DJ, Parsek MR. 2020. The Versatile Pseudomonas aeruginosa Biofilm Matrix Protein CdrA Promotes Aggregation through Different Extracellular Exopolysaccharide Interactions. J Bacteriol 202.

35. Rybtke M, Berthelsen J, Yang L, Høiby N, Givskov M, Tolker-Nielsen T. 2015. The LapG protein plays a role in Pseudomonas aeruginosa biofilm formation by controlling the presence of the CdrA adhesin on the cell surface. MicrobiologyOpen 4:917–930.

36. Reichhardt C, Wong C, Silva DP da, Wozniak DJ, Parsek MR. 2018. CdrA Interactions within the Pseudomonas aeruginosa Biofilm Matrix Safeguard It from Proteolysis and Promote Cellular Packing. mBio 9.

37. Tseng BS, Reichhardt C, Merrihew GE, Araujo-Hernandez SA, Harrison JJ, MacCoss MJ, Parsek MR. 2018. A Biofilm Matrix-Associated Protease Inhibitor Protects Pseudomonas aeruginosa from Proteolytic Attack. mBio 9.

38. Erskine E, MacPhee CE, Stanley-Wall NR. 2018. Functional Amyloid and Other Protein Fibers in the Biofilm Matrix. J Mol Biol 430:3642–3656.

39. Van Gerven N, Klein RD, Hultgren SJ, Remaut H. 2015. Bacterial Amyloid Formation: Structural Insights into Curli Biogensis. Trends Microbiol 23:693–706.

40. Absalon C, Dellen KV, Watnick PI. 2011. A Communal Bacterial Adhesin Anchors Biofilm and Bystander Cells to Surfaces. PLOS Pathog 7:e1002210.

41. Beyhan S, Yildiz FH. 2007. Smooth to rugose phase variation in Vibrio cholerae can be mediated by a single nucleotide change that targets c-di-GMP signalling pathway. Mol Microbiol 63:995–1007.

42. Fong JCN, Karplus K, Schoolnik GK, Yildiz FH. 2006. Identification and characterization of RbmA, a novel protein required for the development of rugose colony morphology and biofilm structure in Vibrio cholerae. J Bacteriol 188:1049–1059.

43. Berk V, Fong JCN, Dempsey GT, Develioglu ON, Zhuang X, Liphardt J, Yildiz FH, Chu S. 2012. Molecular Architecture and Assembly Principles of Vibrio cholerae Biofilms. Science 337:236–239.

44. Giglio KM, Fong JC, Yildiz FH, Sondermann H. 2013. Structural Basis for Biofilm Formation via the Vibrio cholerae Matrix Protein RbmA. J Bacteriol 195:3277–3286.

45. Fong JC, Rogers A, Michael AK, Parsley NC, Cornell W-C, Lin Y-C, Singh PK, Hartmann R, Drescher K, Vinogradov E, Dietrich LE, Partch CL, Yildiz FH.

Structural dynamics of RbmA governs plasticity of Vibrio cholerae biofilms. eLife 6.

46. De S, Kaus K, Sinclair S, Case BC, Olson R. 2018. Structural basis of mammalian glycan targeting by Vibrio cholerae cytolysin and biofilm proteins. PLoS Pathog 14.

47. Kaus K, Biester A, Chupp E, Lu J, Visudharomn C, Olson R. 2019. The 1.9 Å crystal structure of the extracellular matrix protein Bap1 from Vibrio cholerae provides insights into bacterial biofilm adhesion. J Biol Chem 294:14499–14511.

48. Khemiri A, Jouenne T, Cosette P. 2016. Proteomics dedicated to biofilmology: What have we learned from a decade of research? Med Microbiol Immunol (Berl) 205:1–19.

49. Rani A, Babu S. 2018. Environmental proteomic studies: closer step to understand bacterial biofilms. World J Microbiol Biotechnol 34:120.

50. Toyofuku M, Roschitzki B, Riedel K, Eberl L. 2012. Identification of Proteins Associated with the Pseudomonas aeruginosa Biofilm Extracellular Matrix. J Proteome Res 11:4906–4915.

51. Erdmann J, Thöming JG, Pohl S, Pich A, Lenz C, Häussler S. 2019. The Core Proteome of Biofilm-Grown Clinical Pseudomonas aeruginosa Isolates. 10. Cells 8:1129.

52. Park AJ, Murphy K, Krieger JR, Brewer D, Taylor P, Habash M, Khursigara CM. 2014. A Temporal Examination of the Planktonic and Biofilm Proteome of Whole Cell Pseudomonas aeruginosa PAO1 Using Quantitative Mass Spectrometry. Mol Cell Proteomics 13:1095–1105.

53. Nouwens AS, Beatson SA, Whitchurch CB, Walsh BJ, Schweizer HP, Mattick JS, Cordwell SJ. 2003. Proteome analysis of extracellular proteins regulated by the las and rhl quorum sensing systems in Pseudomonas aeruginosa PAO1. Microbiology, 149:1311–1322.

54. Coelho A, Santos E de O, Faria ML da H, Carvalho DP de, Soares MR, Kruger WMA von, Bisch PM. 2004. A proteome reference map for Vibrio cholerae El Tor. PROTEOMICS 4:1491–1504.

55. World Health Organization. 2021. Cholera.

56. King AA, Ionides EL, Pascual M, Bouma MJ. 2008. Inapparent infections and cholera dynamics. 7206. Nature 454:877–880.

57. Ali M, Lopez AL, You YA, Kim YE, Sah B, Maskery B, Clemens J. 2011. WHO | The global burden of cholera. World Health Organ. World Health Organization.

58. Weil AA, Ryan ET. 2018. Cholera: recent updates. Curr Opin Infect Dis 31:455–461.

59. Faruque SM, Biswas K, Udden SMN, Ahmad QS, Sack DA, Nair GB, Mekalanos JJ. 2006. Transmissibility of cholera: in vivo-formed biofilms and their relationship to infectivity and persistence in the environment. Proc Natl Acad Sci U S A 103:6350–6355.

60. Tamayo R, Patimalla B, Camilli A. 2010. Growth in a biofilm induces a hyperinfectious phenotype in Vibrio cholerae. Infect Immun 78:3560–3569.

61. Vuotto C, Donelli G. 2019. Novel Treatment Strategies for Biofilm-Based Infections. Drugs 79:1635–1655.

62. Cegelski L, Pinkner JS, Hammer ND, Cusumano CK, Hung CS, Chorell E, Åberg V, Walker JN, Seed PC, Almqvist F, Chapman MR, Hultgren SJ. 2009. Small-molecule inhibitors target Escherichia coli amyloid biogenesis and biofilm formation. Nat Chem Biol 5:913–919.

63. Baker P, Hill PJ, Snarr BD, Alnabelseya N, Pestrak MJ, Lee MJ, Jennings LK, Tam J, Melnyk RA, Parsek MR, Sheppard DC, Wozniak DJ, Howell PL. 2016. Exopolysaccharide biosynthetic glycoside hydrolases can be utilized to disrupt and prevent Pseudomonas aeruginosa biofilms. Sci Adv 2:e1501632.

64. Nadell CD, Drescher K, Foster KR. 2016. Spatial structure, cooperation and competition in biofilms. Nat Rev Microbiol 14:589–600.

65. Fong JCN, Yildiz FH. 2007. The rbmBCDEF Gene Cluster Modulates Development of Rugose Colony Morphology and Biofilm Formation in Vibrio cholerae. J Bacteriol 189:2319–2330.

66. Blanchard B, Imberty A, Varrot A. 2014. Secondary sugar binding site identified for LecA lectin from Pseudomonas aeruginosa. Proteins Struct Funct Bioinforma 82:1060–1065.

67. Yan Z, Yin M, Chen J, Li X. 2020. Assembly and substrate recognition of curli biogenesis system. Nat Commun 11:241.

68. Harrison KJ, Crécy-Lagard V de, Zallot R. 2018. Gene Graphics: a genomic neighborhood data visualization web application. Bioinformatics 34:1406–1408.

69. Kelley LA, Mezulis S, Yates CM, Wass MN, Sternberg MJE. 2015. The Phyre2 web portal for protein modeling, prediction and analysis. Nat Protoc 10:845–858.

70. Kelly DJ, Thomas GH. 2001. The tripartite ATP-independent periplasmic (TRAP) transporters of bacteria and archaea. FEMS Microbiol Rev 25:405–424.

71. Fischer M, Hopkins AP, Severi E, Hawkhead J, Bawdon D, Watts AG, Hubbard RE, Thomas GH. 2015. Tripartite ATP-independent Periplasmic (TRAP) Transporters Use an Arginine-mediated Selectivity Filter for High Affinity Substrate Binding *. J Biol Chem 290:27113–27123.

72. Mulligan C, Geertsma ER, Severi E, Kelly DJ, Poolman B, Thomas GH. 2009. The substrate-binding protein imposes directionality on an electrochemical sodium gradient-driven TRAP transporter. Proc Natl Acad Sci 106:1778–1783.

73. Mulligan C, Fischer M, Thomas GH. 2011. Tripartite ATP-independent periplasmic (TRAP) transporters in bacteria and archaea. FEMS Microbiol Rev 35:68–86.

74. Omasits U, Ahrens CH, Müller S, Wollscheid B. 2014. Protter: interactive protein feature visualization and integration with experimental proteomic data. Bioinformatics 30:884–886.

75. Enos-Berlage JL, McCarter LL. 2000. Relation of Capsular Polysaccharide Production and Colonial Cell Organization to Colony Morphology in Vibrio parahaemolyticus. J Bacteriol 182:5513–5520.

76. Hartmann R, Jeckel H, Jelli E, Singh PK, Vaidya S, Bayer M, Rode DKH, Vidakovic L, Díaz-Pascual F, Fong JCN, Dragoš A, Lamprecht O, Thöming JG, Netter N, Häussler S, Nadell CD, Sourjik V, Kovács ÁT, Yildiz FH, Drescher K. 2021. Quantitative image analysis of microbial communities with BiofilmQ. Nat Microbiol 6:151–156.

77. Parasuraman P, Murugan V, Selvin JFA, Gromiha MM, Fukui K, Veluraja K. 2014. Insights into the binding specificity of wild type and mutated wheat germ

agglutinin towards Neu5Acα(2-3)Gal: a study by in silico mutations and molecular dynamics simulations. J Mol Recognit JMR 27:482–492.

78. Yildiz F, Fong J, Sadovskaya I, Grard T, Vinogradov E. 2014. Structural Characterization of the Extracellular Polysaccharide from Vibrio cholerae O1 El-Tor. PLOS ONE 9:e86751.

79. Mandal DK, Bhattacharyya L, Koenig SH, Brown RD, Oscarson S, Brewer CF. 1994. Studies of the Binding Specificity of Concanavalin A. Nature of the Extended Binding Site for Asparagine-Linked Carbohydrates. Biochemistry 33:1157–1162.

80. Wang W-F, Cheng X, Molineux IJ. 1999. Isolation and Identification of fxsA, an Escherichia coli Gene that can Suppress F Exclusion of Bacteriophage T7. J Mol Biol 292:485–499.

81. Toulouse C, Metesch K, Pfannstiel J, Steuber J. 2018. Metabolic Reprogramming of Vibrio cholerae Impaired in Respiratory NADH Oxidation Is Accompanied by Increased Copper Sensitivity. J Bacteriol 200.

82. Shikuma NJ, Yildiz FH. 2009. Identification and Characterization of OscR, a Transcriptional Regulator Involved in Osmolarity Adaptation in Vibrio cholerae. J Bacteriol 191:4082–4096.

83. Beyhan S, Bilecen K, Salama SR, Casper-Lindley C, Yildiz FH. 2007. Regulation of Rugosity and Biofilm Formation in Vibrio cholerae: Comparison of VpsT and

VpsR Regulons and Epistasis Analysis of vpsT, vpsR, and hapR. J Bacteriol 189:388–402.

84. Charusanti P, Chauhan S, McAteer K, Lerman JA, Hyduke DR, Motin VL, Ansong C, Adkins JN, Palsson BO. 2011. An experimentally-supported genome-scale metabolic network reconstruction for Yersinia pestis CO92. BMC Syst Biol 5:163.

85. Jones CJ, Utada A, Davis KR, Thongsomboon W, Sanchez DZ, Banakar V, Cegelski L, Wong GCL, Yildiz FH. 2015. C-di-GMP Regulates Motile to Sessile Transition by Modulating MshA Pili Biogenesis and Near-Surface Motility Behavior in Vibrio cholerae. PLOS Pathog 11:e1005068.

86. Conner JG, Zamorano-Sánchez D, Park JH, Sondermann H, Yildiz FH. 2017. The ins and outs of cyclic di-GMP signaling in Vibrio cholerae. Curr Opin Microbiol 36:20–29.

87. Teschler JK, Cheng AT, Yildiz FH. 2017. The Two-Component Signal Transduction System VxrAB Positively Regulates Vibrio cholerae Biofilm Formation. J Bacteriol 199.

88. Dehal PS, Joachimiak MP, Price MN, Bates JT, Baumohl JK, Chivian D, Friedland GD, Huang KH, Keller K, Novichkov PS, Dubchak IL, Alm EJ, Arkin AP. 2010. MicrobesOnline: an integrated portal for comparative and functional genomics. Nucleic Acids Res 38:D396–D400.

89. Graf S, Schmieden D, Tschauner K, Hunke S, Unden G. 2014. The Sensor Kinase DctS Forms a Tripartite Sensor Unit with DctB and DctA for Sensing C4-Dicarboxylates in Bacillus subtilis. J Bacteriol 196:1084–1093.

90. Johnson TL, Fong JC, Rule C, Rogers A, Yildiz FH, Sandkvist M. 2014. The Type II Secretion System Delivers Matrix Proteins for Biofilm Formation by Vibrio cholerae. J Bacteriol 196:4245–4252.

91. Armbruster CR, Lee CK, Parker-Gilham J, de Anda J, Xia A, Zhao K, Murakami K, Tseng BS, Hoffman LR, Jin F, Harwood CS, Wong GC, Parsek MR. 2019. Heterogeneity in surface sensing suggests a division of labor in Pseudomonas aeruginosa populations. eLife 8:e45084.

92. Asally M, Kittisopikul M, Rué P, Du Y, Hu Z, Cagatay T, Robinson AB, Lu H, Garcia-Ojalvo J, Süel GM. 2012. Localized cell death focuses mechanical forces during 3D patterning in a biofilm. PNAS 109 (46): 18891-18896.

93. Yan J, Fei C, Mao S, Moreau A, Wingreen NS, Košmrlj A, Stone HA, Bassler BL. 2019. Mechanical instability and interfacial energy drive biofilm morphogenesis. eLife 8:e43920.

94. Herrero M, de Lorenzo V, Timmis KN. 1990. Transposon vectors containing non-antibiotic resistance selection markers for cloning and stable chromosomal insertion of foreign genes in gram-negative bacteria. J Bacteriol 172:6557–6567.

95. Fürste JP, Pansegrau W, Frank R, Blöcker H, Scholz P, Bagdasarian M, Lanka E. 1986. Molecular cloning of the plasmid RP4 primase region in a multi-host-range tacP expression vector. Gene 48:119–131.